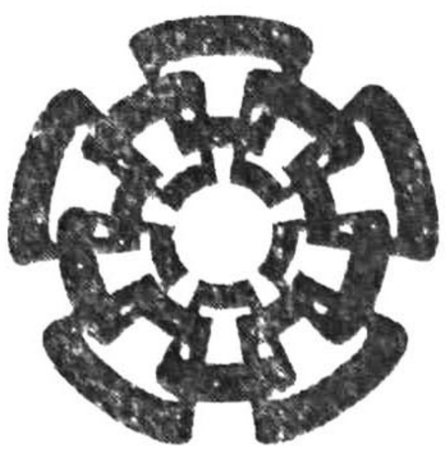

Centro de Investigación y de Estudios Avanzados
del Instituto Politécnico Nacional
Unidad Guadalajara

Avances en el monitoreo de la estabilidad de área amplia en sistemas de potencia mediante el análisis espectral de Koopman

Tesis que presenta:

Marcos Alfredo Hernández Ortega

para obtener el grado de:

Maestro en Ciencias

en la especialidad de:

Ingeniería Eléctrica

Director de Tesis

Dr. Arturo Román Messina

CINVESTAV del IPN Unidad Guadalajara, Guadalajara, Jalisco, Agosto de 2014.

Centro de Investigación y de Estudios Avanzados
del Instituto Politécnico Nacional
Unidad Guadalajara

Advances in wide-area power system stability monitoring using Koopman spectral analysis

A thesis presented by:
Marcos Alfredo Hernández Ortega

to obtain the degree of:
Master in Science

in the subject of:
Electrical Engineering

Thesis Advisor:
Dr. Arturo Román Messina

CINVESTAV del IPN Unidad Guadalajara,Guadalajara, Jalisco, August 2014

CLASIF.. CT00730
ADQUIS.. CT-879-551
FECHA: 29-05-2015
PROCED.. DON-2015
$

Avances en el monitoreo de la estabilidad de área amplia en sistemas de potencia mediante el análisis espectral de Koopman

Tesis de Maestría en Ciencias
Ingeniería Eléctrica

Por:

Marcos Alfredo Hernández Ortega

Ingeniero Eléctrico

Instituto Tecnológico de Morelia 2007-2012

Becario de CONACYT expediente no. 282116

Director de Tesis

Dr. Arturo Román Messina

CINVESTAV del IPN Unidad Guadalajara, Agosto de 2014.

Advances in wide-area power system stability monitoring using Koopman spectral analysis

Master of Science Thesis
In Electrical Engineering

By:

Marcos Alfredo Hernández Ortega
Electrical Engineer
Instituto Tecnológico de Morelia 2007-2012

Scholarship granted by CONACYT, No. 282116

Thesis Advisor:
Dr. Arturo Román Messina

CINVESTAV del IPN Unidad Guadalajara, August, 2014.

Acknowledgements

I would like to express my sincere gratitude to my advisor, Ph.D. Arturo Román Messina, for sharing his knowledge, understanding and patience, and for providing me with the necessary support and enthusiasm required to make this thesis possible.

I would also like to thank to my family for the support that they provided me through my entire life.

To my professors and friends at CINVESTAV Guadalajara, as well as to my friends at Indaparapeo, Michoacán, México.

Finally, acknowledgements are also due to the CONACYT for its support.

Resumen

El monitoreo de área amplia de procesos dinámicos complejos es un problema de gran importancia para el análisis y el control del comportamiento dinámico de los sistemas de potencia. Un monitoreo confiable de la dinámica espacio-temporal mediante unidades de medición fasorial sincronizadas en tiempo, con el objetivo final de su aplicación al diagnóstico, protección y control de sistemas en tiempo real, permanece como un desafío importante de investigación debido a la complejidad de la dinámica y los procesos de control que ocurren simultáneamente a diferentes escalas.

Este trabajo de investigación examina la aplicación de la teoría de modos Koopman para la identificación y extracción de mecanismos coherentes y sus propiedades modales correspondientes, a partir de la respuesta observada del sistema de potencia. Basándose en las propiedades espectrales del operador de Koopman, se desarrollan y se verifican técnicas para extraer el perfil modal y las propiedades de los modos, en conjuntos de datos provenientes tanto de mediciones como de simulaciones de estabilidad transitoria.

Se proporciona además, una interpretación física de los modos Koopman que permita estimar la dinámica global no lineal del sistema. Se muestra que, para el caso de comportamientos lineales, el método converge hacia los modos lineales. En el caso de dinámicos no lineales, el análisis de los modos Koopman tiene una interpretación interesante en términos del análisis de formas normales en la teoría de perturbaciones.

Se plantean avances en el desarrollo de métodos para evaluar la estabilidad de grandes redes de potencia y se identifican direcciones fundamentales de la investigación.

Adicionalmente, se abordan algunos problemas de simulación encontrados en la aplicación de técnicas para la implementación del análisis espectral de Koopman en sistemas de potencia de grandes dimensiones. Las nuevas estrategias desarrolladas para mejorar la eficiencia del análisis por medio de optimización numérica permiten que el método sea capaz de tratar sistemas complejos.

Se realizan algunas comparaciones con otras propuestas existentes para evaluar la eficiencia del marco propuesto.

Abstract

System wide-area monitoring of complex dynamic processes is a problem of great importance in the analysis and control of power system dynamic behavior. Reliable monitoring of the spatial and temporal dynamics by means of time-synchronized phasor measurement units, with the ultimate application to real-time system diagnostics, protection and control, remains a major research challenge due to the complexity of the driving dynamics and control processes occurring at different scales.

This research work examines the application of Koopman mode theory to identify and extract coherent mechanisms and their associated modal properties from power system observed response. Based on the spectral properties of the Koopman operator, techniques to extract mode shapes and modal properties from recorded data at various critical locations are developed and tested in both, synthetic and simulated datasets.

A physical interpretation of the Koopman modes is then provided, which enables assessment of global nonlinear dynamics. It is shown that for linear observables, the method converges towards the linear stability modes. In the case of nonlinear dynamics, Koopman mode analysis has an interesting interpretation in terms of normal form analysis in perturbation theory.

Advances in the development of methods for assessing the stability of large power grids are stated and key research directions in the area of spatio-temporal modeling are discussed.

Numerical issues encountered in the application of Koopman spectral analysis to large scale power systems are also discussed. Newly developed strategies for improving analysis efficiency via numerical optimization enable the analysis method to better handle complex systems. Comparisons with other approaches are provided to assess the efficiency of the proposed framework

Index

Chapter 1
Introduction

Chapter2
Koopman Mode Analysis

Chapter3
Optimized Dynamic Mode Decomposition Methods

Chapter4
Physical Interpretation of KMA

Chapter5
Application

Chapter6
Conclusions

Index of figures and tables

Chapter1
Introduction

This introductory chapter presents a brief description of the research work contained in the thesis.

The background and motivations are explained as well as the statement of the problem that is attached in this document.

Further, a concise review of the previous work related to the topics treated in this thesis is presented. Also, the pursued objectives, the obtained results and limitations of the approach are then stated.

Moreover, the main contributions are summarized.

The last part of the chapter is an outline of the general structure of the thesis.

1.1 Background and motivation

The stability of large interconnected power systems is of primary concern in the power industry. Power system dynamic behavior is intrinsically nonlinear and non-stationary [1], [2].

Transient dynamic processes in power systems exhibit complex phenomena that occur on a wide range of spatial and temporal scales. In practice, system behavior is interpreted in terms of oscillatory modes involving the exchange of swing energy between machines.

The oscillatory modes of electromechanical origin (local and inter-area) are of special concern since they describe global behavior. With a few exceptions, oscillatory activity in the general range of 0.1 Hz to 1.0 Hz is associated with inter-area modes that are related to the swinging of many machines in one part of the system against machines in other parts. They are caused by two or more groups of closely coupled machines being interconnected by weak ties and can be affected by many factors. Modes in the range of 1.0 Hz to perhaps 1.8 Hz are usually local to some particular generator or plant, and not globally observable [1], [2].

Accurate estimation and characterization of electromechanical oscillation modes interacting throughout a large, interconnected grid is a critical part of analyzing, controlling and operating a power system. Mode estimation can be accomplished by modeling the system or by obtaining a mode decomposition that optimally fits a measured system response. Both methodologies have advantages and disadvantages that make them complementary [3].

The process of modeling a power system is based on a certain grade of linearization of the dynamic equations describing the interaction among different variables and elements of the system. The increased use of control devices and the huge dimension of modern interconnected systems in addition to its intrinsic nonlinear behavior make this a very difficult and demanding task.

With the advent of wide area measurement systems (WAMS), and the consequent availability of simultaneous measurements at various system locations coordinated via global positioning systems, there is a need for developing techniques with the capability of efficiently identify dynamical (nonlinear) modes from large amounts of synthetic or measured recorded data [1].

Knowledge of a power system's modal properties may provide critical information for control decisions and thus enable reliable grid operation at higher loading levels [3]. This is the thrust of the present research.

1.2 Problem statement

Methods of investigating and approximating nonlinear system behavior of power system dynamic processes are of special interest to utilities. As emphasized above, this behavior is particularly relevant in the analysis of measured data from wide-area measurements systems involving various temporal and spatial scales [1], [5]-[8].

Techniques for describing global behavior of complex transient processes are of particular interest for characterization of wide-area phenomena. Experience shows that simultaneous analysis of measured data may improve data characterization and result in a better description of global phenomena [6]-[8].

Global stability analyses of measured data may be used to detect impending system breakdown and may be the basis for wide-area control and protection. Direct nonlinear analysis of large data sets, however, may be prohibitive and result in a large amount of data that has to be processed for assessing power system's health.

This research discusses the application of nonlinear analysis techniques to the problem of power system modal identification. Methods based on Koopman mode decomposition are to this end developed and tested on both synthetic and simulated data. The methods extend the notion of linear modal decompositions to the nonlinear setting and can be used to characterize global phenomena.

By extending linear analysis, modal interactions, trends and other artifacts can be accurately identified.

Extracting dynamical features of a power system by global linear analysis require the underlying matrix of the system. In the case of transient stability measurements, this kind of matrices is not available [9]. A bulk of approaches has been proposed over the past two decades to conduct modal analysis using only time-synchronized actual-system measurements [4]. Some of these techniques may represent accurately the entire ensemble of data with a few modes obtained by means of correlation or most energetic trajectories, but without a clear physical meaning of each of them.

There are some other methods, also known as ringdown analyzer algorithms which underlying assumed signal model is a sum of damped sinusoids. For large systems, however, most of these techniques are computationally inefficient and accurate characterization of relevant modal behavior becomes difficult. Moreover, these approaches are mainly based on linear techniques and some of them cannot perform adequately for nonlinear or nonstationary signals.

Further, large stressed interconnected systems when subjected to large disturbances, due to its number of degrees of freedom, and the sparse geographical distribution, exhibit highly complex phenomena including modal interactions, temporarily chaotic vibrations, and intermodulation. To determine the mechanisms governing these physical variations, it is essential to characterize the large-scale interactions between the system modes [2].

The huge number of elements encountered in a power systems and the needed detail to describe their dynamic behavior to obtain a precise description of the evolution of a power system imply an enormous computational effort. Additionally, power systems are continually excited by random inputs with high-order independence. Because of this stochastic nature, no algorithm can exactly estimate the modal properties of the system from finite-time measurements [4].

It is clear from this analysis, that techniques with the ability to simultaneously analyze measured data at various system locations are needed that can account for nonlinear and non-stationary behavior.

The following section briefly describes work in this area and areas of future research are identified.

1.3 A brief review of previous work

Existing approaches to power system dynamic characterization are largely based on linear analysis techniques. Examples include Prony analysis techniques, eigenrealization algorithms, block processing techniques, and recursive algorithms, among others. These procedures have been successfully used to extract modal information from complex data sets [3], [4], [10]-[12].

As the number of measured signal increases, accurate characterization of relevant modal behavior becomes difficult, especially in the presence of noise, trends and abrupt system changes [13]. Some of this sort of approaches have been developed or enhanced in recent years. Even though under relatively high measurement-noise conditions accurate estimates have been provided, the analysis is made via linear techniques, and so is assumed to be the dynamical behavior of the power system [4], [12].

Some techniques which use is efficient with a relatively high number of measured signals (some of them even in the presence of noise) also have been introduced in the last years; the most for analyzing nonstationary and nonlinear phenomena, e.g., proper orthogonal decomposition (POD), empirical orthogonal function (EOF), wavelet-based analysis, and Hilbert spectral analysis [6]-[8], [14]. Nevertheless, the eigenfunctions or modes obtained frequently enclose several electromechanical modes mixed and in some cases mode shape extraction is not addressed [14].

Recently, an interesting and potentially powerful tool based on the Koopman operator has been developed for dynamical analysis of mechanical

systems, mainly in the area of turbulence and fluid dynamics [15]-[18]. The technique is especially useful for describing the behavior of complex nonlinear systems by decomposing snapshots of measured observables into modes determined from spectral analysis of the Koopman operator. It was proposed by Bernard O. Koopman while investigating linear transformations in Hilbert spaces to analyze Hamiltonian systems [19].

Koopman mode analysis was introduced in the power systems literature in [20]–[23]. The technique was used in [20] to identify coherency by performing modal analysis based on nonstationary data of short-term, nonlinear swing dynamics. It was observed that the Koopman modes provide a nonlinear extension of linear oscillatory modes.

In [21] it is suggested a precursor to phenomena of loss of transient stability in multi-machine power systems. Modes are extracted using the Koopman mode decomposition to analyze data provided by sensors or simulations. Also of interest, the Koopman operator has been used for nonlinear dynamical systems in order to enable a data-based approach to stability assessment of power systems without models [22].

In [23] a study for an optimal islanding strategy based on the dynamical properties of the system extracted by means of Koopman mode analysis is developed.

Koopman operator is infinite dimensional even if the governing dynamics are finite dimensional, and does not rely on linearization of the dynamics. Indeed, it captures the full information of any nonlinear system [15]. Modes obtained, referred as Koopman modes are associated with a particular observable, and may be determined directly from measurement data. They have an associated temporal frequency and growth rate and may be viewed as a nonlinear generalization of linear global modes of a linearized system [15], [16].

1.4 Thesis objectives

The primary objective of this thesis is to develop advanced analytical models to characterize power system nonlinear oscillatory behavior from measured data. Extensions and generalizations to Koopman mode decomposition are suggested and tested.

Specific objectives include:

- The development of an analytical framework for nonlinear analysis of measured data based on an optimized dynamical mode decomposition technique.

- The analysis of the physical characteristics of the extracted modes and their comparison with other nonlinear analysis methods.

  The analysis of factors affecting the model performance. In particular, the performance of the technique under limited measurements, noise, and incomplete modal observability.

1.5 Research contributions

The main original contributions of this research work are:

- The development of a rigorous analytical framework for the simultaneous analysis of spatio-temporal data based on advanced Koopman mode decomposition

- The evaluation of optimized dynamic mode decomposition techniques inspired by computational intelligence

- The interpretation of modal behavior in terms of nonlinear mode interaction in perturbation theory

The extension and generalization of Koopman analysis to incorporate observability information into the modal characterization strategy. The evaluation of sources of error arising from incomplete observability of the system

1.6 Organization of the thesis

This thesis is structured in six chapters. After this introductory chapter, Chapter 2 presents a theoretical background on Koopman operator analysis. The theoretical basis of this method are described in the context of the analysis of simultaneous measured data.

Chapter 3 discusses different strategies for an accurate computation of the Koopman modes. These include the dynamic mode decomposition algorithm, an optimized dynamic mode decomposition technique, and some other variants explored through the development of this research work. A brief description of the proposed optimized dynamic mode decomposition technique is given, together with an analysis of synthetic data. A comparison with both, linear and nonlinear analysis techniques is presented.

In Chapter 4, a physical interpretation of the Koopman mode decomposition is provided. It is shown that, under small perturbations, the Koopman modes converge to the linear global modes of the system. A rigorous analytical interpretation is then provided that shows the conditions under which this is achieved. Extension and generalizations to the nonlinear case are investigated and comparisons with perturbation theory are presented.

The application of the proposed technique to simulated data is presented in Chapter 5. Detailed simulation studies show that the proposed framework outperforms existing modal decomposition approaches.

Finally, in Chapter 6 some conclusions, suggestions, and future works are summarized.

1.7 References

[1] J. F. Hauer and J. G. DeSteese, A Tutorial on Detection and Characterization of Special Behavior in Large Electric Power Systems Pacific Northwest Nat. Lab., Richland, WA, 2004, Rep. PNNL-14655.

[2] P. Kundur, Power System Stability and Control, New York, Mc-Graw-Hill, 1994.

[3] J. W. Pierre, D. J. Trudnowski, and M. K. Donnelly, "Initial results in electromechanical mode identification from ambient data," IEEE Trans. Power Syst., vol. 12, no. 3, pp. 1245–1251, Aug. 1997.

[4] D. J. Trudnowski and J. W. Pierre, "Overview of algorithms for estimating swing modes from measured responses", in Proc. 2009 IEEE PES General Meeting, Calgary, AB, Canada, Jul. 2009.

[5] A. R. Messina, Inter-area Oscillations in Power Systems: A Nonlinear and Nonstationary Perspective, New York, Springer, 2009.

[6] A. R. Messina and V. Vittal, "Extraction of dynamic patterns from wide-area measurements using empirical orthogonal functions", IEEE Trans. Power Syst., vol. 22, no. 2, pp. 682–692, May 2007

[7] A. R. Messina, V. Vittal, D. Ruiz-Vega, and G. Enríquez-Harper, "Interpretation and visualization of wide-area PMU measurements using Hilbert analysis," IEEE Trans. Power Syst., vol. 21, no. 4, pp. 1763–1761, Nov. 2006.

[8] A. R. Messina and V. Vittal, "Nonlinear, non-stationary analysis of inter-area oscillations via Hilbert spectral analysis," IEEE Trans. Power Syst., vol. 21, no. 3, pp. 1234–1241, Aug. 2006.

[9] P. J. Schmid, "Dynamic mode decomposition of numerical and experimental data," J. Fluid Mechanics, vol. 656, Cambridge University Press 2010, pp. 5–28.

[10] J. J. Sanchez-Gasca and J. Chow, "Performance comparison of three identification methods for the analysis of electromechanical oscillations", IEEE Trans. Power Syst., vol. 14, no. 3, pp. 995–1002, Aug. 1999.

[11] R. W. Wies, A. Balasubramanian, and J. W. Pierre, "Combining least mean adaptive filter and auto-regressive block processing techniques for estimating the low-frequency electromechanical modes in power systems," in Proc. IEEE Power Engineering Society General Meeting, Montreal, Que., Canada, Jul. 2006.

[12] L. Dosiek, N. Zhou, J. W. Pierre, Z.Huang, and D. J. Trudnowski, "Mode shape estimation algorithms under ambient conditions: a comparative review," IEEE Trasn. Power Syst., vol. 28, no. 2, May 2013.

[13] D. J. Trudnowski, J. M. Johnson, and J. F. Hauer, "Making Prony analysis more accurate using multiple signals", IEEE Trans. Power Syst., vol. 14, no. 1, pp. 226–231, Feb. 1999.

[14] J. L. Rueda, C. A. Juárez, and I. Erlich, "Wavelet-based analysis of power system low-frequency electromechanical oscillations", IEEE Trans. Power Syst., vol. 26, no. 3, Aug. 2011.

[15] C. W. Rowley, I. Mezic, S. Bagheri, P. Schlatter, & D. S. Henningson, "Spectral analysis of nonlinear flows", J. Fluid Mechanics, vol. 641, Cambridge University Press 2009, pp. 115–127

[16] I. Mezić, "Analysis of fluid flows via spectral properties of Koopman operator", Annu. Rev. Fluid Mech., vol. 45, pp. 357-378, 2013.

[17] I. Mezić, "Spectral properties of dynamical systems, model reduction and decompositions," Nonlinear Dyn., vol. 41, pp. 309–325, Aug. 2005

[18] I. Mezić and A. Banaszuk, "Comparison of systems with complex behavior," Physica D, vol. 197, pp. 101–133, Oct. 2004

[19] B. O. Koopman, "Hamiltonian systems and transformations in Hilbert space," Proc. Nat. Acad. Sci. USA, vol. 17, no. 5, pp. 315–318, May 1931.

[20] Y. Susuki and I. Mezić, "Nonlinear Koopman modes and coherency identification of coupled swing dynamics," IEEE Trans. Power Syst., vol. 26, no. 4, pp. 1894-1904, Nov 2011.

[21] Y. Susuki and I. Mezić, "Nonlinear Koopman modes and precursor to power system swing instabilities," IEEE Trans. Power Syst., vol. 27, no. 3, pp. 1182-11191, Aug. 2012.

[22] Y. Susuki and I. Mezić, "Nonlinear Koopman modes and power system assessment without models," IEEE Trans. Power Syst., vol. 29, no. 2, pp. 899–907, March. 2014.

[23] J. F. Raak, "Investigation of power grid islanding based on nonlinear Koopman modes", M.S. thesis, Sch. Elect. Eng., Roy. Inst. of Tech., Stockholm, Sweden, 2013.

Chapter2
Koopman Mode Analysis

The expansion of a complicated function of space and time into a sum of simpler components is a problem of current interest. The most common methods of analysis are based on the Taylor and Fourier expansions. This idea, though has provided important information about the process dynamics, is called into question since the equations describing the behavior of dynamical systems are nonlinear.

An alternate concept has emerged: the problem of decomposing the evolution of a set of observables from the perspective of operator theory, namely based on the projection onto eigenfunctions of the Koopman operator. Koopman mode analysis (KMA) captures the full information of a (nonlinear) system through the spectral analysis of the Koopman operator. It does not rely in any linearization process and can represent any nonlinear response as a linear combination of an infinite sum of linear and nonlinear functions. It is considered as a nonlinear generalization of linear global analysis.

In this chapter, a brief description of Koopman mode analysis and the Koopman operator is presented to analyze discrete systems. The main properties of this technique are developed, and special attention is focused on its mathematical formulation. A brief comparison with other methods, such as the discrete Fourier transformation (DFT) and the proper orthogonal decomposition (POD) is provided.

2.1 Mapping onto basis functions

Power systems dynamics exhibit complex phenomena that occur on a wide range of scales in both space and time. Even with large amounts of information available from simulations and measurements, analysis of complex dynamical phenomena directly from raw time histories is usually not fruitful.

In practice, analyses of dynamic structures are often performed by decomposing measured data into modes. Common techniques include global eigenmodes for linearized dynamics, discrete Fourier transform (DFT), proper orthogonal decomposition (POD) for nonlinear flows, balancing modes for linear systems, and many variants of these techniques [1],[2].

Many of the methods used for capturing coherent structures and for model reduction involve projecting known, high-dimensional dynamics onto a set of modes. A problem of particular importance is the analysis of n state variables $\mathbf{x}(t) \in \Re^n$ function of time t with known dynamics

$$\dot{\mathbf{x}}(t) = f(\mathbf{x}), \tag{2.1}$$

where $f(\cdot) \in \Re^n$ denotes the intrinsic function of the dynamics.

From linear system theory, the vector of states $\mathbf{x}(t)$ can be expanded in terms of a set of N basis functions, or modes, $\varphi_j(\mathbf{x}) \in \mathbb{C}^n$ [3]:

$$\mathbf{x}(t) = \sum_{j=1}^{N} a_k(t)\varphi_j(\mathbf{x}), \tag{2.2}$$

with $a_k(t) \in \mathbb{C}$ being coefficients of the basis functions and j,k are integer indexes.

If the modes $\varphi_j(\mathbf{x})$ are orthonormal, the dynamics can be projected as

$$\dot{a}_j(t) = \left\langle f(\mathbf{x}(t)), \varphi_j(\mathbf{x}(t)) \right\rangle, \tag{2.3}$$

where $\langle \cdot \rangle$ denotes the inner product.

If the modes are not orthonormal, then there is a complementary set of adjoint modes $\psi_j(\mathbf{x}) \in \mathbb{C}^N$ that satisfy

$$\langle \varphi_j(\mathbf{x}), \psi_k(\mathbf{x}) \rangle = \delta_{jk}. \tag{2.4}$$

Here, δ_{jk} denotes the Kronecker delta. In this case, the expansion (2. 2) can still be determined, but the projected dynamics are given by

$$\dot{a}_j(t) = \langle f(\mathbf{x}(t)), \psi_j(\mathbf{x}(t)) \rangle. \tag{2.5}$$

In such a projection method, the main choices are therefore how to choose the modes $\varphi_j(\mathbf{x})$ and $\psi_k(\mathbf{x})$ [3].

When the equations that describe the behavior of a dynamical system are summarized as a function of an operator, it can be analyzed from the perspective of (linear) operator theory. The Koopman operator theory deals with operator theory to analyze dynamical systems. Using the Koopman operator, the spectral properties of the system can be determined and so obtained a set of basis functions related to its intrinsic dynamical response [4].

In what follows, the main theoretical aspects related to the analysis of (linear) operators and the Koopman operator are discussed.

2.2 Operator theory

The theory of operators has, as its object, the study of functions defined on infinite-dimensional spaces. There are important parts of mathematics which cannot be understood in depth without the help of theory of operators. Some examples are the theory of functions of a real variable, integral equations, and the calculus of variations, among others [5].

In order to state the same framework and following [6]-[8], all the concepts below are defined in a complex abstract Hilbert space H which is charac-

terized by five properties: linearity, the existence of a unitary metric, the non-existence of a finite basis, completeness, and separability [6].

The notion of linear operator can be defined as follows.

Definition 2.1 (Linear operator). Let G_1, G_2 be subspaces such that $G_1, G_2 \subset H$ and $T: G_1 \to G_2$ be a function (operator, transformation) under which an element $y \in G_2$ corresponds to each element $x \in G_1$ in the following manner $y = T(x)$. If, for any $x_1, x_2 \in G_1$ and $\alpha, \beta \in \mathbb{C}$, then $T(\alpha x_1 + \beta x_2) = \alpha T(x_1) + \beta T(x_2)$, the operator T is said to be additive. If, in addition, G_1 and G_2 are metric spaces, that is to say that in each space the distance between pairs of elements is defined, one can consider continuous operators T Operators which are both additive and continuous are called linear [5][5].

The fundamental problem of the theory of linear transformations is to prove the existence of linear subspaces of H invariant under a given transformation T and to determine these subspaces [6]. An important type of linear operators for this purpose are the unitary operators U

2.2.1 Unitary operators

Definition 2.2 (Unitary operator). The operator U with $H \subset \Re^n$ as its domain and range is unitary if

$$\langle U x_1, U x_2 \rangle = \langle x_1, x_2 \rangle \tag{2.6}$$

for $x_1, x_2 \in H$ [8][8].

Another definition of the unitary operator is the following

Definition 2.3 (Unitary operator). A bounded linear operator U on a space $H \subset \Re^n$ into itself is unitary if and only if

$$U^{-1} = U^* \tag{2.7}$$

where U is the adjoint operator of U [9].

The unitary operator U has an inverse operator U^{-1} which is also unitary. Moreover, the unitary operator is necessarily linear and is an isometry [10], [8].

A solution of the problem of the existence of linear subspaces of H invariant under T may be formulated by means of the resolution of the identity and the spectral analysis of unitary operators.

2.2.2 *Resolution of the identity*

Assume that T is an operator in H, and that it has a finite or countable set of pairwise orthogonal and normalized eigenvectors $\mathbf{e}_1, \mathbf{e}_2, \ldots, \mathbf{e}_k$, which correspond to nonzero complex eigenvalues $\lambda_1, \lambda_2, \ldots, \lambda_k$. The set H_0 of all vectors from H which are orthogonal to each vector $\mathbf{e}_k$ is a subspace.

It follows that for $\mathbf{x} \in \mathrm{H}_0$, $T\mathbf{x} = 0$. Therefore, it is possible to consider H_0 as the eigenmanifold of the operator T which belongs to the eigenvalue $\lambda_0 = 0$.

As far as H is separable and $\{\mathbf{e}_k\}$ is an orthonormal basis for it, the space $\mathrm{H} \ominus \mathrm{H}_0$ can be represented in the form of an orthogonal sum of eigenmanifolds H_k, which belongs to distinct eigenvalues. Then

$$\mathrm{H} = \mathrm{H}_0 \oplus \mathrm{H}_1 \oplus \mathrm{H}_2 \oplus \cdots, \tag{2.8}$$

where

$$T\mathbf{v}_k = \lambda_k \mathbf{v}_k \tag{2.9}$$

for each eigenvector $\mathbf{v}_k \in H_k$ [10].

Designating the operator of projection on H_k by P_k, we can write

$$I = P_0 + P_1 + P_2 + \cdots. \tag{2.10}$$

For each $\mathbf{x} \in \mathrm{H}$,

$$T\mathbf{x} = \lambda_1 P_1 \mathbf{x} + \lambda_2 P_2 \mathbf{x} + \cdots \tag{2. 11}$$

Now let G_t be the subspace spanned by the eigenvectors which belong to the eigenvalues less than t in some sense. Let E_t be the operator of projection on G_t; then E_t has a limit both for increasing and for decreasing t. Therefore, E_{t-0} and E_{t+0} exist, and $E_{t-0} = E_t$. Thus, E_t is a function of t that is continuous from the left, If $\lambda_k \in \mathbb{C}$ is an eigenvalue, then the difference $E_{\lambda_k+0} - E_{\lambda_k} = P_k$ is the operator of projection into the eigenmanifold H_k.

Now, the terms $\mathbf{x}$ and $T\mathbf{x}$ can be represented in the form:

$$\mathbf{x} = E\mathbf{x} = \int_{\alpha}^{\beta} d\, E_t \mathbf{x} \tag{2. 12}$$

$$T\mathbf{x} = \int_{\alpha}^{\beta} t d\, E_t \mathbf{x} \tag{2. 13}$$

where the integrals are taken over an interval $[\alpha, \beta]$ which contains all the eigenvalues of the operator T. Then, by generalizing the above ideas, the following definition arises.

Definition 2.4 (Resolution of the identity). A resolution of the identity is a one-to-one parameter family of projection operators E_t defined through a finite or infinite interval $[\alpha, \beta]$, which satisfy the following conditions (If the interval $[\alpha, \beta]$ is infinite it can be defined $E_\alpha = E_{-\infty} = \lim_{t \to -\infty} E_t$, and $E_\beta = E_\infty = \lim_{t \to \infty} E_t$) [10]:

(i). $E_\alpha = 0,\ E_\beta = I$. (2. 14)

(ii). $E_{t-0} = E_t \ (\alpha < t < \beta)$, (2. 15)

(iii). $E_u E_v = E_s \ (s = \min\{u, v\})$ (2. 16)

An important subject is that the eigenmanifold constitutes a set of invariant subspaces under T. Hence, the spectral analysis of linear operators allows to obtain this set of invariant subspaces. Moreover, the spectral analysis of unitary operators has some interesting properties useful for the analysis of dynamical systems.

2.2.3 Spectral theory

Let T be a linear operator which domain $\mathrm{D}(T)$ and range $\mathrm{R}(T)$ both lie in H. It is considered the linear operator

$$T_\lambda = \lambda I - T \tag{2. 17}$$

where λ is a complex number and I the identity operator. The distribution of the values λ for which T_λ has an inverse and the properties of the inverse when it exists, are called the spectral theory for the operator T [9].

Definition 2.5 (Spectrum and resolvent). If $\lambda_k \in \mathbb{C}$ is such that the range $\mathrm{R}(T_{\lambda_k})$ is dense in H and T_{λ_k} has a continuous inverse $(\lambda_k I - T)^{-1}$, it is said that λ_k is in the resolvent set $\rho(T)$ of T, and we denote this inverse $(\lambda_k I - T)^{-1}$ by $\mathrm{R}(\lambda_k, T)$ and call it the resolvent of T All complex numbers λ_k not in $\rho(T)$ form a set called the spectrum of T The spectrum $\sigma(T)$ is decomposed into disjoint sets $\mathrm{P}_\sigma(T)$, $\mathrm{C}_\sigma(T)$, and $\mathrm{R}_\sigma(T)$ with the following properties [9]:

(i). $\mathrm{P}_\sigma(T)$ is the totality of complex numbers λ for which T_λ does not have an inverse; $\mathrm{P}_\sigma(T)$ is called the point spectrum of T

(ii). $\mathrm{C}_\sigma(T)$ is the totality of complex numbers λ for which T_λ has a discontinuous inverse with domain dense in H; $\mathrm{C}_\sigma(T)$ is called the continuous spectrum of T.

(iii). $R_\sigma(T)$ is the totality of complex numbers λ for which T_λ has an inverse whose domain is not dense in H; $R_\sigma(T)$ is called the residual spectrum of T

Definition 2.6 (Normal operator). An operator T defined on H is normal if and only if

$$TT^* = T^*T \tag{2. 18}$$

The main assertion of the spectral theorem is that every bounded normal operator T on a Hilbert space induces a resolution E of the identity on the Borel subsets of its spectrum $\sigma(T)$ and that T can be reconstructed from E. A large part of the theory of normal operators depends on this fact [8].

Theorem 2.1. If $T \in$ H and T is normal, then there exists a unique resolution of the identity E on the Borel subsets of $\sigma(T)$ which satisfies:

$$T = \int_{\sigma(T)} \lambda dE(\lambda). \tag{2. 19}$$

E is referred as the *spectral decomposition* of T. Sometimes it is convenient to think of E as being defined for all Borel sets in $\mathbb{C}$; to achieve this put $E(\omega) = 0$ if $\omega \cap \sigma(T) = \emptyset$ [8].

Then, recalling that the eigenvectors of an operator T span eigenmanifolds that indeed are invariant subspaces, the following theorem can be stated.

Theorem 2.2. Let $\sigma(T)$ be the spectrum of a normal operator T, and $\lambda_k \in \mathbb{C}$. If $\sigma(T) = \{\lambda_1, \lambda_2, \ldots, \lambda_k\}$ is a countable set, then every $\mathbf{x} \in$ H has a unique expansion of the form

$$\mathbf{x} = \sum_{i=1}^{\infty} \mathbf{x}_i, \tag{2. 20}$$

where $T_i \mathbf{x}_i = \lambda_i \mathbf{x}_i$. Also, $\mathbf{x}_i \perp \mathbf{x}_j$ whenever $i \neq j$ [8].

Furthermore, analysis of the spectral decomposition of the unitary operators shows that these type of operators are suitable for the spectral analysis of dynamical systems as can be seen below.

Theorem 2.3. A normal operator U defined on H is unitary if and only if $\sigma(T)$ lies on the unit circle [8].

Following Theorem 2.3, as U is a unitary operator, all of its eigenvalues have absolute value unity, i.e., each has the form e^{λ} where λ is a complex number that contains a term called *eigenfrequency* of the unitary operator. The equation

$$U^k \mathbf{v}_k = e^{k\lambda} \mathbf{v}_k \tag{2. 21}$$

holds for integer k if $\mathbf{v}_k \in \mathbb{C}^N$ is an eigenvector associated with the eigenvalue $\lambda_k \in \mathbb{C}$, and also if $U^k \left(-\infty < k < \infty\right)$ is a continuous group of unitary operators [8], [10].

2.2.4 The Koopman operator

In [8], the concepts presented above were extended to include classical Hamiltonian mechanics. The equations of the system which state variables are $\mathbf{x}_k \in \Re^N$ define the operator S_t which has the following properties:

(i). $S_t(\mathbf{x}_0) \rightarrow \mathbf{x}_t$ for an initial condition $\mathbf{x}_0$ and a determined time t. (2. 22)

(ii). $S_{t_1} S_{t_2} = S_{(t_1+t_2)}$, for any times t_1 and t_2, and (2. 23)

(iii). $S_0 = I$ for $t = 0$. (2. 24)

In the search of invariant surfaces where the operator S_t projects the dynamics of a certain subspace of a space $\mathrm{H} \subset \Re^n$ onto itself, it can be defined a set of characteristic functions $\varphi_k(\mathbf{x})$ which are complex single-valued, measurable and bounded for all $\mathbf{x} \in \mathrm{H}$.

Then, the transformation U_t which eigenfunctions are $\varphi_k(\mathbf{x})$ is defined by

$$U_t \varphi_k(\mathbf{x}) = \varphi_k(S_t(\mathbf{x})) \tag{2. 25}$$

and is continuous in $\varphi_k(\mathbf{x})$; also is defined and continuous for all real t. Thus, $U_t \varphi_k(\mathbf{x})$ has at $\mathbf{x}$ the value which $\varphi_k(\mathbf{x})$ has at the point $S_t\mathbf{x}$ into which $\mathbf{x}$ flows after the lapse of time t. The transformation U_t is unitary, and so it arises that [8]:

$$\begin{aligned} U_t \left[a\varphi_j(\mathbf{x}) + b\varphi_k(\mathbf{x})\right] &= a\varphi_j(S_t(\mathbf{x})) + b\varphi_k(S_t(\mathbf{x})) \\ &= aU_t\varphi_j(\mathbf{x}) + bU_t\varphi_k(\mathbf{x}) \end{aligned} \tag{2. 26}$$

There exists a resolution of the identity E_t corresponding with U_t, which consists of a family of operators as defined in Section 2.1.2. Analogously to (2.13) and (2.19), effectuates a spectral resolution of U_t:

$$U_t\varphi_k(\mathbf{x}) = \int_{-\infty}^{\infty} e^{it\lambda_t} dE_t\varphi_k(\mathbf{x}) \tag{2. 27}$$

An evident property of U_t is that, for an arbitrary single-valued function of several variables F

$$U_t F(\varphi_1(\mathbf{x}), \varphi_2(\mathbf{x}), \dots) = F(U_t\varphi_1(\mathbf{x}), U_t\varphi_2(\mathbf{x}), \dots), \tag{2. 28}$$

where $\varphi_1(\mathbf{x}), \dots, \varphi_k(\mathbf{x}) \in \mathbb{C}$ are characteristic functions corresponding to the characteristic values $\lambda_1, \dots, \lambda_k \in \mathbb{C}$, which indeed are of the form e^{λ_k} and are distributed around the unit circle.

2.3 Koopman operator for continuous-time dynamical systems

For a continuous-time dynamical system evolving on a manifold $M \subset \Re^n$ such that for $\mathbf{x} \in M$, where $f(\cdot)$ is a possible nonlinear mapping from M onto itself

and is assumed to be approximately the same over the full interval of time [12]

$$\mathbf{x} = f(\mathbf{x}) \tag{2.29}$$

it can be defined a family of operators U^t, the Koopman operator of the continuous time, just as have been defined in the previous section.

Recalling, that the Koopman operator is a linear operator that acts on a vector-valued function $g : \mathrm{M} \to \Re^n$, mapping $g(\mathbf{x}_0)$ into $g(t, \mathbf{x}_0)$, in the following manner:

$$g(t, \mathbf{x}_0) = U^t\, g(\mathbf{x}_0) = g\left(S^t(\mathbf{x}_0)\right), \tag{2.30}$$

where $S^t(\mathbf{x}_0)$ denotes the position in time t of the trajectory defined by (2.28) that starts at time zero at point $\mathbf{x}_0$.

2.3.1 Koopman eigenfunctions

In analogy with linear stability analysis, Koopman mode analysis provides a set of eigenvalues and eigenfunctions that describe the dynamical behavior of the system and constitutes a set of structures which the observables,can be decomposed in.

According with the concepts presented in the previous section, the following definition can be provided:

Definition 2.7 (Koopman eigenfunction and Koopman eigenvalue). Let $\mathrm{M} \subset \Re^n$ and $\phi_j(\mathbf{x}) : \mathrm{M} \to \mathbb{C}$ denote eigenfunctions; $\dot{\lambda}_j \in \mathbb{C}$ denote eigenvalues of the Koopman operator, then the evolution in time of the dynamical system is given by [1]:

$$U^t \phi_j(\mathbf{x}_0) = \phi\left(S^t(\mathbf{x}_0)\right) = \exp(\lambda_j t)\varphi_j(\mathbf{x}_0), \quad j = 1, 2, \ldots. \tag{2.31}$$

Despite the dynamics itself being linear, the eigenfunctions of the Koopman operator are not necessarily linear. These eigenfunctions span the

space of real-analytic functions on $\mathfrak{R}$, and thus nonlinear observables evolving under linear dynamics can be represented by a spectral expansion using Koopman eigenfunctions. This can be seen from the properties of the Koopman operator described below [1].

2.3.2 Properties of the Koopman operator

In order to understand the power and applicability of Koopman mode analysis for dynamical systems, the main and more important properties of the Koopman operator are listed below. Although some have been presented above, here are rewritten with the aim of provide a clearer description.

Property 2.1 (Linearity). Although the dynamical system is nonlinear and evolves on a finite-dimensional manifold $M \subset \Re^n$ the Koopman operator is linear and infinite-dimensional. Since U is linear, it holds that

$$U^t(\alpha g_1 + \beta g_2)(\mathbf{x}_0) = \alpha U^t g_1(\mathbf{x}_0) + \beta U^t g_2(\mathbf{x}_0) \tag{2.32}$$

for any functions g_1, g_2 and scalars α, β [2].

Property 2.2 (Potency). Let $\phi(x) = x^n, x \in \Re, n \in \mathbb{Z}^+$, and $\lambda \in \mathbb{C}$. Then

$$U^t\phi(x) = \phi(x\exp(\lambda t)) = x^n \exp(n\lambda t) = \exp(n\lambda t)\phi(x), \tag{2.33}$$

and thus the functions $\phi(x) = x^n$ are eigenfunctions of U^t associated with eigenvalues $n\lambda$.

Now, by considering the Taylor expansion of the evolution of any real-analytic observable $g(x)$:

$$g(x) = \sum_{j=0}^{\infty} g_j x^j \tag{2.34}$$

where $g_j = (1/j!)\, d^j g / dx^j(0)$.

Its evolution, given by $g(t,x)=U^t g(x)$, can be represented as

$$g(t,x)=U^t g(x)=U^t\left(\sum_{j=0}^{\infty} g_j x^j\right)=\sum_{j=0}^{\infty} g_j \exp(j\lambda t)x^j \tag{2.35}$$

For n real or negative, x^n is also an eigenfunction; provided those, the space of observables can be expanded in which that are of interest [1].

Property 2.3 (Modal interaction). Let $\mathbf{x}_t \in \mathrm{M}$ where $\mathrm{M} \subset \Re^n$ If $\phi_{\lambda_1} : \mathrm{M} \to \Re$ is an eigenfunction of U^t at $\lambda_1 \in \mathbb{C}$ and $\phi_{\lambda_2}^* : \mathrm{M} \to \Re$ is an eigenfunction of U^t at $\lambda_2 \in \mathbb{C}$, then $\phi_{\lambda_1} \cdot \phi_{\lambda_2}$ is an eigenfunction at $\lambda_1 + \lambda_2$ [1]:

$$\begin{aligned} U^t\left(\phi_{\lambda_1}(\mathbf{x})\phi_{\lambda_2}(\mathbf{x})\right) &= \phi_{\lambda_1}\left(S^t(\mathbf{x})\right)\phi_{\lambda_2}\left(S^t(\mathbf{x})\right) \\ &= \exp(\lambda_1 t)\phi_{\lambda_1}(\mathbf{x})\exp(\lambda_2 t)\phi_{\lambda}(\mathbf{x}) \\ &= \exp\left((\lambda_1+\lambda_2)t\right)\phi_{\lambda_1}(\mathbf{x})\phi_{\lambda_2}(\mathbf{x}). \end{aligned} \tag{2.36}$$

Thus, the properties 2.35 and 2.36 allow express the Taylor expansion of a set of real-analytic nonlinear observables that capture the behavior of a dynamical system in terms of nonlinear interaction of linear modes in similar way to the method of normal forms [13]. This affirmation is further developed and analyzed in the following sections and in Chapter 4.

2.3.3 Koopman modes

It can be assumed now a vector-valued observable $g(\mathbf{x}) \in \Re^n$, with $\mathbf{x} \in \mathrm{M}$ where $\mathrm{M} \subset \Re^n$ is the state space of the dynamical system.

Definition 2.8 (Koopman mode). The Koopman mode $\mathbf{v}(\mathbf{x}) \in \mathbb{C}^n$ at isolated eigenvalue $\lambda \in \mathbb{C}$ of algebraic multiplicity 1 is the projection of $g(\mathbf{x})$ onto the eigenfunction $\phi_\lambda(\mathbf{x})$ of U^t at λ [1].

The projection in question can be obtained as an inner product with the eigenfunction $\bar{\phi}_{\lambda}^{c}(\mathbf{x})$ at λ^{c} of the adjoint of U' - the Perron-Frobenius operator. This would, however, require an explicit calculation of such an eigenfunction. Alternatively, some other ways for Koopman modes computation have been developed; these are described in Chapter 3.

Koopman modes are independent of initial conditions and form a basis for the expansion of the evolution of the observable $g(\mathbf{x})$ starting from any initial condition in the state space. They are of interest because they are akin to the eigenvector expansion utilized in linear analysis. In fact, for linear systems the Koopman modes coincide with its eigenvectors as shown below [1].

2.4 Koopman mode analysis for discrete-time dynamical systems

Owing to the discrete nature of the data that is available to perform an analysis, it is convenient to state Koopman operator theory in terms of discrete-time. Thus a discrete sequence $U^{n\Delta t}, n = 0,1,\ldots,N$ is obtained and if $\lambda_k \in \mathbb{C}$ is an eigenvalue of U' with mode $\mathbf{v}_k(\mathbf{x}) \in \mathbb{C}^n$, then the obtained evolution associated with that mode is $\alpha^n \mathbf{v}_k(\mathbf{x}) = \exp(n\lambda_k \Delta t)\mathbf{v}_k(\mathbf{x})$ yielding $\log_e(\alpha) = (\lambda_k \Delta t)$, and the eigenvalue is plotted at $\exp[(\log_e \alpha)/\Delta t]$ [1].

Then the operator $U^{\Delta t}$ that composes the family of operators U^t is referred just as the Koopman operator U Thus, henceforth the analysis and contains of the thesis are developed into a discrete-time frame. It is appropriate to make mention that the definitions and properties defined previously can be extended to discrete-time framework.

Similarly to the previous section, it is considered a dynamical system evolving on a manifold $\mathrm{M} \subset \Re^n$ such that for $\mathbf{x}_k \in \mathrm{M}$,

$$\mathbf{x}_{k+1} = f(\mathbf{x}_k), \tag{2.37}$$

where $f(\cdot)$ is a map from $\mathbf{M}$ to itself and k is an integer index. It is important to highlight that as in the previous section, the mapping $f(\cdot)$ is assumed to be approximately the same over the full interval of time [12].

The Koopman operator is a linear operator U that acts on vector-valued functions $g : \mathbf{M} \to \Re$, mapping g into a new function given by

$$U g(\mathbf{x}) = g(f(\mathbf{x})). \tag{2.38}$$

Let $\varphi_j : \mathbf{M} \to \mathbb{C}$ denote eigenfunctions and $\lambda_j \in \mathbb{C}$ denote eigenvalues of the Koopman operator [2],

$$U\varphi_j(\mathbf{x}) = \lambda_j \varphi_j(\mathbf{x}), \quad j = 1, 2, \ldots, \tag{2.39}$$

and consider a vector-valued observable $g : \mathbf{M} \to \Re^n$

In addition, the existence of a continuous spectrum possess a largely open problem on how to represent the part of the dynamics in terms of structures that are local (but not associated with linearization) in time, frequency, and space but that also possess aspects of collective motion [1].

Following [14], for dynamics that have not continuous spectrum in frequency domain (practical experience suggests this situation in power system analysis [15]), and if each of the n components of g lies within the span of the eigenfunctions φ_j, then the observables may be expressed exactly by expanding the vector-valued g in terms of those eigenfunctions as

$$g(\mathbf{x}) = \sum_{j=1}^{\infty} \varphi_j(\mathbf{x})\, \mathbf{v}_j . \tag{2.40}$$

The eigenfunctions φ_j are referred to as the Koopman eigenfunctions (KFs) and the corresponding vectors $\mathbf{v}_j \in \mathbb{C}^n$ are called the Koopman modes (KMs) of f, corresponding to g.

Iterates of $\mathbf{x}_0$ are then given by

$$g(\mathbf{x}_k) = \sum_{j=1}^{\infty} U^k \varphi_j(\mathbf{x}_0)\, \mathbf{v}_j = \sum_{j=1}^{\infty} \lambda_j{}^k \varphi_j(\mathbf{x}_0)\, \mathbf{v}_j \,. \tag{2.41}$$

The Koopman eigenvalues (KVs) λ_j characterize the temporal behavior of the corresponding Koopman mode $\mathbf{v}_j$: the phase of λ_j determines its frequency, and its magnitude determines the growth rate. For a system evolving on an attractor, the Koopman values always lies on the unit circle [2].

These modes have the property that they represent the dynamics of the system, in which a spatial shape is multiplied by a time-dependent function of the form $\exp(\lambda_j k \Delta t)$ for complex $\lambda_j = \sigma_j + i\omega_j$ (time dependence can be more complicated in the case of degenerate eigenvalues). The real part σ_j is the damping coefficient and ω_j the angular frequency. Therefore, each Koopman mode has by construction just one frequency.

The resulting modes are not necessarily orthogonal. They are also a natural extension of the concept of linear eigenmodes as collective motions occurring at the same frequency, growth, or decay rate [1].

2.4.1 Linear dynamical systems

Suppose $\mathrm{M} \subset \Re^n$ is an n–dimensional linear space, and suppose the map $f : \mathrm{M} \to \Re^n$ is a linear scheme determined by $f(\mathbf{x}) = \mathbf{A} \cdot \mathbf{x}$. It turns out that the eigenvalues of $\mathbf{A}$ are also eigenvalues of U, and its eigenvectors are related to the eigenfunctions of U as well. Let $\mathbf{v}_j \in \mathbb{C}^n$ and $\lambda_j \in \mathbb{C}$ denote the eigenvectors and eigenvalues of $\mathbf{A}$, $\mathbf{A}\mathbf{v}_j = \lambda \mathbf{v}_j$, and let $\mathbf{v}_j \in \mathbb{C}^n$ be corresponding functions of the adjoint $\mathbf{A}$ (i.e., $\mathbf{A}\ \mathbf{v}_j = \bar{\lambda}\mathbf{v}_j$), normalized so that $\langle \mathbf{v}_j, \mathbf{v}_k \rangle = \delta_{jk}$.

Next, define the real-scalar-valued function

$$\varphi_j(\mathbf{x}) = \langle \mathbf{x}, \mathbf{v}_j \rangle, \quad j = 1, \ldots, n \,. \tag{2.42}$$

Then, the φ_j are eigenfunctions of U since

$$U\varphi_j(\mathbf{x}) = \varphi_j(\mathbf{A}\mathbf{x}) = \langle \mathbf{A}\mathbf{x}, \mathbf{v}_j \rangle = \langle \mathbf{x}, \mathbf{A}^*\mathbf{v}_j \rangle = \lambda_j \langle \mathbf{x}, \mathbf{v}_j \rangle = \lambda_j \varphi_j(\mathbf{x}). \tag{2.43}$$

Unlike $\mathbf{A}$, the operator U has a countable infinite number of eigenvalues since λ_j^k is also an eigenvalue with eigenfunction $\varphi_j(\mathbf{x})^k$ for any integer k. Now, for any $\mathbf{x} \in \mathbf{M}$, as long as $\mathbf{A}$ has a full set of eigenvectors, it may be written

$$\mathbf{x} = \sum_{j=1}^{n} \langle \mathbf{x}, \mathbf{v}_j \rangle \mathbf{v}_j = \sum_{j=1}^{n} \varphi_j(\mathbf{x}) \mathbf{v}_j. \tag{2.44}$$

Thus, for linear systems the Koopman modes coincide with the eigenvectors of $\mathbf{A}$ [2]. Moreover, any nonlinear analytic observable can be expanded in the same way as is established in the following subsection.

2.4.2 Nonlinear dynamical systems

Koopman mode analysis is based on the fact discovered in [14], that normal modes of linear oscillations have their natural analogs, the Koopman modes, in the context of nonlinear dynamics; consequently, the Koopman modes are more effective at decoupling and isolating dynamics [2]. To pursue this analogy the state-space representation of the system must be changed into the dynamics governed by the linear Koopman operator on an infinite-dimensional space of observables.

Additionally, as stated in [1], despite the dynamics itself being linear, the eigenfunctions of the Koopman operator are not necessarily linear. These functions span the space of real-analytic functions on $\Re$, and thus nonlinear observables evolving under linear dynamics can be represented by a spectral expansion using the Koopman modes. Moreover, any nonlinear analytic observable can be expanded according to properties 2.2 and 2.3 where products of eigenfunctions are used in the expansion. Indeed, all linear combinations of the frequencies excite higher modes [2].

In the case of a nonlinear setting that form a periodic solution of (2.37), the Koopman modes as defined above are vectors given by the discrete Fourier transform (DFT) and the phases of corresponding eigenvalues are frequencies of the form $2\pi j/m$ [2].

In fact, above statement applies more generally to non-periodic systems when dynamics are restricted to any attractor and the Koopman modes may be calculated by harmonic averages [14], [16] [17].

Conséquently, the Koopman mode analysis is a method capable to extract the intrinsic dynamics of a (non)linear system by means of the spectral analysis of the Koopman operator. In order to point out the main advantages and disadvantages of Koopman mode analysis, in the following section is made a comparison against other methods commonly used.

2.5 Comparison with other methods

In this section a brief comparison between Koopman mode analysis and three decomposition methods commonly used, namely discrete Fourier transform (DFT), proper orthogonal decomposition (POD), and Prony analysis is presented.

2.5.1 Discrete Fourier transform

The discrete Fourier transform (DFT) of a data vector $x(n)$ is defined as the evaluation of its Fourier transform $X(\omega)$ in a set of N discrete frequencies equally separated and can be determined by means of [18]

$$X(k)=\sum_{n=0}^{N-1}x(n)\exp\left(-j2\pi kn/N\right),\quad k=0,1,2,\ldots,N-1. \tag{2.45}$$

A key limitation of the DFT is that its frequencies depends only on the number of data points and not on the data content. In consequence, to ensure that a particular frequency is properly captured, the data must cover an integer number of corresponding periods. If multiple frequencies are of interest, then

this constraint may be prohibitive, especially if the frequencies are unknown or are not related by a simple rational number.

In addition, as the longest period the DFT can capture is the time span of the data, the algorithms for computation of Koopman modes have no theoretical lower bound on the frequencies that can capture, although they are still subjected to the Nyquist frequency constraint.

Moreover, the DFT is incapable of determine modal growth rates, and many modes are needed to be retained to reproduce the non-periodic data correctly, as shown in [17].

2.5.2 *Proper orthogonal decomposition*

A common technique for identifying coherent structures is the proper orthogonal decomposition (POD) method, introduced in fluid dynamics in [19]. This method, as originally developed, is capable of extracting information from snapshots of the dynamic field by decomposing it into a sum of spatially orthogonal modes, and is thus applicable to experimental data.

POD method determines the most energetic structures by diagonalizing the spatial correlation matrix computed from the snapshots. The resulting decomposition is closest to the original field in the least-squares sense [14]. Two major drawbacks that are tacitly acknowledged by employing this method are associated with this technique: (i) the energy may not in all circumstances be the correct measure to rank the flow structures and (ii) due to the choice of second-order statistics as a basis for the decomposition, valuable phase information is lost [12]. POD models can work well, nonetheless they often require careful tuning and there is always the awareness that low-energy modes can be critically important to the dynamics [3].

Although some variants of POD have been studied to overcome these situations, this family of methods are applicable only to linear systems and furthermore, they do not have the physical meaning inherent to Koopman modes.

They are fundamentally decoupled from any sense of time or dynamics, and therefore may not provide the best mode basis for constructing dynamical models [17]. Whereas POD concentrates on a representation based on spatial orthogonality, Koopman mode analysis focuses on a representation based on temporal orthogonality (frequencies) [12].

2.5.3 Prony analysis

Prony analysis is a widely used algorithm in oscillation mode parameter identification, whose principle is to fit a linear combination of exponential terms to the analytical signal. In principle, Prony analysis methods assume the system to be single output, and individual signals are analyzed independently often resulting in conflicting frequency and damping estimates [20].

It is considered a general continuous signal $y(t)$ that is modeled by:

$$\hat{y}(t) = \sum_{m=1}^{p} B_m e^{\lambda_m t} \tag{2.46}$$

where $B_m \in \mathbb{C}$ is the output residue for the continuous-time pole $\lambda_m \in \mathbb{C}$, $\lambda_m \neq \lambda_n$ for $m \neq n$. These parameters are obtained by fitting, in a least squares sense, $\hat{y}(t)$ to the system output $y(t)$. The signal fit given by (2.46), in conjunction with the system input signal, allow for the identification of a low order linear system [21].

There also exists extensions to Prony analysis that allow multiple signals to be analyzed simultaneously resulting in one set of mode estimates [20]. Nevertheless, this is computational demanding.

Although this method have been widely studied and developed, it is linear, and when the signal is non-stationary it can provide spurious modes. Furthermore, for a few quantity of snapshots it may obtain erroneous results, whereas with a large amount of data the time of convergence is considerably increased. In some sense, Prony analysis is an extension of DFT [20][20]-[22].

2.6 Concluding remarks

In this chapter the theoretical background and main properties and aspects of the Koopman operator have been stated. The Koopman operator theory provides a rigorous framework that unifies a number of different concepts including linear stability analysis, triple decomposition, and Koopman mode decomposition; as well as linear stability theory and the discrete Fourier transform [1], [3].

Unlike many decomposition techniques, the data needed to compute Koopman mode decomposition does not need to be neither periodic nor from a linear process to construct a meaningful modal decomposition [17]. Koopman mode analysis is not based on the linearization of the system; instead, it projects the dynamics onto an infinite-dimensional space that is predetermined by the spectral properties of the Koopman operator. Aside, the spectrum of the Koopman operator is constructed by the intrinsic linear modes of the dynamics, and their interactions, defining in this way an infinite-dimensional space.

Nonetheless, all the theoretical background presented in this chapter is not useful if there exists no way for computing Koopman mode analysis. This is treated in the following chapter.

2.7 References

[1] I. Mezić, "Analysis of fluid flows via spectral properties of Koopman operator", Annu. Rev. Fluid Mech., vol. 45, pp. 357-378, 2013.

[2] C.W. Rowley, I. Mezic, S. Bagheri, P. Schlatter, & D. S. Henningson, "Spectral analysis of nonlinear flows", J. Fluid Mechanics, vol. 641, Cambridge University Press 2009, pp. 115–127

[3] C. W. Rowley, I. Mezić, S. Bagheri, P. Schlatter, and D. S. Henningson, "Reduced-order models for flow control: balanced models and Koopman modes," in Seventh IUTAM Symposium on Laminar-Turbulent Transition, IUTAM Bookseries Volume 18, 2010, pp 43-50.

[4] M. Budi sic, R. Mohr, and I. Mezic, "Applied Koopmanism," Chaos, vol. 22, no. 4, 2012.

[5] S. Banach, Theory of Linear Operations, Netherlands, vol. 38 of North-Holland Mathematical Library, Elsevier, 1987.

[6] M.H. Stone, "Linear transformations in linear spaces I. Geometrical aspects," Proc. Nat. Acad. Sci. USA, vol. 15, no. 3, pp. 198-200, Mar 1929.

[7] M. H. Stone, "Linear transformations in linear spaces III. Operational Methods and Group Theory," Proc. Nat. Acad. Sci. USA, vol. 16, no. 2, pp. 172-175, Feb 1930.

[8] N. I. Akhiezer and I. M. Glazman, Theory of Linear Operators in Hilbert Space, NY, USA, Dover Publications, 1993.

[9] B.O. Koopman, "Hamiltonian systems and transformations in Hilbert space", Proc. Nat. Acad. Sci. USA, vol. 17, no. 5, pp. 315-318, May 1931.

[10] K. Yosida, Functional Analysis, NY, USA, Springer-Verlag, 1980.

[11] W. Rudin, Functional Analysis, NJ, USA, McGraw-Hill, 1991.

[12] P. J. Schmid, "Dynamic mode decomposition of numerical and experimental data," J. Fluid Mechanics, vol. 656, Cambridge University Press 2010, pp. 5–28.

[13] J. J. Sanchez-Gasca, V. Vittal, M. J. Gibbard, A. R. Messina, D. J. Vowles, S. Liu, and U. D. Annakkage, "Inclusion of higher order terms for small-signal (modal) analysis: committee report – task force on assessing the need to include higher order terms for small-signal (modal) analysis", *IEEE Trans. Power Syst.*, vol. 20, no. 4, pp. 1886-1904, Nov. 2005.

[14] I. Mezić, "Spectral properties of dynamical systems, model reduction and decompositions," Nonlinear Dyn., vol. 41, pp. 309–325, Aug. 2005

[15] Y. Susuki and I. Mezić, "Nonlinear Koopman modes and coherency identification of coupled swing dynamics," IEEE Trans. Power Syst., vol. 26, no. 4, pp. 1894-1904, Nov 2011.

[16] I. Mezić and A. Banaszuk, "Comparison of systems with complex behavior," Physica D, vol. 197, pp. 101–133, Oct. 2004

[17] K. K. Chen, J.H. Tu, C. W. Rowley, "Variants of Dynamic Mode Decomposition: Boundary Condition, Koopman, and Fourier Analyses", J. of Nonlinear Science, vol. 22, no. 6, pp. 887–915, Dec. 2012.

[18] J. G. Proakis and D. K. Manolakis, Digital Signal Processing, USA, Pearson Prentice-Hall, 2006.

[19] P. Holmes, J. L. Lumley, and G. Berkooz, Turbulence, Coherent Structures, Dynamical Structures and Symmetry, Cambridge, UK, Cambridge Univ. Press, 1998.

[20] D. J. Trudnowski, J. M. Johnson, and J. F. Hauer, "Making Prony analysis more accurate using multiple signals", IEEE Trans. Power Syst., vol. 14, no. 1, pp. 226–231, Feb. 1999.

[21] J. J. Sanchez-Gasca and J. Chow, "Performance comparison of three identification methods for the analysis of electromechanical oscillations", IEEE Trans. Power Syst., vol. 14, no. 3, pp. 995–1002, Aug. 1999.

[22] R.W. Wies, A. Balasubramanian, and J. W. Pierre, "Combining least mean adaptive filter and auto-regressive block processing techniques for estimating the low-frequency electromechanical modes in power systems," in Proc. IEEE Power Engineering Society General Meeting, Montreal, Que., Canada, Jul. 2006.

Chapter3

Optimized Dynamic Mode Decomposition Methods

In this chapter, a critical evaluation of dynamic mode decomposition methods is provided. Variants of the Koopman operator based on Arnoldi algorithms are developed and tested on synthetic and simulated data.

First, a review of the existing Koopman analysis methods is presented. Variants of Koopman analysis based on the notion of a dynamic mode decomposition are presented and connections with the Koopman operator are given. Advantages and limitations of the dynamic mode decomposition algorithms are pointed out.

The chapter concludes with a discussion of the observability issues in the developed modal decompositions.

Example simulations of synthetic and simulated data are presented to demonstrate the usefulness of the developed algorithms.

3.1 Generalized Laplace analysis

The Generalized Laplace Analysis (GLA) theorem gives an iterative procedure to compute projections onto an eigenspace [1]. The theory behind generalized Laplace analysis is briefly described here in the context of the Koopman mode decomposition.

Theorem 3.1 (Generalized Laplace analysis). Let $\{\lambda_1, \ldots, \lambda_k\}$, $\lambda_j \in \mathbb{C}$ be a (finite) set of simple eigenvalues of U^t such that $|\exp(\lambda_1 t)| \geq |\exp(\lambda_2 t)| \geq \cdots \geq |\exp(\lambda_N t)|$, and let $\varphi_j \in \mathbb{C}$ and $\mathbf{v}_j \in \mathbb{C}^n$ be an eigenfunction and a Koopman mode, respectively, corresponding to λ_j. Define now the vector-valued observable at time t, as $g(S^t(\mathbf{x})) \in \Re^n$, which is function of the vector of (state) variables $\mathbf{x} \in \Re^n$ [1].

Then, the Koopman mode associated with λ_k can be obtained via

$$\phi_k(\mathbf{x})\mathbf{v}_k(\mathbf{x}) = \lim_{T\to\infty} \frac{1}{T}\int_0^T \exp(-\lambda_k t)\left[g(S^t(\mathbf{x})) - \sum_{j=1}^{k-1} \exp(\lambda_j t)\phi_j(\mathbf{x})\mathbf{v}_j(\mathbf{x})\right] dt . \quad (3.1)$$

Analogously, for discrete time holds that

$$\phi_k(\mathbf{x})\mathbf{v}_k(\mathbf{x}) = \lim_{K\to\infty} \frac{1}{K}\sum_{k=0}^{K-1} \exp(-\lambda_k t)\left[g(S^t(\mathbf{x})) - \sum_{j=1}^{k-1} \exp(\lambda_j t)\phi_j(\mathbf{x})\mathbf{v}_j(\mathbf{x})\right], \quad (3.2)$$

where T (K) is the sampling interval in the real (discrete) time-domain.

It is noted that for Theorem 3.1, a set of eigenvalues is needed but they are not computed as part of the theorem. The generalized Laplace analysis starts by identifying or estimating the largest Koopman eigenvalue associated with the evolution of the observable and removing its contribution.

The caveat here is that different observables in principle will present different spectra, so the whole Koopman spectrum and its modes might not be revealed. Moreover, this can lead to an unstable computation as for large t in-

volves multiplication of a very large number with a very small number. An alternative to estimating the Koopman modes is provided by the Arnoldi-type methods described below, which reveal a richer spectrum [1], [2].

3.2 Dynamic mode decomposition

In practice, it is not possible to have an explicit representation of the Koopman operator U. Its behavior can only be ascertained by its action on an observable g and commonly only at a finite number of initial conditions [1].

Dynamic mode decomposition (DMD) is based on a variant of the Arnoldi algorithm by utilizing companion matrices, described in [4]. It was introduced in [5] as a method able to extract dynamical information from flow fields generated by numerical simulation or measured data and to describe the underlying physical mechanisms captured.

3.2.1 Computation from snapshots

A standard method for computing estimates of the eigenvalues of a dynamical system governed by (2.37) is a Krylov method. These methods produce approximations to the eigenvalues of Koopman operator and their corresponding modes. Given a vector of initial conditions, $\mathbf{x}_0 \in \Re^n$, after $m-1$ time steps, it has been generated a collection of m vectors that span a Krylov subspace, given by $\{\mathbf{x}_0,\ f(\mathbf{x}_0),\ \ldots,\ f^{(m-1)}(\mathbf{x}_0)\}$. The approximate eigenvalues and eigenvectors are found by projecting f onto this subspace [3], [5].

Further, for any state $\mathbf{x}_j$ measured in a vector-valued observable $g(\mathbf{x}_j) \in \Re^n$, the data can be represented as a snapshot sequence $\mathbf{X} \in \Re^{n\times(m+1)}$ defined as:

$$\mathbf{X} = [\mathbf{x}_0 \quad \mathbf{x}_1 \quad \cdots \quad \mathbf{x}_m], \tag{3.3}$$

where $\mathbf{x}_j$ stands for the j th snapshot.

Let now the data vectors be stacked into a matrix $\mathbf{K} \in \Re^{n \times m}$ defined as follows:

$$\mathbf{K} = \begin{bmatrix} \mathbf{x}_0 & f(\mathbf{x}_0) & f(f(\mathbf{x}_0)) & \cdots & f^{(m-1)}(\mathbf{x}_0) \end{bmatrix} \tag{3.4}$$

$$\mathbf{K} = \begin{bmatrix} \mathbf{x}_0 & \mathbf{x}_1 & \mathbf{x}_2 & \cdots & \mathbf{x}_{m-1} \end{bmatrix}. \tag{3.5}$$

As the number of snapshots increases, it is reasonable to assume that, beyond a critical number of snapshots $(n < m)$, the vectors given by (3.5) become linearly dependent. In such a case, the vector $\mathbf{x}_m$ can be expressed as a linear combination of the previous snapshots according to:

$$\mathbf{x}_m = f(\mathbf{x}_{m-1}) = c_0 \mathbf{x}_0 + \cdots + c_{m-1} \mathbf{x}_{m-1} = \mathbf{K}\mathbf{c} \tag{3.6}$$

where $\mathbf{c} = \begin{bmatrix} c_0 & \cdots & c_{m-1} \end{bmatrix}^T$ and $c_j \in \Re$ [4]. Then, it follows that

$$\mathbf{K}_* = f(\mathbf{K}) = \mathbf{K}\mathbf{C}, \tag{3.7}$$

where $\mathbf{K}_*$ is an index-shifted data matrix defined as [6]:

$$\mathbf{K}_* = \begin{bmatrix} \mathbf{x}_1 & \mathbf{x}_2 & \cdots & \mathbf{x}_{m-1} \end{bmatrix}, \tag{3.8}$$

and $\mathbf{C} \in \Re^{m \times m}$ is a companion matrix given by

$$\mathbf{C} = \begin{bmatrix} 0 & 0 & \cdots & 0 & c_0 \\ 1 & 0 & & 0 & c_1 \\ 0 & 1 & & 0 & c_2 \\ \vdots & & & \vdots & \vdots \\ 0 & 0 & \cdots & 1 & c_{m-1} \end{bmatrix}. \tag{3.9}$$

The eigenvalues of $\mathbf{C}$ are then a subset of the eigenvalues of f. As a consequence, the decomposition into eigenmodes for the companion matrix $\mathbf{C}$ can be expressed in terms of $\tilde{\lambda} \in \mathbb{C} \quad \mathbf{a} \in \mathbb{C}^n$, as

$$\mathbf{C}\mathbf{a} = \tilde{\lambda}\mathbf{a}. \tag{3.10}$$

Then, using (3.7)

$$\mathbf{K}_{\bullet}\mathbf{a} = f(\mathbf{K})\mathbf{a} = \mathbf{KCa} = \tilde{\lambda}\mathbf{Ka}, \tag{3.11}$$

it can be shown that $\tilde{\mathbf{v}} \in \mathbb{C}^n$, defined as

$$\tilde{\mathbf{v}} = \mathbf{Ka} \tag{3.12}$$

is an eigenvector of f with eigenvalue $\tilde{\lambda}$.

More generally, if the m th vector is not a linear combination of previous snapshots, then instead of (3.6) we have a residual $\mathbf{r} \in \Re^n$:

$$\mathbf{r} = \mathbf{x}_m - \mathbf{Kc}, \tag{3.13}$$

which is minimized when $\mathbf{c}$ is chosen such that $\mathbf{r}$ is orthogonal to $span\{\mathbf{x}_0, \ldots, \mathbf{x}_{m-1}\}$. In this case, the relation (3.7) becomes $f(\mathbf{K}) = \mathbf{KC} + \mathbf{re}_{m-1}^T$, where $\mathbf{e}_{m-1} = [0 \ \ldots \ 1] \in \Re^m$

The eigenvalues of $\mathbf{C}$ are then approximations to the eigenvalues of f called empirical Ritz values; the corresponding approximate eigenvectors given by (3.12), are called the empirical Ritz vectors [5]. In physical terms, the finite-dimensional companion matrix $\mathbf{C}$ can be thought of as an approximation to the action of the Koopman operator U on the associated finite-dimensional Krylov subspace [2].

3.2.2 Algorithm for computation of Koopman modes

Algorithms for the computation of the Koopman modes are discussed below. It is assumed that the snapshots are sampled at regular times; i.e., it is not required explicit knowledge of f

To formalize the process, consider a sequence $[\mathbf{x}_0, \ldots, \mathbf{x}_m]$ where $\mathbf{x}_j \in \Re^n$ The empirical Ritz values $\tilde{\lambda}_j \in \mathbb{C}$ and empirical Ritz vectors $\tilde{\mathbf{v}}_j \in \mathbb{C}^n$ of the sequence are determined by the following algorithm:

(i). Define $\mathbf{K}$ by (3.5) and find the real constants c_j such that

$$\mathbf{r} = \mathbf{x}_m - \mathbf{K}\mathbf{c} = \mathbf{x}_m - \sum_{j=0}^{m-1} c_j \mathbf{x}_j, \quad \mathbf{r} \perp span\left\{\mathbf{x}_0, \ldots, \mathbf{x}_{m-1}\right\}. \tag{3.14}$$

(ii). Construct the companion matrix, $\mathbf{C}$ in (3.9) and find its eigenvalues and eigenvectors:

$$\mathbf{C} = \mathbf{T}^{-1}\mathbf{\Lambda}\mathbf{T}, \quad \mathbf{\Lambda} = diag\left(\lambda_1, \cdots, \lambda_m\right) \tag{3.15}$$

where the eigenvectors of $\mathbf{C}$ are columns of $\mathbf{T}^{-1}$

(iii). Define $\tilde{\mathbf{v}}_j$ to be the columns of $\mathbf{V} = \mathbf{K}\mathbf{T}^{-1}$

Consider now a set of data $[\mathbf{x}_0, \ldots, \mathbf{x}_m]$ governed by (2.37) and let $\tilde{\lambda}_j$, $\tilde{\mathbf{v}}_j$ be the empirical Ritz values and vectors of this sequence. Assuming that $\tilde{\lambda}_j \neq \tilde{\lambda}_k$ for all $j \neq k$, then it can be shown that

$$\mathbf{x}_k = \sum_{j=0}^{m-1} \tilde{\lambda}_j^k \, \tilde{\mathbf{v}}_j, \quad k = 0, \ldots, m-1, \tag{3.16}$$

and

$$\mathbf{x}_m = \sum_{j=0}^{m-1} \tilde{\lambda}_j^k \, \tilde{\mathbf{v}}_j + \mathbf{r}, \quad \mathbf{r} \perp span\left\{\mathbf{x}_0, \ldots, \mathbf{x}_{m-1}\right\}. \tag{3.17}$$

Equation (3.5) may be rewritten as

$$\mathbf{K} = \begin{bmatrix} \mathbf{x}_0 & \mathbf{x}_1 & \mathbf{x}_2 & \cdots & \mathbf{x}_{m-1} \end{bmatrix},$$

$$\mathbf{K} = \begin{bmatrix} \tilde{\mathbf{v}}_1 & \cdots & \tilde{\mathbf{v}}_m \end{bmatrix} \begin{bmatrix} 1 & \tilde{\lambda}_1 & \tilde{\lambda}_1^{\,2} & \cdots & \tilde{\lambda}_1^{\,m-1} \\ 1 & \tilde{\lambda}_2 & \tilde{\lambda}_2^{\,2} & \cdots & \tilde{\lambda}_2^{\,m-1} \\ \vdots & \vdots & \vdots & \cdot & \vdots \\ 1 & \tilde{\lambda}_m & \tilde{\lambda}_m^{\,2} & \cdots & \tilde{\lambda}_m^{\,m-1} \end{bmatrix} \tag{3.18}$$

The rightmost matrix above is a Vandermonde matrix, which actually is the matrix $\mathbf{T}$ of (3.15) that diagonalizes the companion matrix $\mathbf{C}$ as long as the eigenvalues $\{\tilde{\lambda}_1, \ldots, \tilde{\lambda}_m\}$ are distinct.

Comparison of (3.16) and (3.17) with (2.41), it follows that the empirical Ritz values $\tilde{\lambda}_j$ and vectors $\tilde{\mathbf{v}}_j$ behave in the same manner as the eigenvalues λ_j and modes $\mathbf{v}_j$ of U, but for a finite number of them, instead of an infinite sum.

On one hand, if $\mathbf{r} = \mathbf{0}$ in (3.17), the approximate modes are indistinguishable from the eigenvalues and modes of U with the expansion (2.40) consisting only of a finite number of terms. On the other hand, if $\mathbf{r} \neq \mathbf{0}$, then there is some error, but in fact, this is the same as the smallest possible error in projecting $g(\mathbf{x}_m)$ onto any modes $\tilde{\mathbf{v}}_j$ formed from linear combinations of the first m data vectors [5].

Therefore, empirical Ritz values $\tilde{\lambda}_j$ and vectors $\tilde{\mathbf{v}}_j$ are (usually) good approximations of the true Koopman eigenvalues λ_j and Koopman modes $\mathbf{v}_j$ respectively. The terms $\mathbf{v}_j$ are scaled by the constant values $\varphi_j(\mathbf{x}_0)$.

3.2.3 Stability and convergence

The well-known Arnoldi method is closely related to the decomposition above. When $f(\mathbf{x}_j) = \mathbf{A}\mathbf{x}_j$, $\mathbf{A} \in \Re^{n \times n}$ the Arnoldi method successively orthogonalizes the vectors of $\mathbf{K}$ resulting in a decomposition of the form $\mathbf{AQ} \approx \mathbf{QH}$ with $\mathbf{K} = \mathbf{QR}$ and $\mathbf{H} = \mathbf{RSR}^{-1}$ as a Hessenberg matrix. The eigenvalues of $\mathbf{H}$ approximate some of the eigenvalues of $\mathbf{A}$.

In practice, the Arnoldi method is accomplished by a sequence of projections onto successive Krylov subspaces. This yields a more stable algorithm, but for these projections the matrix $\mathbf{A}$ has to be available. In contrast, the dynamic mode decomposition algorithm has less favorable stability (and convergence) properties since it is assumed that there is no information about f [4].

Furthermore, in [6] it has been proved that the dynamical mode decomposition is unique, provided that eigenvalues are isolated and snapshots are independent. It is also observed that the mean subtraction leads to all possible eigenvalues being on the unit circle and the companion matrix analysis reducing to the discrete Fourier transform matrix. However, the problem with subtracting the mean of the sequence of snapshots is in fact related to the observation that the companion matrix $\mathbf{C}$ is an approximation to the Koopman operator representation on a finite-dimensional set of functions.

In general, the computation of the Koopman modes by the dynamic mode decomposition method needs to be done without subtracting the mean if decaying or growing modes are to be captured [2].

Additionally, the above algorithm is tied to the initial conditions. This dependence rises since the empirical Ritz values and vectors are found using a Krylov subspace generated by a sequence of vector-valued observations along a finite trajectory with a vector of initial conditions $\mathbf{x}_0 \in \mathrm{M}$. Since f can be decomposed into eigenspaces that are invariant subspaces, and recalling (2.11), it follows that $f(\mathbf{x}_j)$ can be expressed as:

$$\mathbf{x}_{j+1} = f(\mathbf{x}_j) = \lambda_1 P_1 \mathbf{x}_j + \lambda_2 P_2 \mathbf{x}_j + \cdots \tag{3.19}$$

where P_j is a projection operator $P_j : \mathrm{M} \to \mathrm{M}_j$ being M_j the eigenmanifold corresponding to the eigenvalue λ_j.

Then, if $\mathbf{x}_0 \notin \mathrm{M}_j$, its projection into M_j is $P_j \mathbf{x}_0 = \mathbf{0}$; i.e., the spectral dynamics inherent to f are not present in the observables and consequently that part of the spectrum is not revealed. Thus, different initial conditions can reveal different parts of the spectrum [1].

Numerically there is another concern with the convergence of the method: experiments show that its results are more sensitive to variations in $\mathbf{x}_m$ than to variations in other data vectors. This is because the Ritz values are the

eigenvalues of the companion matrix $\mathbf{C}$; which dictates this reconstruction. The presence of noise in $\mathbf{x}_n$ could drastically change the contents, and hence the eigenvalues, of the companion matrix [6].

Moreover, even though the above decomposition is mathematically correct, a practical implementation yields an ill-conditioned algorithm that is often not capable of extracting more than the first or first two dominant dynamic modes [4]. To address these problems, two more techniques are presented for Koopman mode analysis computation.

3.3 SVD-based dynamic mode decomposition

In order to avoid the practical problems exposed in the last paragraph of the previous section, it has been proposed in [4] a more robust implementation that results in a reduced matrix $\tilde{\mathbf{C}} \in \Re^{n' \times n'}$ related to $\mathbf{C}$ via a similarity transformation.

3.3.1 SVD projection

Robustness is achieved by a preprocessing step using a singular value decomposition (SVD) of the data sequence $\mathbf{K} = \mathbf{U}\boldsymbol{\Sigma}\mathbf{W}^H$ where $\mathbf{U} \in \Re^{n \times n'}$ $\boldsymbol{\Sigma} \in \Re^{n' \times n'}$ is a diagonal matrix and $\mathbf{W} \in \Re^{m \times n'}$ Substituting the SVD of $\mathbf{K}$ into (3.7), and rearranging the resulting expression we obtain

$$\tilde{\mathbf{C}} = \mathbf{U}^H \mathbf{K}_{\cdot} \mathbf{W}\boldsymbol{\Sigma}^{-1} = \boldsymbol{\Sigma}\mathbf{W}^H \mathbf{C}\mathbf{W}\boldsymbol{\Sigma}^{-1}. \tag{3.20}$$

In the particular case that $f(\mathbf{x}_j) = \mathbf{A}\mathbf{x}_j$ the previous expression can be also expressed as

$$\tilde{\mathbf{C}} = \mathbf{U}^H \mathbf{A}\mathbf{U}. \tag{3.21}$$

The above operation amounts to a projection of the companion matrix $\mathbf{C}$, the linear operator $\mathbf{A}$ for (3.21), over (onto for $\mathbf{A}$) a basis from the singular value decomposition. A further advantage is the opportunity to account for a rank-

deficiency in the data sequence $\mathbf{K}$ via a restriction to a limited projection basis given by the non-zero singular values of $\mathbf{\Sigma}$ (or by singular values above a prescribed threshold) [4], [6].

Then the modes can be obtained from the matrix $\tilde{\mathbf{C}}$ by solving the diagonalization problem

$$\tilde{\mathbf{C}} = \mathbf{Y}\mathbf{\Lambda}\mathbf{Y}^{-1} \tag{3. 22}$$

where the eigenvectors of $\tilde{\mathbf{C}}$ are columns of $\mathbf{Y}$; $\mathbf{\Lambda}$ is as in (3.15). The modal structures can be obtained as presented below [4], [6].

3.3.2 Algorithm for computation

Consider a sequence $[\mathbf{x}_0,\ldots,\mathbf{x}_m]$ of snapshots sampled at regular times, where $\mathbf{x}_j \in \Re^n$ Then the Koopman operator behavior approach based on the singular value decomposition can be implemented by the following algorithm:

(i). Define $\mathbf{K}$ by (3.5), find the real constants c_j as in (3.14) and define the companion matrix $\mathbf{C}$ by (3.9).

(ii).Define the projected companion matrix $\tilde{\mathbf{C}}$ by (3.20) and find its eigenvalues and eigenvectors in accordance to (3.22)

(iii). Project the eigendecomposition of $\tilde{\mathbf{C}}$ into the basis of $\mathbf{C}$ and define the matrices $\mathbf{\Phi}$ and $\mathbf{V}$ to represent the samples matrix $\mathbf{K}$ as

$$\mathbf{K} = \mathbf{\Phi}\mathbf{V} \tag{3. 23}$$

that is equivalent to (2.41) but for all the ensemble of data and considering $g(\mathbf{x}_k) = \mathbf{x}_k$. Similarly, the index-shifted data matrix can be expressed as

$$\mathbf{K}_* = \mathbf{\Phi}\mathbf{\Lambda}\mathbf{V} \tag{3. 24}$$

The definition of the matrices $\mathbf{\Phi}$ and $\mathbf{V}$ can be determined by substituting (3.22) into (3.20) and rearranging:

$$\mathbf{K}_{\cdot} = \mathbf{U}\mathbf{Y}\mathbf{\Lambda}\mathbf{Y}^{-1}\mathbf{\Sigma}\mathbf{W}^{H} \tag{3.25}$$

Then by comparing with (3.24), we can define the matrices $\mathbf{\Phi}$ and $\mathbf{V}$ as follows

$$\mathbf{\Phi} = \mathbf{U}\mathbf{Y}, \tag{3.26}$$

$$\mathbf{V} = \mathbf{Y}^{-1}\mathbf{\Sigma}\mathbf{W}^{H} \tag{3.27}$$

The previous formulation, albeit is mathematically correct and computationally stable, indeed is similar to the proper orthogonal decomposition exposed in the preceding chapter.

This affirmation rises from the fact that the product $\mathbf{Y}^{-1}\mathbf{\Sigma}\mathbf{W}^{H}$ depends on the singular values contained in $\mathbf{\Sigma}$ that are related to the energy, and is not conformed by functions of a single frequency as has been shown in Section 2.4.

Another variant following [6] keeps the matrices $\mathbf{\Lambda}$ and $\mathbf{\Phi}$ defined as above, and assuming that the $\tilde{\lambda}_j$ are approximated to the Koopman eigenvalues, $\mathbf{V}$ must be estimated in such a way to satisfy (3.24).

The dynamic mode decomposition based on the calculation of the singular values may provide good approximations to the Koopman eigenvalues λ_j, but the approximated Koopman modes can be quite inaccurate. This method is useful mainly to obtain a first approximation of the true Koopman values for the method described below, though it is not applicable to all classes of data sequences.

3.4 Optimized dynamic mode decomposition

Inspired by the work in [6], an optimized version of the dynamic mode decomposition is now proposed, in which instead of a residual error at the last snap-

shot, it is allowed for errors at all snapshots but optimizing the eigenvalues to fit the data.

As in principle, the observables are fitted accurately with m empirical Ritz eigenmodes, this optimized approach regards p modes with $p < m$, where p can be predefined or optimized in base of an accuracy criterion.

3.4.1 Optimized DMD formulation

Suppose that $\{\mathbf{x}_k\}_{k=0}^{m-1}$ is a set of vector-valued observables. Given $p < m$, the target is to find a set of complex scalars $\{\tilde{\lambda}_j\}_{j=1}^{p}$ and complex vectors $\{\tilde{\mathbf{v}}_j\}_{j=1}^{p}$ such that

$$\mathbf{x}_k = \sum_{j=1}^{p} \tilde{\lambda}_j^k \tilde{\mathbf{v}}_j + \mathbf{r}_k, \quad k = 0,\ldots,m-1 \tag{3.28}$$

whereas $\Gamma \in \Re$,

$$\Gamma \equiv \sum_{k=0}^{m-1} \| \mathbf{r}_k \|_2^2 \tag{3.29}$$

is minimized.

Then, let $\mathbf{K}$ be as above, where $\mathbf{V}$ and $\mathbf{T}$ are redefined by:

$$\mathbf{V} = \begin{bmatrix} \tilde{\mathbf{v}}_1 & \cdots & \tilde{\mathbf{v}}_p \end{bmatrix}, \tag{3.30}$$

$$\mathbf{T} = \begin{bmatrix} 1 & \tilde{\lambda}_1 & \tilde{\lambda}_1^2 & \cdots & \tilde{\lambda}_1^{m-1} \\ 1 & \tilde{\lambda}_2 & \tilde{\lambda}_2^2 & \cdots & \tilde{\lambda}_2^{m-1} \\ \vdots & \vdots & \vdots & & \vdots \\ 1 & \tilde{\lambda}_p & \tilde{\lambda}_p^2 & \cdots & \tilde{\lambda}_p^{m-1} \end{bmatrix} \tag{3.31}$$

Now the residue matrix $\mathbf{R} \in \Re^{n \times m}$ is constructed as follows

$$\mathbf{R} = \begin{bmatrix} \mathbf{r}_1 & \cdots & \mathbf{r}_m \end{bmatrix}, \tag{3.32}$$

Furthermore, instead of (3.18) it can be written

$$\mathbf{K} = \mathbf{VT} + \mathbf{R}. \tag{3.33}$$

The matrix $\mathbf{V}$ and the Vandermonde matrix $\mathbf{T}$ are sought in order to minimize the squared Frobenius norm $\Gamma = \|\mathbf{R}\|_F^2$, which is indeed a least-squares problem for $\mathbf{V}$ The choice of $\mathbf{V}$ with the smallest Frobenius norm is

$$\mathbf{V} = \mathbf{K}\mathbf{T}^{+} \tag{3.34}$$

where $\mathbf{T}^{+}$ is the Monroe-Penrose pseudo-inverse matrix of $\mathbf{T}$ if $\lambda_j \neq \lambda_k$ for $j \neq k$.

3.4.2 Computation of optimized DMD

At this point there is no analytic algorithm for computing the optimized dynamic mode decomposition. In [6], two optimization methods are proposed to compute a global mode decomposition:

a). A global optimization technique that combines simulated annealing and the Nelder-Mead simplex method, and

b). The Broyden-Fletcher-Goldfarb-Shanno quasi-Newton iterator for purely local minimization,. taking the results of the SVD-based dynamical mode decomposition as initial conditions.

In this research work, a highly flexible approach to estimating the optimized dynamic mode decomposition is developed using a genetic algorithm. Results are compared with the algorithms above.

3.5 Illustrative examples

In this section, the three above algorithms for computation of Koopman modes (DMD, SVD-based DMD, and optimized DMD) are examined in terms of their ability to extract and characterize electromechanical behavior.

3.5.1 Application to synthetic signals

As a first example, the method is applied to a set of sinusoidal signals. Let $\mathbf{X}=[\mathbf{u}_1(t)\cdots\mathbf{u}_m(t)]^T$ be a $n\times m$ matrix of data as in (3.3) where $n=9$ and m is the number of snapshots of the functions.

Each snapshot $u_j(t)$ is a damped sinusoidal function of the form $u_j(t)=a_j\exp(-\sigma_j t)\sin(2\pi f_j t)$, with amplitude a_j damping coefficient σ_j and frequency f_j where $f_{1,2,3}=0.3125\,\text{Hz}$, $f_{4,5,6}=0.5562\,\text{Hz}$, and $f_{7,8,9}=0.8321\,\text{Hz}$.

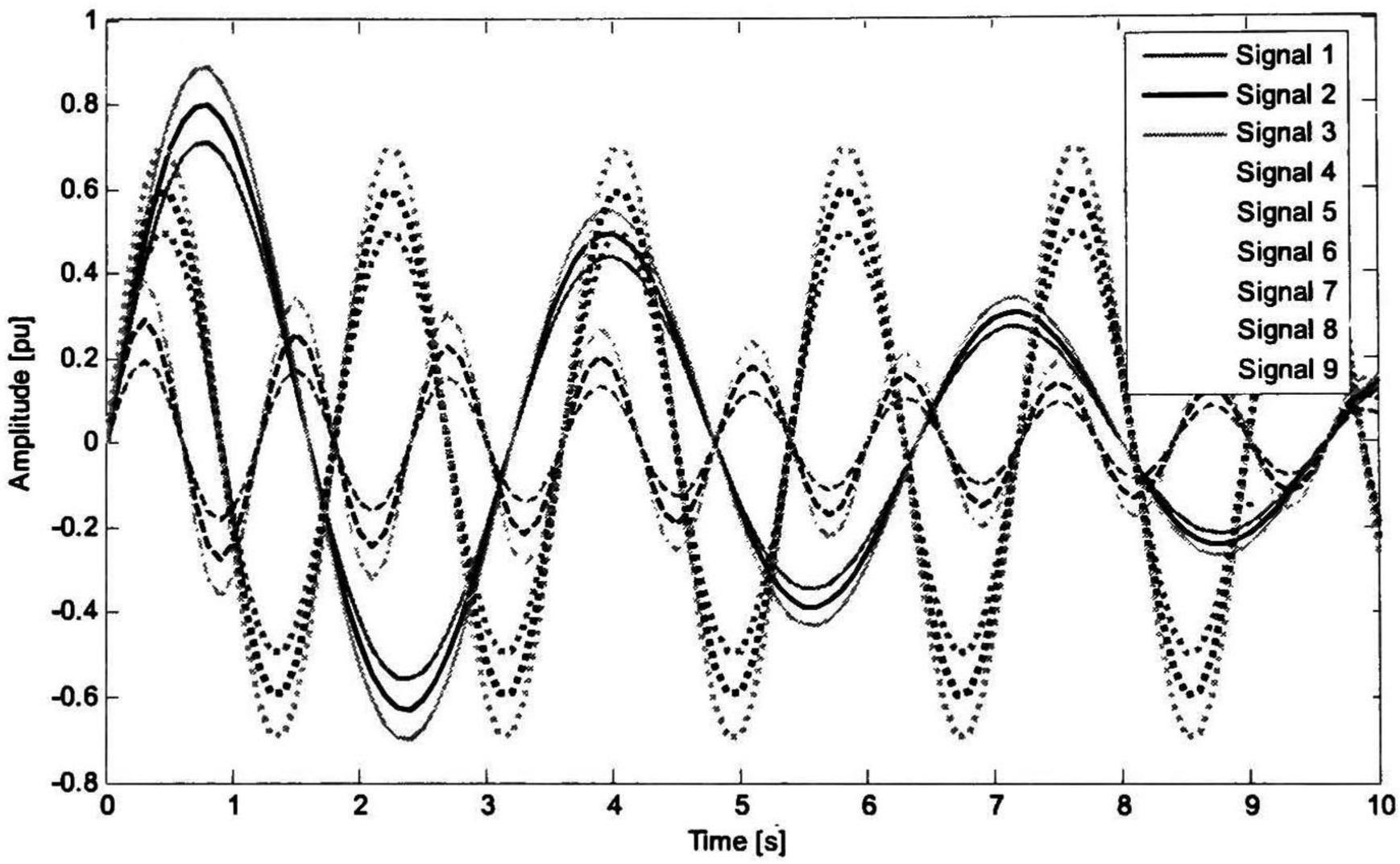

Fig. 3.1. Synthetic signals.

The associated vector of frequencies is defined as $\mathbf{f}=[f_1\ \ f_2\cdots f_n]^T$; the damping coefficients vector is $\boldsymbol{\sigma}=[\sigma_1\ \ \sigma_2\cdots\sigma_n]^T$, where $\sigma_{1,2,3}=-0.15$, $\sigma_{4,5,6}=0.00$, and $\sigma_{7,8,9}=-0.10$ Np/s, i.e., the functions have damping ratios of 7.6172 %, 0.0000 %, and 1.9123 %, respectively. The vector of time begins with $t_0=0$ s up to $t_m=10$ s with $\Delta t=0.01$ s, and the vector of amplitudes is $\mathbf{a}=[0.8\ \ 0.9\ \ 1.0\ \ 0.5\ \ 0.6\ \ 0.7\ \ 0.2\ \ 0.3\ \ 0.4]^T$

Figure 3.1 shows the time evolution of the test signals.

The data set is analyzed by the first alternative of computation which gives 100 empirical Ritz eigenmodes. Table 3.1 summarizes the first 10 modes, ordered by the absolute value of the respective Ritz values.

The entire set of Ritz eigenmodes has a maximum reconstruction error of 3.2930×10^{-14} with respect to the original data set.

Table 3.1. Dominant Ritz eigenmodes obtained by the DMD algorithm for the data set in Fig. 3.1.

Mode j	$\lvert\tilde{\lambda}_j\rvert$	Frequency [Hz]	Damping [%]	Norm $\lVert\tilde{\mathbf{v}}_j\rVert$
1	0.9883	0.8198	2.2816	**0.3218**
2	0.9821	0.5899	4.8802	**1.5981**
3	0.9797	0.3274	9.9153	**1.1534**
4	0.9787	0.7035	4.8694	**0.4484**
5	0.9757	0.9412	4.1494	**0.2027**
6	0.9751	0.2063	19.1148	**0.4957**
7	0.9721	0.1022	40.3011	**0.5353**
8	0.9714	0.0000	100.0000	**0.5500**
9	0.9702	0.4472	10.7057	**1.7605**
10	0.9694	1.0441	4.7350	**0.2717**

It can be seen from Table 3.1 that the first three modes have frequencies and damping coefficients similar to the original data. Nonetheless, the norm values on the fifth column do not correspond to the ordering, so this is not an adequate parameter to identify those modes containing more physical information.

Reconstructed signals resulting from the first few modes were compared. First, the set of signals obtained by using only the three first modes are given in Fig. 3.2. As can be observed, the amplitudes of the signals 4 through 6 have an additional frequency and another attenuation that adds error mainly at the beginning of the period of time, whereas the amplitudes of the rest of the signals are quite similar to the respective signals of Fig. 3.1.

The maximum mismatch was about 2.3746 unities of magnitude.

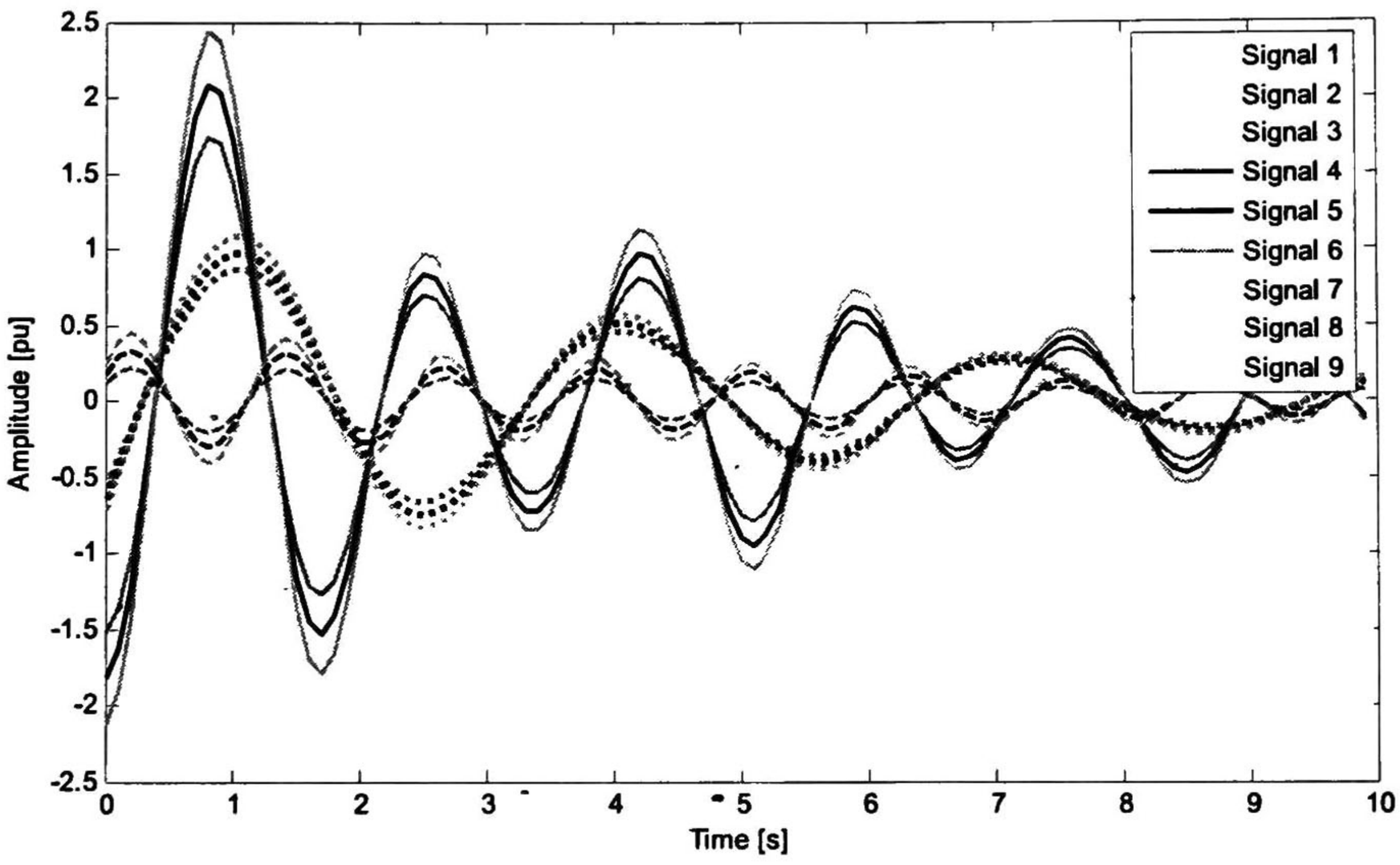

Fig. 3.2. Reconstructed signals by taking the first three modes of Table 3.1.

Moreover, it has been introduced a phase into the signals of Fig. 3.2, albeit the percentage of participation of the frequencies in the conformation of the signals is almost preserved.

On the other hand, the second technique fails to extract information about the dynamics of the signals. This can often occur with this method since it depends on the singular value decomposition. In other words, it is based on the singular values, which are related to the signals energy. This approach is more suitable for large sets of observables.

Finally, the optimized dynamic mode decomposition is used to analyze the signals in Fig. 3.1, beginning with the 5 modes of Table 3.1 and an initial error of 3.0202 unities of magnitude.

The results are summarized in Table 3.2, where the maximum error was minor to 0.02 %.

Table 3.2. Modes of the signals of Example 3.1 obtained by the DMD and optimized DMD algorithms compared with the true modes of the data.

Mode	Original data		DMD		Optimized DMD	
j	Frequency [Hz]	Damping [%]	Frequency [Hz]	Damping [%]	Frequency [Hz]	Damping [%]
1	0.3125	7.6172	0.3274	9.9153	0.3125	7.6174
2	0.5562	0.0000	0.5899	4.8802	0.5562	0.0001
3	0.8321	1.9123	0.8198	2.2816	0.8321	1.9117

3.5.2 Application to simulated data from an electric circuit

As a second example, the developed methods are applied to a simple electric circuit. The analysis focuses on the ability of the dynamic mode decomposition schemes to extract the linear modes from the simulated circuit responses to small perturbations.

Figure 3.3 shows a single line diagram of the test circuit. For the purposes of this analysis, it is assumed that $v_{C_1}(0)=1$ V with all the other initial conditions equal to zero.

The observables are the voltages at each node; the $n\times m$ observation matrix is defined as $\mathbf{X}=[\mathbf{x}_1 \quad \mathbf{x}_2 \quad \cdots \quad \mathbf{x}_m]=[\mathbf{u}_1(t)\cdots\mathbf{u}_n(t)]^T$ where each snapshot is $\mathbf{x}_k=[u_{1k}\cdots u_{1n}]^T = \left[v_{C_1}(k) \quad v_{C_2}(k) \quad v_{C_3}(k) \quad v_{L_1}(k) \quad v_{L_2}(k) \quad v_{L_3}(k)\right]^T$ The voltages are sampled using a constant sampling period $\Delta t=0.001$ s. A window width equal to 5 seconds was selected for analysis.

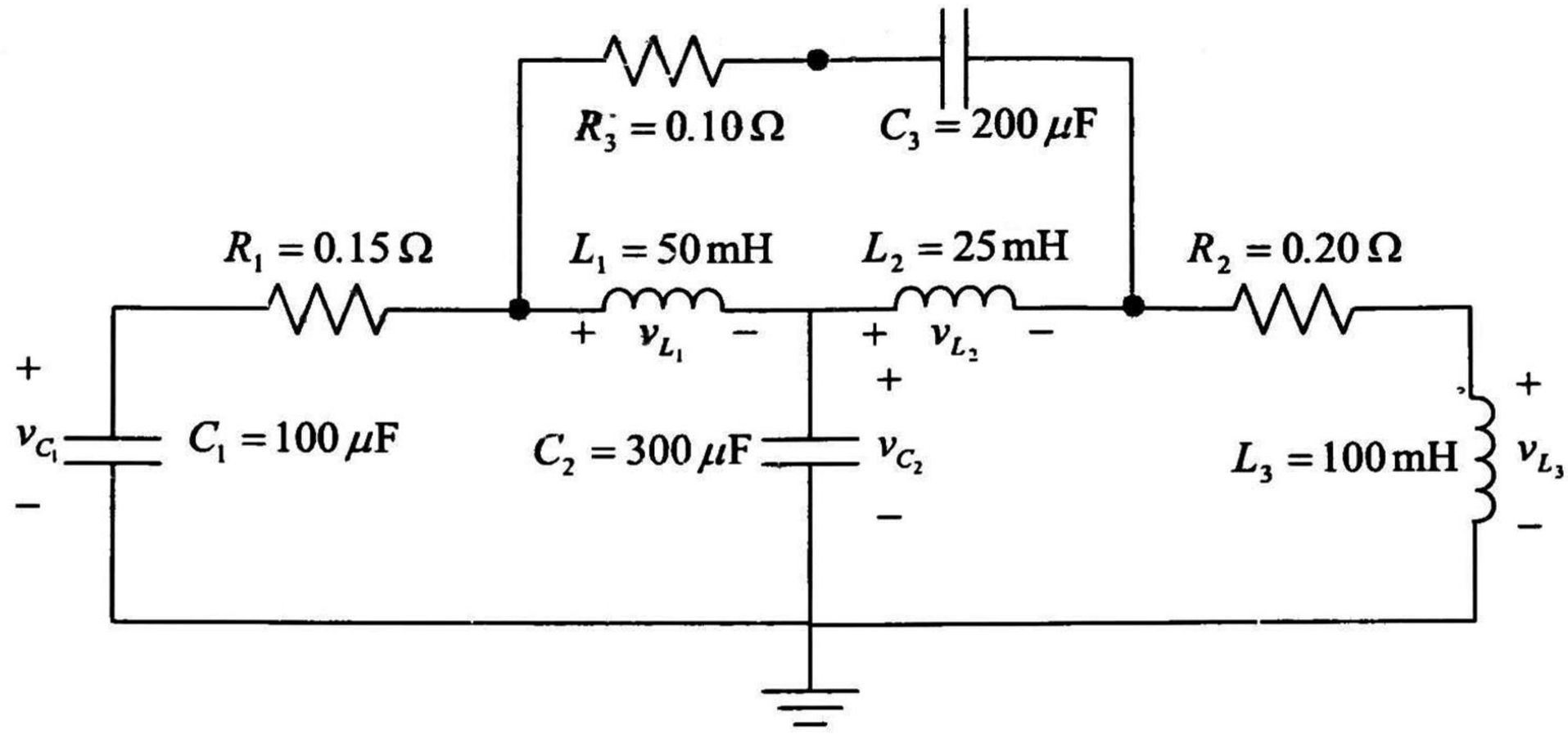

Fig. 3.3 RLC Circuit of Example 3.2 showing parameters used in the analysis.

As a first step, the linear model of the system $\dot{\mathbf{x}} = \mathbf{A}\mathbf{x}$ was obtained. Then, an eigenanalysis is performed to determine the natural frequencies and linear modes of the system, and a matrix of observations is created from model simulations.

Figure 3.4 shows selected simulations which are representative of the observed system response.

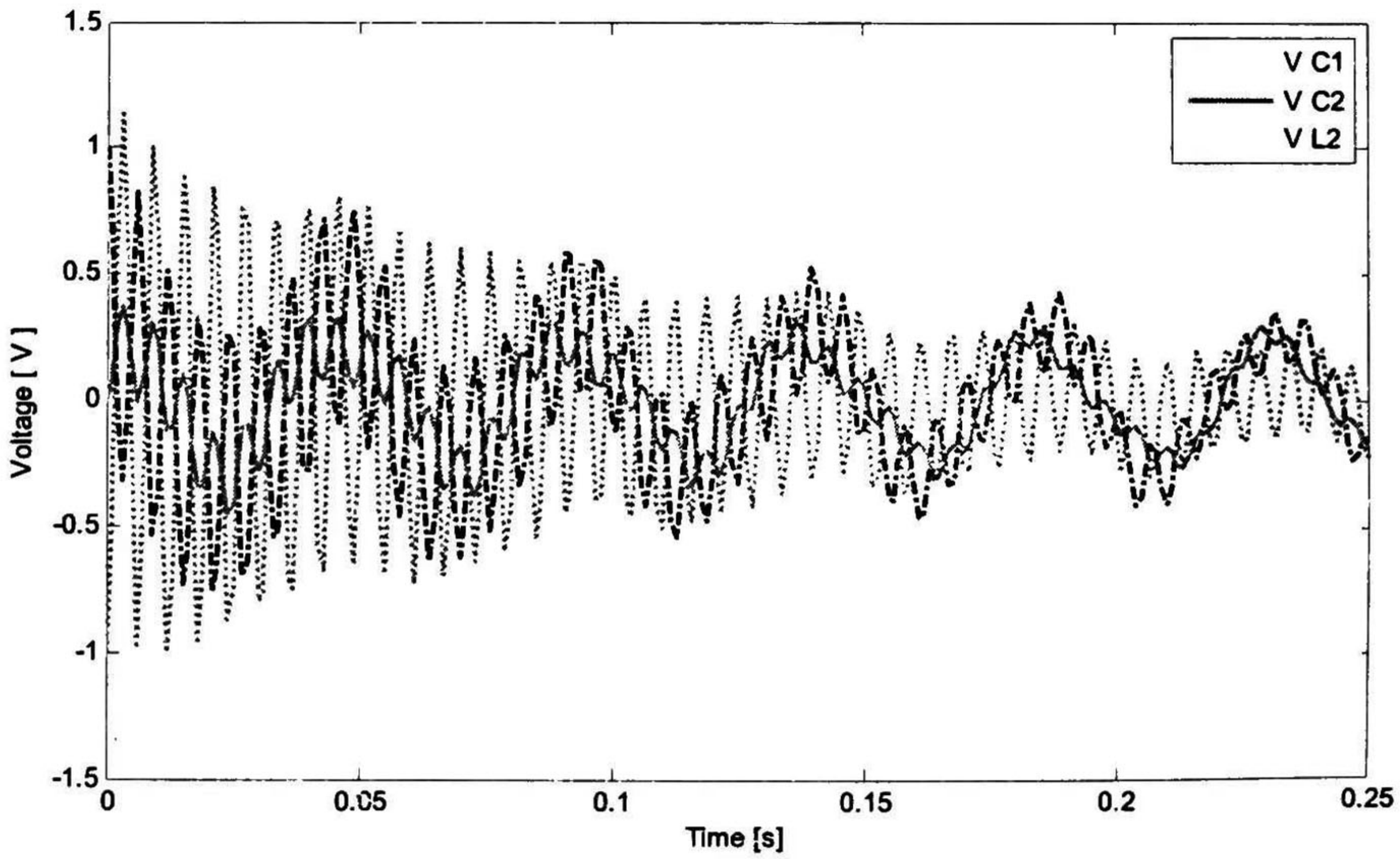

Fig. 3.4 Signals of Example 3.2 used for KMA.

The results of the three versions of the dynamical mode decompositions are shown in Table 3.3. As can be seen from this Table, the numerical errors are 4.4395×10^{-12} V (with the first four modes), 0.6603 V, and 1.9584×10^{-13} V, respectively.

As seen in Table 3.3, the SVD-based dynamical mode decomposition fails to characterize the frequency and damping of modes 2 and 3. This is consistent with our numerical results in Chapter 5.

Also of interest, the norm of the second approximate Koopman mode of the dynamical mode decomposition in Table 3.3, and the norms of the rest of the Ritz eigenmodes are almost zero, showing the appropriateness of the model.

Table 3.3. Comparison of the linear modes extracted by the DMD, SVD-based DMD, and optimized DMD algorithms.

Mode	Eigenmodes		DMD		SVD-based DMD		Optimized DMD	
j	Freq. [Hz]	Damp. [%]	Freq. [Hz]	Damp. [%]	Freq. [Hz]	Damp. [%]	Freq. [Hz]	Damp. [%]
1	164.1186	0.7331	164.1171	0.7331	161.1328	1.8237	164.1171	0.7331
2	41.5651	0.3310	46.3997	2.5806	33.3555	2.0238	41.5651	0.3310
3	21.5788	0.2402	41.5651	0.3310	7.6690	15.7060	21.5788	0.2402
4			21.5788	0.2402				

When applied to linear process, Koopman mode analysis recovers the global stability modes of the flow. When decomposing a nonlinear process, the analysis allows identification of the dominant frequencies and their associated spatial structures.

3.6 Modal observability

In this section, a strategy based on the observability of the modes is sought in order to provide a criterion to select the best entrances that provide an accurate

Koopman modes computation. The basic idea of the proposed method derives from the modal controllability and observability notions advocated in [7].

3.6.1 Background

Consider a general linear system described by the state-space model

$$\dot{\mathbf{x}}(t) = \mathbf{A}\mathbf{x}(t) + \mathbf{B}\mathbf{u}(t), \quad \mathbf{x}(0) = \mathbf{x}_0 \tag{3.35}$$

$$\mathbf{y}(t) = \breve{\mathbf{C}}\mathbf{x}(t) \tag{3.36}$$

where $\mathbf{x}(t) \in \Re^n$ are the state variables, $\mathbf{A} \in \Re^{n \times n}$ is the system matrix, $\mathbf{B} \in \Re^{n \times m}$ is the input matrix, $\mathbf{u}(t) \in \Re^m$ is the vector of system inputs, $\mathbf{x}_0$ is the vector of initial conditions, $\breve{\mathbf{C}} \in \Re^{p \times n}$ is the outputs matrix, and $\mathbf{y}(t) \in \Re^p$ is the vector of system outputs.

The solution to this system can be written as

$$\mathbf{y}(t) = H(\mathbf{x}_0) + \breve{\mathbf{C}} L(\mathbf{u}) \tag{3.37}$$

where $H(\cdot)$ and $L(\cdot)$ are linear operators defined as

$$L(\mathbf{u}) = \int e^{\mathbf{A}(t-\tau)} \mathbf{B}\mathbf{u}(\tau) d\tau \tag{3.38}$$

and

$$H(\mathbf{x}_0) = \breve{\mathbf{C}} e^{\mathbf{A}t} \mathbf{x}_0 . \tag{3.39}$$

The system described by (3.36) and (3.37) is said to be completely observable if the state variables $\mathbf{x}(t_0)$ at time t_0 can be found from the observation of $\mathbf{y}(t)$ during a finite interval of time, i.e. if H has a void null space. Therefore, the system is completely observable if all the state transitions affect eventually all the elements of the output vector [8].

This approach, however, is not satisfactory in most cases because the information it provides is qualitative in nature, it can say, at best, what parts of the

system are observable and what parts are not, but it is not capable to make quantitative statements about the different parts of the system.

Observability for the aims of this research work refers to the sensor's ability to see the internal states of the system. In what follows, method for evaluating a quantitative measure of observability of a linear dynamical system by taking into account the mode shape as well as the system outputs is suggested.

3.6.2 Quantitative measures

A quantitative measure of observability is motivated by the following expression for $\mathbf{y}(t)$ [7]:

$$\mathbf{y}(t)=\sum_{i=1}^{n}\left(\breve{\mathbf{C}}\mathbf{v}_i\left[\mathbf{w}_i^T\mathbf{x}_0+\mathbf{w}_i^T\mathbf{B}\int_0^t e^{-\lambda_i\tau}\mathbf{u}(\tau)d\tau\right]e^{\lambda_i t}\right) \tag{3.40}$$

where $\lambda_i \in \mathbb{C}$ is the ith eigenvalue, and $\mathbf{v}_i \in \mathbb{C}^n$ and $\mathbf{w}_i \in \mathbb{C}^n$ are the corresponding right and left eigenvectors.

It is clear from this equation that the extent to which the ith mode appears at the different outputs is determined by the elements of the vector $\breve{\mathbf{C}}\mathbf{v}_i$. If the matrix $\breve{\mathbf{C}}$ is written as

$$\breve{\mathbf{C}}=row\left[\mathbf{c}_1^T,\mathbf{c}_1^T\ \ldots,\mathbf{c}_p^T\right], \tag{3.41}$$

then the matrix $\breve{\mathbf{C}}\mathbf{V}$ given by

$$\breve{\mathbf{C}}\mathbf{V}=\begin{bmatrix}\mathbf{c}_1^T\mathbf{v}_1 & \mathbf{c}_1^T\mathbf{v}_2 & \cdots & \mathbf{c}_1^T\mathbf{v}_n\\ \vdots & \vdots & . & \vdots\\ \mathbf{c}_p^T\mathbf{v}_1 & \mathbf{c}_p^T\mathbf{v}_2 & \cdots & \mathbf{c}_p^T\mathbf{v}_n\end{bmatrix} \tag{3.42}$$

have a useful interpretation: the magnitude of the entry $\mathbf{c}_i^T\mathbf{v}_j$ of $\breve{\mathbf{C}}\mathbf{V}$ measures how much the jth mode appears in the ith output of $\mathbf{y}(t)$.

Based on this reasoning, the elements of **CV** are treated as measures of observability.

Additionally, in [7] it is introduced the notion of the unit momentum scaling, mainly thought to determine in a better way the controllability of the states that allows a better performance of the controllers. In our case, this is not of interest. Instead, a quantitative measure of the presence of the modes in the data sequence is useful.

The observability measure $\mathbf{c}_k^T\mathbf{v}_i$ can be interpreted as the k th output signal at $t=0^+$, subject to an initial condition $\mathbf{x}(0)=\mathbf{v}_i$. More precisely,

$$y_k(0^+)=\mathbf{c}_k^T\mathbf{v}_i(\mathbf{w}_i^T\mathbf{v}_i)$$

$$y_k(0^+)=\mathbf{c}_k^T\mathbf{v}_i. \tag{3.43}$$

Then, the vector of initial conditions $\mathbf{x}(0)$ can be expressed as a linear combination of the right eigenvectors $\mathbf{x}(0)=a_1\mathbf{v}_1+a_2\mathbf{v}_2+\ldots+a_n\mathbf{v}_n$, $a_j\in\mathbb{C}$. Consequently, the observability measures are now $a_i\mathbf{c}_k^T\mathbf{v}_i$, which are the elements of the matrix $\breve{\mathbf{C}}\mathbf{VK}$, where $\mathbf{K}\in\mathbb{C}^{n\times n}$ is a diagonal matrix which elements are the coefficients a_j.

$$\breve{\mathbf{C}}\mathbf{VK}_a=\begin{bmatrix}\mathbf{c}_1^T\mathbf{v}_1 & \mathbf{c}_1^T\mathbf{v}_2 & \cdots & \mathbf{c}_1^T\mathbf{v}_n\\ \vdots & \vdots & \ddots & \vdots\\ \mathbf{c}_p^T\mathbf{v}_1 & \mathbf{c}_p^T\mathbf{v}_2 & \cdots & \mathbf{c}_p^T\mathbf{v}_n\end{bmatrix}\begin{bmatrix}a_1 & & \mathbf{0}\\ & & \\ \mathbf{0} & & a_n\end{bmatrix} \tag{3.44}$$

This matrix changes with each new initial condition, but as it was stated in Section 3.2, for Koopman mode analysis generally there are available just a finite number of initial conditions, and the algorithms for its computation are highly dependent on this fact.

The main objective of the evaluation of the matrix $\breve{\mathbf{C}}\mathbf{VK}$ is to determine the minimum quantitative value of observability of a mode where it can still be identified in the analysis of the Koopman operator.

3.7 Concluding remarks

Koopman eigenvalues and modes at a spatial point can be determined by the generalized Laplace analysis provided even a single point but also a long time trace of data.

Conversely, the variants of the dynamic mode decomposition methods based on Arnoldi-type algorithms seem to be able to capture the Koopman values and their corresponding modes over a shorter period from data that have a larger spatial extent. Nonetheless, in contrast with Definition 2.8, the Koopman modes obtained by the Arnoldi-type algorithms depend on initial conditions.

In practice, the Koopman operator does not have to be realized to obtain the Koopman modes. Generalized Laplace analysis and the dynamic mode decomposition deals with snapshots sequences whereas linear stability analysis relies on linearization [2].

An interesting conclusion of the Section 3.5 is that the complete and the optimized dynamic mode decomposition algorithms capture the eigenvalues and eigenvectors relatively well. The first algorithm obtains good approximations to the frequency and damping coefficients for the main modes, but the representation has an error of considerable magnitude. On the other hand the optimized dynamic mode decomposition obtains a set of very accuracy approximations to the Koopman modes, although it generally needs much more time.

Additionally, it has been observed that when the empirical Ritz values are close enough to the true Koopman eigenvalues, their norm is a good parameter to distinguish among the true and spurious approximations to the Koopman modes.

In the examples presented in this section, the approach based on the singular value decomposition was not useful, albeit it may provide good results for larger sets of data, in the sense of spatial dimension. In some cases, it is just useful to obtain good approximations of the λ_j or their own frequencies.

Finally, a method to evaluate quantitatively the observability of the modes of a linear dynamical system was described in Section 3.6, allowing to evaluate how is that this observability measure can affect the accuracy and convergence of the Arnoldi-type algorithms. This measure as well as other parameters can be used posteriorly to develop better strategies for an efficient computation of the Koopman operator analysis.

3.8 References

[1] M. Budi˘sic, R. Mohr, and I. Mezic, "Applied Koopmanism," *Chaos*, vol. 22, no. 4, 2012.

[2] I. Mezić, "Analysis of fluid flows via spectral properties of Koopman operator", *Annu. Rev. Fluid Mech.*, vol. 45, pp. 357-378, 2013.

[3] A. Ruhe, "Rational Krylov sequence methods for eigenvalue computations," *Linear Alg. Appl.*, vol. 58, pp. 279–316, 1984.

[4] P. J. Schmid, "Dynamic mode decomposition of numerical and experimental data," *J. Fluid Mechanics*, vol. 656, Cambridge University Press 2010, pp. 5–28.

[5] C.W. Rowley, I. Mezic, S. Bagheri, P. Schlatter, & D. S. Henningson, "Spectral analysis of nonlinear flows", *J. Fluid Mechanics*, vol. 641, Cambridge University Press 2009, pp. 115–127

[6] K. K. Chen, J.H. Tu, C. W. Rowley, "Variants of Dynamic Mode Decomposition: Boundary Condition, Koopman, and Fourier Analyses", *J. of Nonlinear Science*, vol. 22, no. 6, pp. 887–915, Dec. 2012.

[7] S. M. Chan, "Modal controllability and observability of power-system models", *Electrical Power & Energy Systems*, vol. 6, No. 2, 1984.

[8] K. Ogata, *Modern Control Engineering*, New Jersey, Prentice Hall, 2002.

Chapter4
Physical Interpretation of KMA

Koopman mode analysis provides a powerful method for analyzing empirical data generated by nonlinear dynamical processes.

In this chapter, a physical interpretation of the Koopman modes is provided in the context of system oscillatory response. It is observed that when the Koopman mode decomposition is applied to a linear process, the dynamic decomposition allows recovering the linear stability modes of the linearized system.

For a nonlinear process, the Koopman decomposition identifies the dominant frequencies and their associated spatial structures, which provides a physical interpretation of the decomposition for nonlinear systems similar to the decomposition provided by the method of normal forms.

4.1 Linear observables

In this section, a physical interpretation of the Koopman modes when a set of linear observables is analyzed is provided. In this sense, the linear observables are defined as the output signals $\mathbf{y}(t)$ of a linear system defined by (3.35) and (3.36), which can be totally described by the linear stability modes obtained through a linear stability analysis (small-signal stability analysis for electric power systems).

It has been suggested that the Koopman modes are related to the linear global modes of the linear system in such a manner that the (optimized) dynamic mode decomposition indeed extracts them whereas the empirical Ritz values and vectors converge towards the true Koopman modes and Koopman eigenvalues.

4.1.1 Small-signal stability analysis

Small-signal stability analysis refers to the analysis of the system response to small perturbations.

In order to illustrate the physical significance of the modes, consider a classical power system model. The dynamic behavior of the system is given by the nonlinear model [1]:

$$\frac{d}{dt}\Delta\delta_j = \omega_0 \Delta\omega_j , \tag{4.1}$$

$$2H_j \frac{d}{dt}\Delta\omega_j = P_{M_j} - P_{E_j} - K_{D_j}\Delta\omega_j , \tag{4.2}$$

$j = 1,2,\ldots,ng$, where ng is the number of generators.

Here, $\Delta\delta_j$ is the angular position of the rotor of generator j with respect to a synchronously rotating reference, ω_0 is the synchronous speed in rad/s, $\Delta\omega_j$ is the deviation of the normalized rotor speed relative to the normalized synchronous speed in pu.

$H_j \in \Re$, the inertia constant in s, $K_{D_j} \in \Re$, is the damping coefficient in pu, $P_{M_j} \in \Re$, is the input mechanical power pu, and $P_{E_j} \in \Re$, is the output electrical power, pu. Loads are represented as constant impedances.

The linearized system is obtained through the Taylor's series expansion of (4.1) and (4.2) with terms involving second and higher order powers of the states neglected. Conventionally, the dynamical behavior of the system is represented by a constant coefficients matrix $\mathbf{A} \in \Re^{2ng \times 2ng}$

$$\dot{\mathbf{x}} = \mathbf{A}\mathbf{x} \tag{4.3}$$

where $\mathbf{x} = \left[\Delta\delta_1, \ldots, \Delta\delta_{ng}, \Delta\omega_1, \ldots, \Delta\omega_{ng}\right]^T$

The solution of (4.3) with initial conditions $\mathbf{x}_0$, is given by [1]:

$$\mathbf{x}(t) = \mathbf{u}'_1 \mathbf{x}_0 \mathbf{v}'_1 e^{\lambda_1 t} + \cdots + \mathbf{u}'_{2ng} \mathbf{x}_0 \mathbf{v}'_{2ng} e^{\lambda_{2ng} t} \tag{4.4}$$

Here $\mathbf{v}'_j$, $\mathbf{u}'_j$ are the right and left eigenvectors associated with the eigenvalue λ'_j of matrix $\mathbf{A}$, satisfying

$$\mathbf{A}\mathbf{v}'_j = \lambda'_j \mathbf{v}'_j \quad j = 1,2,\ldots,2ng\,. \tag{4.5}$$

Equation (4.4) provides a decomposition of the system response into single-frequency modal components; the terms $\mathbf{u}'_j \mathbf{x}_0$ give the initial excitation of each mode, while the vectors $\mathbf{v}'_j$ are the mode shapes associated with a given modal component [1].

4.1.2 Physical interpretation for linear observables

Koopman modes are of particular interest here because they are similar to the eigenvector expansion utilized in linear dynamics [2]. As discussed in Chapter 2, each snapshot $\mathbf{x}_k$ of the matrix $\mathbf{X}$ can be decomposed into a linear combination of Koopman modes multiplied by their respective values of Koopman eigenfunctions evaluated at time instant, t_k.

More formally, we can rewrite (3.18) or (3.33) as:

$$\mathbf{x}_k = \tilde{\lambda}_1^k \tilde{\mathbf{v}}_1 + \tilde{\lambda}_2^k \tilde{\mathbf{v}}_2 + \cdots + \tilde{\lambda}_p^k \tilde{\mathbf{v}}_p \tag{4.6}$$

where n is the number of snapshots, and $p \leq n$ is the number of Koopman modes obtained by any of the algorithms described in Chapter 3.

By comparison of (4.5) with (4.6), and assuming that the contribution of p empirical Ritz vectors, $p \leq 2ng$, accurately represents the observables $\mathbf{x}_k$, that is, the $\tilde{\lambda}_j$ are different each other, and that the frequencies and damping ratios captured by the p empirical Ritz eigenvalues are very similar to those given by the linear modal decomposition, namely

$$\mathbf{u}'_j \, \mathbf{x}_0 \mathbf{v}'_j \approx \tilde{\mathbf{v}}_j . \tag{4.7}$$

Then, given that the eigenanalysis of the Koopman operator allows to capture the intrinsic dynamics of the system, it can be stated that the Koopman mode decomposition of the linear observables is equivalent to that determined by means of the linear stability analysis and so:

$$\mathbf{u}'_j \, \mathbf{x}_0 \mathbf{v}'_j = \varphi(\mathbf{x}_0)\mathbf{v}_j , \tag{4.8}$$

where $\varphi(\mathbf{x}_0)$ is the value of the jth Koopman eigenfunction for the initial conditions $\mathbf{x}_0$, and $\mathbf{v}_j$ is the jth (normalized) Koopman mode.

Finally, it can be derived that

$$\mathbf{u}'_j \, \mathbf{x}_0 \mathbf{v}'_j = \varphi(\mathbf{x}_0)\mathbf{v}_j \approx \tilde{\mathbf{v}}_j = a_0 \hat{\mathbf{v}}_j , \tag{4.9}$$

where $\hat{\mathbf{v}}_j$ is the normalized empirical Ritz vector and a_0 is a real constant value.

Consequently,

$$\mathbf{v}'_j = \mathbf{v}_j \approx \frac{1}{a_0} \tilde{\mathbf{v}}_j = \hat{\mathbf{v}}_j \tag{4.10}$$

4.2 Nonlinear observables

Koopman modes have an interesting interpretation in terms of normal form analysis in perturbation theory [3]-[4]. This is an aspect of the analysis that has not been addressed in the literature.

Though in general, the analysis of normal forms can be formulated for any order of approximation, the analysis here is restricted to second-order perturbations, following the recommendations in [5].

4.2.1 Normal form analysis

The equations that describe the dynamical behavior of the power system are nonlinear. As a result, linear modes may interact with each other and result in nonlinear interactions between the linear modes. It has been observed in [6] that, under stressed system conditions, linear analysis may fail to characterize the observed system response.

The method of normal forms (MNF) is a well-established mathematical procedure to simplify nonlinear differential equations. The set of nonlinear differential equations are transformed up to a specified order, into a collection of linear differential equations by means of a sequence of nonlinear coordinate transformations. These linear transformed equations allow the study of the essential modal characteristics [5].

Here, the MNF is briefly described in the power systems framework, for a deeper treatment of the techniques, the reader is referred to [5] and references therein.

In its most elementary form, normal form analysis begins by performing a Taylor series expansion of the nonlinear system in the neighborhood of certain linear or nonlinear operation point. The expansion can be carried out up to a specified order that in this case is fixed at the second order of a proximation. This is because of the high computational effort required to compute higher order terms.

The Taylor series expansion of the nonlinear system up to second order is given by

$$\mathbf{x} = \mathbf{A}\mathbf{x} + \mathbf{X}_2 + O(3) \tag{4. 11}$$

where $O(3)$ denotes an expression containing residual terms of order 3 and higher.

For the i th state variable, neglecting the terms of third and higher order, one has

$$\dot{x}_i = \mathbf{A}_i x_i + \frac{1}{2}\mathbf{x}^T \mathbf{H}^i \mathbf{x}, \tag{4. 12}$$

where $\mathbf{A}_i$ is the i th row of the Jacobian matrix $\mathbf{A}$, and $\mathbf{H}^i$ is a Hessian matrix; the jk th element of $\mathbf{H}^i$ is given by

$$h^i_{jk} = \frac{\partial^2 f_i}{\partial x_j \partial x_k} \tag{4. 13}$$

Equation (4.12) can be transformed to its Jordan form by applying the similarity transformation $\mathbf{x} = \mathbf{U}\mathbf{y}$, where $\mathbf{U}$ is the matrix of right eigenvectors of $\mathbf{A}$. Use of this assumption in (4.12) results in the decoupled system

$$\dot{\mathbf{y}} = \Lambda\mathbf{y} + \frac{1}{2}\mathbf{V}^T \begin{bmatrix} \mathbf{y}^T\mathbf{U}^T\mathbf{H}^1\mathbf{U}\mathbf{y} \\ \mathbf{y}^T\mathbf{U}^T\mathbf{H}^2\mathbf{U}\mathbf{y} \\ \vdots \\ \mathbf{y}^T\mathbf{U}^T\mathbf{H}^p\mathbf{U}\mathbf{y} \end{bmatrix} \tag{4. 14}$$

The elements of the diagonal matrix Λ are the eigenvalues of $\mathbf{A}$, $\lambda_1, \lambda_2, \ldots, \lambda_p$, and $\mathbf{V}$ is the matrix of left eigenvectors of $\mathbf{A}$. It follows that, the j th Jordan form variable can be expressed as

$$\dot{y}_j = \lambda_j y_j + \sum_{k=1}^{p}\sum_{l=1}^{p} C^j_{kl}\, y_k y_l \,. \tag{4. 15}$$

where C_{kl}^{j} is the kl th element of the matrix $\mathbf{C}^{j}$ defined by

$$\mathbf{C}^{j} = \frac{1}{2}\sum_{q=1}^{p} v_{jq}\left[\mathbf{U}^{T}\mathbf{H}^{q}\mathbf{U}\right]. \tag{4.16}$$

We note that, in (4.16) the bracketed term is a $p \times p$ matrix and v_{jq} is the jq th element of the matrix $\mathbf{V}$

The next step is to transform (4.13) into its simpler form, the *normal form*, by eliminating the nonlinear terms. Use of the nonlinear transformation

$$\mathbf{y} = \mathbf{z} + h_{(2)}(\mathbf{z}) \tag{4.17}$$

in (4.15) gives

$$y_j = z_j + \sum_{k=1}^{p}\sum_{l=1}^{p} h_{(2)_{kl}}^{\ j} z_k z_l\,, \tag{4.18}$$

where $\mathbf{z}$ is a vector of normal form state variables.

It can be shown that the nonlinear coefficients, $h_{(2)_{kl}}^{\ j}$ can be computed from

$$h_{(2)_{kl}}^{\ j} = \frac{C_{kl}^{j}}{\lambda_k + \lambda_l - \lambda_j} \qquad j,k,l = 1,2,\ldots,n \tag{4.19}$$

provided that $\lambda_k + \lambda_l - \lambda_j \neq 0$. By means of (4.17), the second-order terms are removed from (4.14). This is known as the non-resonant condition.

The transformed equation is a set of decoupled first-order linear differential equations

$$\dot{\mathbf{z}} = \mathbf{\Lambda}\,\mathbf{z} + O(3); \qquad \dot{z}_j = \lambda_j z_j + O(3), \qquad j = 1,2,\ldots,p \tag{4.20}$$

where $O(3)$ denotes third and higher order terms, while the second-order terms have been transformed into elements of first order.

Neglecting third and higher order terms, the time evolution of the normal form variables, $z_j(t)$, given by

$$z_j(t) = z_{j0} e^{\lambda_j t} \tag{4. 21}$$

where z_{j0} denotes the initial condition associated with the state variable z_j.

The vector of initial conditions $\mathbf{z}_0$ is computed by solving the nonlinear equation (4.17) for a given initial condition $\mathbf{y}_0$:

$$f(\mathbf{z}) = \mathbf{z} - \mathbf{y}_0 + h_{(2)}(\mathbf{z}) = \mathbf{0} \tag{4. 22}$$

The solution to the above equation provides the initial condition $\mathbf{z}_0$, and then the solution of the original set of equations (4.11) is obtained by transforming the $\mathbf{z}$ variables back to the original state variables $\mathbf{x}$. This is done by first using (4.17) to compute $y_j(t) = z_{j0} e^{\lambda_j t} + \sum_{k=1}^{p} \sum_{l=1}^{p} h_{(2)_{kl}}^{j} z_{k0} z_{l0} e^{(\lambda_k + \lambda_l)t}$ followed by the application of the similarity transformation $\mathbf{x} = \mathbf{U}\mathbf{y}$ to compute $\mathbf{x}$.

Transforming the normal form solutions into the physical states gives the second-order approximation

$$x_i(t) = \sum_{j=1}^{p} u_{ij} z_{j0} e^{\lambda_j t} + \sum_{j=1}^{p} u_{ij} \left[\sum_{k=1}^{p} \sum_{l=1}^{p} h_{(2)_{kl}}^{j} z_{k0} z_{l0} e^{(\lambda_k + \lambda_l)t} \right] \tag{4. 23}$$

where u_{ij} is an element of the matrix of right eigenvectors $\mathbf{U}$.

Equation (4.23) expresses the system response for $x_1, x_2, \ldots, x_p$, in terms of the individual system modes $\lambda_1, \lambda_2, \ldots, \lambda_p$, and the second-order modes $\lambda_1 + \lambda_1$, $\lambda_1 + \lambda_2, \ldots, \lambda_{n-1} + \lambda_n, \lambda_n + \lambda_n$. The terms associated with the mode pairs $\lambda_k + \lambda_l$, provide information not available from the linear approximation of the power system equations.

These terms represent "modal interactions" that arise due to the inclusion of the higher order terms. Moreover, the coefficients of the exponential terms $e^{(\lambda_k+\lambda_l)t}$ give a measure of the participation of the mode combination $\lambda_k + \lambda_l$ in a given variable.

Of paramount importance, equations (4.23) reveals that, if the system is stable, the second term involving $e^{(\lambda_k+\lambda_l)t}$ will be more heavily damped than the first-order modes $e^{\lambda_k t}$ or $e^{\lambda_l t}$ as discussed in [5].

4.2.2 Physical interpretation for nonlinear observables

In Section 4.1 it has been suggested that, for linear observables, the normalized empirical Ritz eigenmodes converges towards the Koopman modes which in fact are equivalent to the linear stability modes.

For nonlinear observables the Koopman mode analysis provides a similar decomposition of the space generated by the snapshots. In this subsection is provided a physical interpretation of the Koopman mode analysis as a decomposition of the nonlinear behavior of the system in its intrinsic nonlinear components. These nonlinear structures are interpreted as dynamics analogous to the method of normal forms.

To begin with the comparison among both nonlinear decomposition techniques, we start by developing the nonlinear expansion of the Koopman mode decomposition; a comparison is then provided with normal form analysis.

Let each snapshot $\mathbf{x}_k$ of the matrix $\mathbf{X}$ be decomposed into the linear combination

$$\mathbf{x}_k = \tilde{\lambda}_1^k \tilde{\mathbf{v}}_1 + \tilde{\lambda}_2^k \tilde{\mathbf{v}}_2 + \cdots + \tilde{\lambda}_p^k \tilde{\mathbf{v}}_p + \cdots + \tilde{\lambda}_q^k \tilde{\mathbf{v}}_q \qquad (4.24)$$

where n is the number of snapshots, $q \le n-1$ is the number of Koopman modes obtained by any of the algorithms described in Chapter 3, and $p \le q$ is the number of linear stability modes of the system.

Recalling properties 2.2 and 2.3, it can be stated that the combinations of the Koopman eigenvalues that approximate the linear eigenvalues of the system originate another Koopman eigenvalues with its respective Koopman modes and Koopman eigenfunctions. Consequently, it can be assumed that the j th Koopman mode, $p < j \leq q$, is a combination of the previous Koopman modes:

$$\tilde{\lambda}_j \tilde{\mathbf{v}}_j = \left(\tilde{\lambda}_k \tilde{\lambda}_l\right)\tilde{\mathbf{v}}_{kl} \approx e^{(\lambda_k+\lambda_l)t}\mathbf{v}_{kl} \tag{4. 25}$$

where λ_k and λ_l are the k th and l th linear eigenvalues of the system, and $\mathbf{v}_{kl}$ is the corresponding mode. Then, if it is assumed that the first p Koopman modes are approximations to the linear stability modes, it can be hypothesized that the rest of the Koopman modes are nonlinear structures of the form (4.25), and so (4.24) can be rewritten as

$$\mathbf{x}_k = \tilde{\lambda}_1^k \tilde{\mathbf{v}}_1 + \tilde{\lambda}_2^k \tilde{\mathbf{v}}_2 + \cdots + \tilde{\lambda}_p^k \tilde{\mathbf{v}}_p + \tilde{\lambda}_{1,1}^k \tilde{\mathbf{v}}_{1,1} + \tilde{\lambda}_{1,2}^k \tilde{\mathbf{v}}_{1,2} \cdots + \tilde{\lambda}_{p-1,p}^k \tilde{\mathbf{v}}_{p-1,p} + \tilde{\lambda}_{p,p}^k \tilde{\mathbf{v}}_{p,p}$$

$$= \tilde{\phi}_1(\mathbf{x}_0)\tilde{\lambda}_1^k \hat{\mathbf{v}}_1 + \tilde{\phi}_2(\mathbf{x}_0)\tilde{\lambda}_2^k \hat{\mathbf{v}}_2 + \cdots + \tilde{\phi}_p(\mathbf{x}_0)\tilde{\lambda}_p^k \hat{\mathbf{v}}_p + \tilde{\phi}_{1,1}(\mathbf{x}_0)\tilde{\lambda}_{1,1}^k \hat{\mathbf{v}}_{1,1} +$$

$$+ \tilde{\phi}_{1,2}(\mathbf{x}_0)\tilde{\lambda}_{1,2}^k \hat{\mathbf{v}}_{1,2} \cdots + \tilde{\phi}_{p-1,p}(\mathbf{x}_0)\tilde{\lambda}_{p-1,p}^k \hat{\mathbf{v}}_{p-1,p} + \tilde{\phi}_{p,p}(\mathbf{x}_0)\tilde{\lambda}_{p,p}^k \hat{\mathbf{v}}_{p,p}. \tag{4. 26}$$

where $\tilde{\phi}_j(\mathbf{x}_0), \tilde{\phi}_j(\mathbf{x}_0) \in \mathbb{C}$ are the norms of the vectors $\tilde{\mathbf{v}}_j$ and $\tilde{\mathbf{v}}_{kl}$, respectively. The vectors $\hat{\mathbf{v}}_j$ and $\hat{\mathbf{v}}_{kl}$ are the normalized vectors $\tilde{\mathbf{v}}_j$ and $\tilde{\mathbf{v}}_{kl}$.

It is observed that, although in (4.24) the term $\mathbf{x}_k$ is decomposed by means of q modes, in (4.26) we have used $p + p!$ terms with the aim of emphasizing that all the modes of second-order can be present in the decomposition. Moreover, in the decomposition of (4.26) may be any nonlinear Koopman mode of any order, and not just second-order terms. Only the second-order terms have been added with the assumption that the higher-order terms have minimal participation and with the target of establish a comparison with normal forms.

Just as in the case of the method of normal form analysis, in the Koopman mode decomposition, it is assumed that a nonlinear system can be decomposed

in an infinite sum of terms of different order. Whether is taken into account that for both methods the terms of third and higher order are neglected, the nonlinear behavior of the system is ruled by (4.23) for normal forms analysis. Then, the set of nonlinear observables can be expressed by means of (4.26) with Koopman mode analysis.

Insight into the nature of the observed behavior can be obtained by rewriting (4.23) in the more interesting form

$$\mathbf{x}_k(t) = \sum_{j=1}^{p} \phi_j(\mathbf{x}_0) e^{\lambda_j k\Delta t} \mathbf{v}'_{(2)_j} + \sum_{k=1}^{p}\sum_{l=1}^{p} \phi_{kl}(\mathbf{x}_0) e^{(\lambda_k+\lambda_l)k\Delta t} \mathbf{v}'_{(2)_{kl}} \qquad (4.27)$$

where $\phi_j(\mathbf{x}_0), \phi_{kl}(\mathbf{x}_0) \in \mathbb{C}$ are constant values dependent on the initial conditions $\mathbf{x}_0$, and the vectors $\mathbf{v}'_{(2)_j}, \mathbf{v}'_{(2)_{kl}} \in \mathbb{C}^m$ are the modes related to λ_j and $(\lambda_k + \lambda_l)$, respectively.

The following conclusions can be drawn from this analysis:

By assuming that the Koopman mode decomposition accurately represents the nonlinear observables $\mathbf{x}_k$, then from the comparison of (4.26) with (4.27), it can be assumed that the first p Koopman modes approximate the linear stability modes of the system as was stated in the preceding section. It results that for the first-order terms

$$\phi_j(\mathbf{x}_0)\mathbf{v}'_{(2)_j} \approx \tilde{\phi}_j(\mathbf{x}_0)\hat{\mathbf{v}}_j, \qquad (4.28)$$

whereas for the second-order terms

$$\phi_{kl}(\mathbf{x}_0)\mathbf{v}'_{(2)_{kl}} \approx \tilde{\phi}_{kl}(\mathbf{x}_0)\hat{\mathbf{v}}_{kl}, \qquad (4.29)$$

Finally, it can be shown that

$$\phi_j(\mathbf{x}_0)\mathbf{v}'_{(2)_j} = \varphi_j(\mathbf{x}_0)\mathbf{v}_j \approx \tilde{\mathbf{v}}_j = \phi_j(\mathbf{x}_0)\hat{\mathbf{v}}_j, \qquad (4.30)$$

and

$$\phi_{kl}(\mathbf{x}_0)\mathbf{v}_{(2)kl} = \varphi_{kl}(\mathbf{x}_0)\mathbf{v}_{kl} \approx \tilde{\mathbf{v}}_{kl} = \phi_{kl}(\mathbf{x}_0)\hat{\mathbf{v}}_{kl}, \tag{4.31}$$

where $\varphi_j(\mathbf{x}_0), \varphi_{kl}(\mathbf{x}_0)$ are the true Koopman frequencies, and $\mathbf{v}_j, \mathbf{v}_{kl}$ are the true Koopman vectors.

4.2.3 Comparison between KMA and the MNF

As discussed above, the Koopman mode decomposition can be interpreted in terms of normal form analysis in perturbation theory. These methods, however, differ in several ways, most significantly in the way to be applied to describe the nonlinear response of an electric power system.

First, the method of normal forms works with the nonlinear model of the power system, linearizing it around a specified point, the Koopman mode analysis works just with recorded data.

This means that the method of normal forms has the possibility of study each one of the dynamics interacting in the response of the system. Also, the computational effort required to carry out the decomposition is very high, in such a way that this study in most cases is not achieved farther than the second order of approximation.

On the other hand, Koopman mode analysis requires the same effort to calculate the approximate Koopman modes regardless of the dynamics described. Koopman mode decomposition computational demand is mainly related with the amount of information to be analyzed (number of observables and the quantity of snapshots). As a consequence, Koopman mode analysis is capable to identify and extract efficiently nonlinear structures related with any order of nonlinearity, i.e. it can identify nonlinearities related to normal forms of second and higher order of approximation.

Though this may seem a great advantage, the closeness of the true Koopman eigenvalues and the absence of physical information make the distinc-

tion between the Koopman modes that describe the linear behavior and those that describe the nonlinear behavior and the spurious modes generated by the numerical method difficult.

In the light of the above observations, the following strategy is proposed:

1. Perform the linear stability analysis for the electric power system for the post-fault condition to obtain the linear stability modes.

2. Through the theory of normal forms determine the nonlinear Koopman eigenvalues that could describe the nonlinear behavior of the system

3. By means of the number of snapshots, the extent of the time increasing step, and the main dynamics that can be excited (mainly those related to the inter-area linear modes), provide a set of true Koopman eigenvalues that probably decompose the observables accurately.

4. Use the set of true Koopman modes as initial conditions for the dynamical mode decomposition or as the initial approximate setting to perform the optimal dynamic mode decomposition.

This strategy was not used in this thesis because it is not part of the objectives pursued, but its application to assess system dynamic behavior is envisioned in future work.

4.2.4 Nonlinear Koopman structures

In this section is established a theoretical procedure to obtain nonlinear structures of the Koopman mode analysis that contain information of the spatial evolution of the dynamics related with a nonlinear mode. These structures are analogous to the linear right eigenvectors and allow to perform a nonlinear mode shape analysis.

In the method of normal forms this nonlinear structures are calculated by means of multiplications of the elements of the right eigenvectors, the nonlinear coefficients, $h_{(2)_{kl}}^{j}$ and the initial conditions of the normal form state variables z_{k0} and z_{l0}, as can be observed in (4.23). This nonlinear structures do not have a clear relation with the linear right eigenvectors.

In the case of Koopman mode analysis, nonlinear structures of the Koopman eigenvalues can be theoretically determined in the following manner.

First, by recalling Property 2.3, which shows that the interaction of Koopman modes generate another Koopman mode, and rewriting it for the discrete-time domain, one has

$$U^k\left(\phi_{\lambda_1}(\mathbf{x})\phi_{\lambda_2}(\mathbf{x})\right)=\phi_{\lambda_1}\left(S^k(\mathbf{x})\right)\phi_{\lambda_2}\left(S^k(\mathbf{x})\right)$$

$$=\exp\left(\lambda_1 k\Delta t\right)\phi_{\lambda_1}(\mathbf{x})\exp\left(\lambda_2 k\Delta t\right)\phi_{\lambda_2}(\mathbf{x})$$

$$=\exp\left((\lambda_1+\lambda_2)k\Delta t\right)\phi_{\lambda_1}(\mathbf{x})\phi_{\lambda_2}(\mathbf{x}), \qquad (4.32)$$

and then recalling how an observable $g(\mathbf{x})$ is decomposed into Koopman modes:

$$g(\mathbf{x})=\sum_{j=1}^{\infty}\varphi_j(\mathbf{x})\,\mathbf{v}_j\,,$$

it can be expressed the time evolution of the observables with initial conditions $g(\mathbf{x}_0)$ at t_0 as:

$$U\,g(\mathbf{x}_0)=\sum_{j=1}^{\infty}U\,\varphi_j(\mathbf{x}_0)\,\mathbf{v}_j \qquad (4.33)$$

Then, by regarding the evolution of the dynamics associated to a modal interaction,

$$U^k\left[\left(\varphi_j(\mathbf{x}_0)\,\mathbf{v}_j\right)\cdot\left(\varphi_l(\mathbf{x}_0)\,\mathbf{v}_l\right)\right]=\varphi_j\left(S^k(\mathbf{x}_0)\right)\varphi_l\left(S^k(\mathbf{x}_0)\right)\left(\mathbf{v}_j\cdot\mathbf{v}_l\right)$$

$$= \exp\left(\lambda_j\, k\Delta t\right)\varphi_j(\mathbf{x}_0)\exp\left(\lambda_l\, k\Delta t\right)\varphi_l(\mathbf{x}_0)(\mathbf{v}_k \cdot \mathbf{v}_l)$$

$$= \exp\left(\left(\lambda_j + \lambda_l\right)k\Delta t\right)\varphi_j(\mathbf{x}_0)\,\varphi_l(\mathbf{x}_0)(\mathbf{v}_k \cdot \mathbf{v}_l)$$

$$= \exp\left(\left(\lambda_j + \lambda_l\right)k\Delta t\right)\varphi_{jl}(\mathbf{x}_0)\, b_{kl}\mathbf{v}_{kl} \qquad (4.34)$$

where $(\cdot)$ denotes a term by term product, b_{kl} is the norm of the vectorial term $(\mathbf{v}_k \cdot \mathbf{v}_l)$, $\varphi_{jl}(\mathbf{x}_0)$ is the Koopman eigenfunction product of the multiplication of the j th and l th Koopman eigenfunctions, and $\mathbf{v}_{kl}$ is the resulting normalized nonlinear structure related to the Koopman eigenvalue $(\lambda_j + \lambda_l)$.

In particular, for the nonlinear Koopman mode corresponding to the Koopman eigenvalue $(\lambda_j + \lambda_j) = (2\lambda_j)$,

$$U^k\left[\left(\varphi_j(\mathbf{x}_0)\,\mathbf{v}_j\right)\cdot\left(\varphi_j(\mathbf{x}_0)\,\mathbf{v}_j\right)\right] = \varphi_j\left(S^k(\mathbf{x}_0)\right)\varphi_j\left(S^k(\mathbf{x}_0)\right)\left(\mathbf{v}_j \cdot \mathbf{v}_j\right).$$

$$= \exp\left(2\lambda_j\, k\Delta t\right)\varphi_j^2(\mathbf{x}_0)\left(\mathbf{v}_j\right)^2$$

$$= \exp\left(2\lambda_j\, k\Delta t\right)\varphi_{jj}(\mathbf{x}_0)\,\mathbf{v}_{jj} \qquad (4.35)$$

Here, the term $\mathbf{v}_{jj}$ represent the vector of the squared values of each element of $\mathbf{v}_j$.

This theoretical result is based on the Koopman operator theory and is used in Chapter 5 to determine a theoretical mode shape of a nonlinear Koopman mode to demonstrate its validity.

4.3 Concluding remarks

It can be observed that the Koopman modes capture the dynamics of a dynamical linear or nonlinear system in a manner analogous to small-signal analysis and the method of normal forms (though in this Chapter has been shown approximations up to the second order), respectively.

Also, an interesting result associated to the determination of nonlinear Koopman structures has been presented, which may be used for an easy determination of the spatial behavior of the nonlinear dynamics. The validity of this result is been proved in Chapter 5, where its usefulness is demonstrated.

Nevertheless, as the empirical Ritz vectors are an estimation of the Koopman modes, the dynamics will not be captured accurately. Numerical experience in Chapter 5, however, shows that the empirical Ritz vectors converge towards the Koopman modes even for complex systems.

4.4 References

[1] P. Kundur, *Power System Stability and Control*, New York, Mc-Graw-Hill, 1994.

[2] I. Mezić, "Analysis of fluid flows via spectral properties of Koopman operator", Annu. Rev. Fluid Mech., vol. 45, pp. 357-378, 2013.

[3] S. Wiggins, *Introduction to Applied Nonlinear Dynamical Systems and Chaos.* New York, Springer-Verlag, 1990.

[4] A. H. Nayfeh, *Method of Normal Forms*. New York, Wiley, 1993.

[5] J. J. Sanchez-Gasca, V. Vittal, M. J. Gibbard, A. R. Messina, D. J. Vowles, S. Liu, and U. D. Annakkage, "Inclusion of higher order terms for small-signal (modal) analysis: committee report – task force on assessing the need to include higher order terms for small-signal (modal) analysis", *IEEE Trans. Power Syst.*, vol. 20, no. 4, pp. 1886-1904, Nov. 2005.

[6] V. Vittal, N. Bhatia, and A. A. Fouad, "Analysis of the inter-area mode phenomenon in power systems following large disturbances", *IEEE Trans. on Power and Systems*, vol. 11, No. 4, Nov. 1996

Chapter5
Application

This chapter describes the application of nonlinear mode decompositions techniques based on the Koopman operator to extract and characterize nonlinear behavior in measured data. Three approaches are considered: dynamic mode decomposition (DMD), SVD-based dynamic mode decomposition and the optimized dynamic mode decomposition.

The techniques are demonstrated on a wide range of examples, including data generated by transient stability simulations and synthetic data. Simulation results show that Koopman mode analysis may be used to assess global stability from simultaneously recorded data.

The effects of observability of critical modes on the accuracy and robustness of the various modeling approaches are examined in detail. In all cases, the optimized dynamic mode decomposition methodology is seen to provide more accurate approximations to system dynamic behavior than those of the (SVD-based) dynamic mode decomposition.

5.1 Outline of the study

The accuracy and robustness of the various modeling approaches was evaluated for observational data obtained from detailed transient stability simulations.

The object of these simulations and analyzes are:

1. To verify the extent to which global mode decomposition techniques can be used to extract and characterize critical intersystem modes of oscillation

2. To verify the accuracy and robustness of the proposed modeling approaches

3. To find robust and stable reduced order models (ROMs) that accurately describe the inter-area dynamics of interest

In the analysis below, attention is focused on the ability of these methodologies to characterize simulated data. First, the test cases are described.

5.1.1 Test cases

Three power systems have been used for analysis of wide-area phenomena.

1. The two-area, four-generator presented in [1]. For the purposes of this study, two models are considered:

    a: A classical system representation

    b. A detailed transient stability model [2]

2. The New-England 16-machine system

3. A 46-machine, 189-bus model of the Mexican interconnected system [3].

5.1.2 Modeling considerations

An initial step before computing the Koopman modes from the data set is to extract the mean speed of each measurement. It is not meant to remove the

mean value of the entire data set, because of the possibility of reaching discrete Fourier transform [4].

With these considerations, the observation matrix, **X**, turns into:

$$\tilde{\mathbf{X}} = \begin{bmatrix} x_{1,1} - \bar{x}_1 & x_{1,2} - \bar{x}_1 & \cdots & x_{1,m+1} - \bar{x}_1 \\ x_{2,1} - \bar{x}_2 & x_{2,2} - \bar{x}_2 & \cdots & x_{2,m+1} - \bar{x}_{21} \\ \vdots & \vdots & & \vdots \\ x_{n,1} - \bar{x}_n & x_{n,2} - \bar{x}_n & \cdots & x_{n,m+1} - \bar{x}_n \end{bmatrix} \tag{5.1}$$

where $\bar{x}_j$ is the mean value of the jth observable, given by $\bar{x}_j = \text{mean}\left(x_{j,1} \; . \; x_{j,2} \quad \cdots \quad x_{j,m+1}\right)$.

The percentage of the error of the representation is calculated as:

$$\text{error}(\%) = \frac{sup\left(\left\| \mathbf{\Phi V} - \tilde{\mathbf{X}} \right\|_2 \right)}{sup\left(\left\| \tilde{\mathbf{X}} \right\|_2 \right)} \times 100 . \tag{5.2}$$

where the term $sup(\cdot)$ denotes the *supremum*, and the matrix $\mathbf{\Phi V}$ gives the decomposition of the original signals in terms of the approximate Koopman modes. That is, $\mathbf{\Phi V}$ is equivalent to (2.41) but for all the ensemble of data assuming $g(\mathbf{x}_k) = \mathbf{x}_k$.

Equation (5.2) is used to evaluate the accuracy of the representations of the original signals obtained by the approximations to the true Koopman modes computed using the different approaches.

We now discuss the application of the proposed techniques.

5.2 Two-area, four-generator system

As a first example, the two-area four-generator system in [1] is used to introduce the application of the proposed techniques to assess system behavior. The base case operating conditions and system parameters are given in [1] for the classical system representation and in [5] for the detailed system representation.

Two disturbance scenarios are considered for analysis:

1) **Case A**. Classical system representation. Loss of 5% of mechanical power in Generator 1.

2) **Case B**. Detailed system representation. Three phase fault applied at Bus 5 cleared in 0.019 s with no line switching.

5.2.1 Classical system representation

Linear analysis was used to benchmark Koopman analysis results.

Table 5.1 summarizes the linear system modes for the classical system representation. The system exhibits an inter-area mode at about 0.56 Hz and two local modes associated with areas 1 and 2 at 1.19 Hz and 1.23 Hz, respectively.

Table 5.1. Small-signal stability analysis eigenvalues.

Mode j	λ_j	Frequency [Hz]	Damping [%]	Mode Description
1	0.0018 + 0.0000i	0.0000	-100.0000	Trend
2	-0.0798+0.0000i	0.0000	100.0000	Mean value
3, 4	-0.3994 ± 3.5602i	0.5666	1.1218	Inter-area
5, 6	-0.0385 ± 7.5344i	1.1991	0.5109	Local Area 1
7, 8	-0.0404 ± 7.7622i	1.2354	0.5211	Local Area 2

Transient stability simulations were recorded over 10 s at a rate of 20 samples per second. Plots of the simulated speed deviations for Case A above are shown in Fig. 5.1. This contingency is found to excite modes 3 and 5 in Table 5.1.

The observation matrix associated with the system response to this perturbation is defined as

$$\mathbf{X} = \begin{bmatrix} \Delta\omega_1 & \Delta\omega_2 & \cdots & \Delta\omega_4 \end{bmatrix}^T \in \Re^{n\times(m+1)} \tag{5.3}$$

with $n = 4$ and $m = 201$.

The five most dominant empirical Ritz eigenmodes obtained by the dynamical mode decomposition are shown in Table 5.2. The frequencies of the second and third empirical Ritz eigenvalues approximate the dynamic of the linear modes 3 and 5 in Table 5.1. The other empirical Ritz eigenmodes are spurious modes.

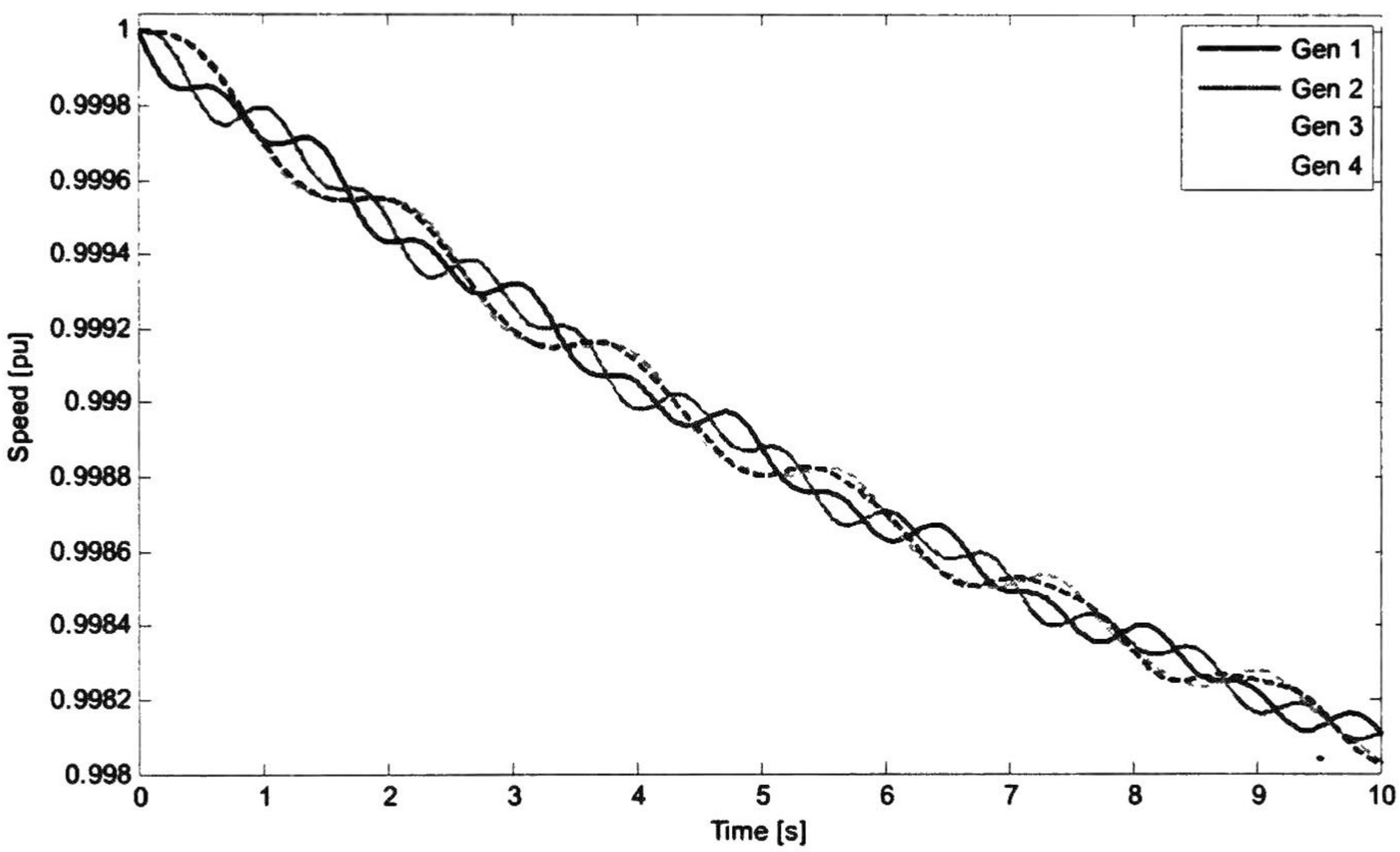

Fig. 5.1. Speed deviations of system generators. Case A.

Table 5.2. Dominant Ritz eigenmodes obtained by DMD for the data shown in Fig. 5.1

Mode	j	$\lvert\tilde{\lambda}_j\rvert$	Frequency (Hz)	Damping (%)	Norm $\lVert\tilde{\mathbf{v}}_j\rVert$
1		1.0003	0.0485	-1.9127	1.000000
2		0.9914	0.5743	1.1036	0.0930
3		0.9871	1.2050	1.2071	0.0717
4		0.9980	0.1638	12.2237	0.1895
5		0.9954	0.2653	9.9980	0.1058

Some discrepancies are noted, especially in the damping of the modal estimates.

The approximation error is of 4.41×10^{-12} % when all 200 modes are included in the modal reconstruction. For comparison, the reconstruction error is 29.67% when the first ten modes are used to reconstruct the simulated signal. This error increases to 36.31% when only three modes are used in the reconstruction.

Also of interest, Tables 5.3 and 5.4 compare the mode shape computed using conventional linear analysis of the linear system representation and the Koopman representation for the 0.56 and 1.20 Hz modes.

Table 5.3. Comparison among mode shapes.

Ritz eigenmode (0.5743 Hz)		Eigenvector $\mathbf{u}_{3,4}$ (0.5666 Hz)	
Amplitude	Phase	Amplitude	Phase
0.36180	179.60181	0.45851	-180.05759
0.26326	179.34981	0.36760	-180.07060
1.00000	0.00000	1.00000	0.00000
0.89860	0.03097	0.87862	0.00330

Table 5.4. Comparison among mode shapes.

Ritz eigenmode (1.2050 Hz)		Vector $\mathbf{u}_{5,6}$ (1.1991 Hz)	
Amplitude	Phase	Amplitude	Phase
0.92670	-175.17165	0.88593	-180.00181
1.00000	0.00000	1.00000	0.00000
0.27763	156.02513	0.24086	-180.40626
0.28833	-54.94551	0.18997	-0.64832

The analysis suggests that dynamic mode decomposition provides a good approximation to mode shapes for the dominant modes of interest.

Using the optimized dynamical mode decomposition method, four Koopman modes that represent the recorded response were obtained. The results are presented en Table 5.5. In contrast to the results from the previous approach, the maximum error value is of almost 0.56%. Again, some discrepancies are noted with the linear estimates.

Additionally, when the eigenvalues of the system are introduced as the Koopman values for the analysis, the error is of 15.49%.

Table 5.5. Approximate KMs obtained by the optimized DMD for the data shown in Fig. 5.1.

Mode j	$\lvert\tilde{\lambda}_j\rvert$	Frequency [Hz]	Damping [%]	Norm $\lVert\tilde{\mathbf{v}}_j\rVert$
1	1.0001	0.0000	-100.00	1.0000
2	0.9997	1.2009	0.1623	0.0049
3	0.9991	0.5742	1.0184	0.0098
4	0.9979	0.0000	100.00	0.6581

The associated mode shape for the first and second Koopman modes are presented in tables 5.6 and 5.7. Similar conclusions to the dynamic mode decomposition case are drawn.

Table 5.6. Comparison among mode shapes.

Ritz eigenmcde (0.5742 Hz)		Vector $\mathbf{u}_{3,4}$ (0.5666 Hz)	
Amplitude	Phase	Amplitude	Phase
0.46927	-179.55802	0.45851	179.9492
0.38215	179.48726	0.36760	179.9294
1.00000	0.00000	1.00000	0.00000
0.87793	-0.19867	0.87862	0.00330

Table 5.7. Comparison among mode shapes

Ritz Mode (1.1973 Hz)		Vector $\mathbf{u}_{5,6}$ (1.1991 Hz)		Vector $\mathbf{u}_{7,8}$ (1.2354 Hz)	
Amplitude	Phase	Amplitude	Phase	Amplitude	Phase
0.91452	178.92790	0.88593	-180.00181	0.07849	-0.56741
1.00000	0.00000	1.00000	0.00000	0.10069	-180.50397
0.21264	169.49399	0.24086	-180.40626	0.81162	-179.99498
0.17766	-13.42432	0.18997	-0.64832	1.00000	0.00000

Results show that both, the dynamic mode decomposition and the optimized dynamic mode decomposition identify in similar way the mode of 0.5666 Hz and have difficulties to identify separately the modes of 1.1991 and 1.2345 Hz, though the optimized approach has lower error of representation.

Then, by comparing the signals of the original data set and the reconstructed signals obtained by dynamic mode analysis, is obtained the Fig. 5.2. It can be seen the error between both groups of signals.

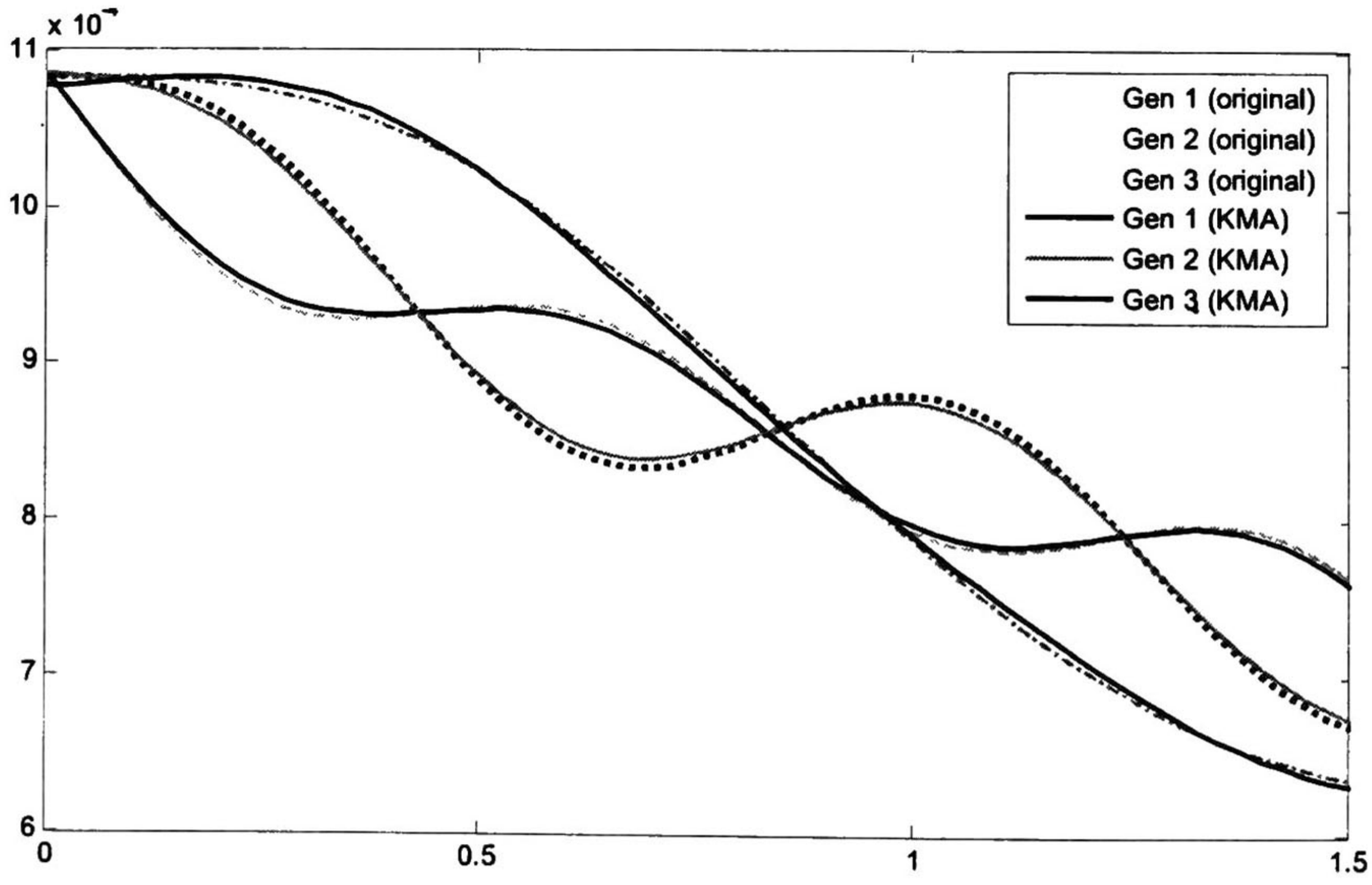

Fig. 5.2. Original signals of the case of study A and the signals reconstructed with the KMs. Here are drawn just the first 1.5 seconds of the transient to make the error more seeable.

5.2.2 Detailed system representation

As a further measure of the performance of the decomposition techniques, modal decompositions were obtained for a detailed system representation. Comparisons are provided with the method of normal form analysis in [2], [5].

For reference and comparison, Table 5.8 shows the linear system modes, whilst Fig. 5.3 shows the system response to a three phase stub fault applied at bus 5 cleared in 0.019 s.

Table 5.8. Oscillatory modes of the system.

Mode j,k	$\lambda_{j.k}$	Frequency [Hz]	Damping [%]	Mode Description
1, 2	-1.1021 ± 7.7247i	1.2294	14.1236	Local Area 1 (δ_1, δ_2)
3, 4	-1.9594 ± 7.5176i	1.1965	25.2211	Local Area 2 (δ_3, δ_4)
5, 6	-1.4668 ± 2.2223i	0.3537	55.0851	$E'_{d4}, \omega_4, \delta_4, \omega_3, \delta_3$
7, 8	-0.1084 ± 1.3809i	0.2198	7.8278	Inter-area $(\delta_1, \delta_2, \delta_3, \delta_4)$
9, 10	-1.2160 ± 0.7717i	0.1228	84.4320	Controls unit Generator 4
11, 12	-0.2727 ± 0.5169i	0.0823	46.6663	Controls unit Generator 1
13, 14	-0.3340 ± 0.4559i	0.0726	59.1008	Controls unit Generator 3
15, 16	-2.8790 ± 0.4097i	0.0652	99.0025	$E'_{q1}, E'_{q2}, E'_{q3}, E'_{q4}$

In order to build the matrix of observables, it has been taken 401 samples with a sample frequency of 20 Hz through a time window of 20 s.

Optimized dynamic mode decomposition of the system results in 20 modes. A reconstruction error of 1.71×10^{-2} % is obtained from the method. Table 5.9 shows the extracted Koopman modes. As seen, optimized dynamical mode decomposition provides a good estimate of the inter-area mode 7 in Table 5.8

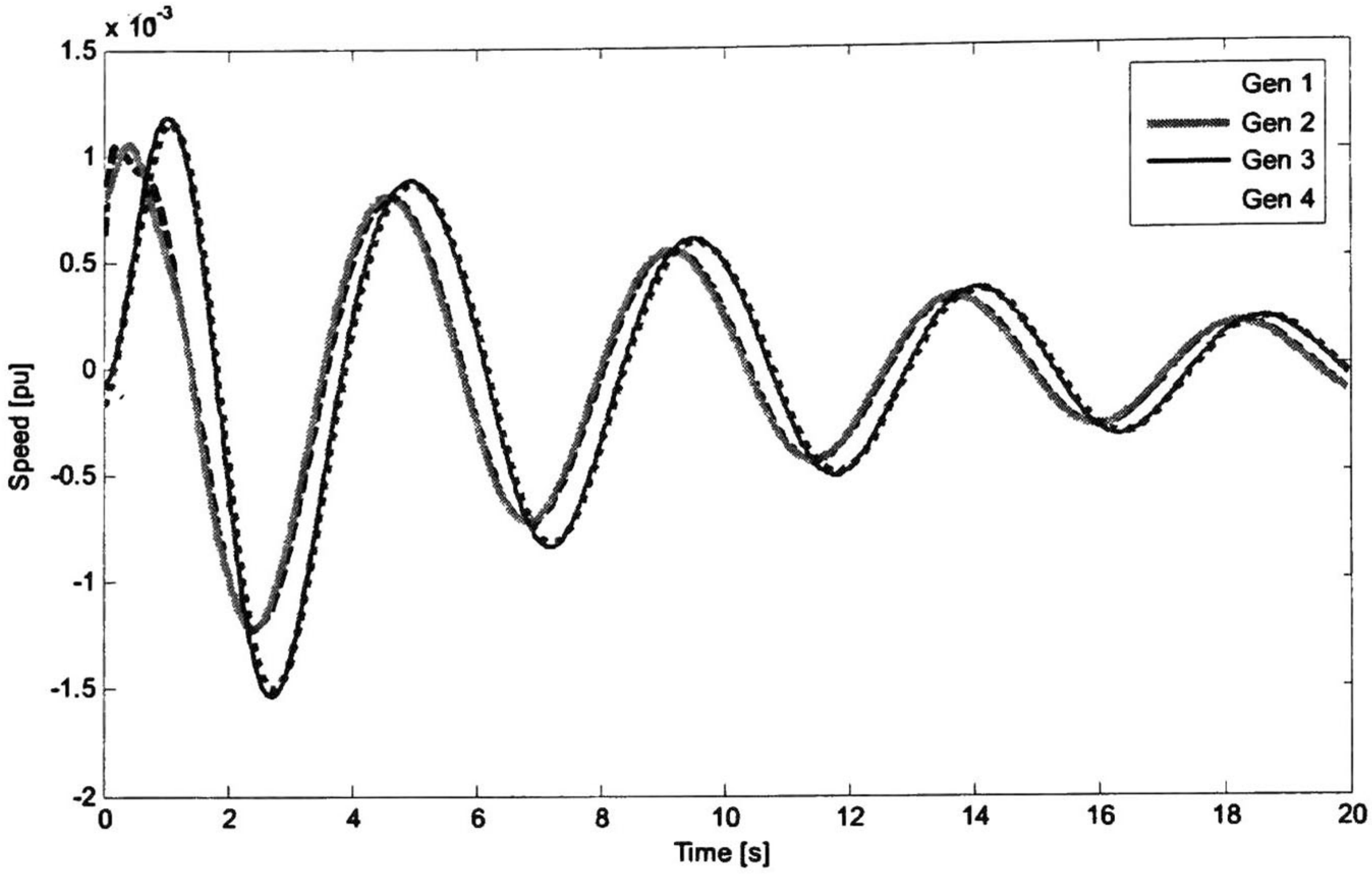

Fig. 5.3. Speed deviations of system generators following a three-phase stub fault at bus 5.

Table 5.9. Main approximate KMs obtained by the optimized DMD for the data of Fig. 5.3.

Mode j	$\lvert\tilde{\lambda}_j\rvert$	Frequency [Hz]	Damping [%]	Norm $\lVert\tilde{\mathbf{v}}_j\rVert$
5	0.9945	0.2207	7.9443	2.7304E-02
6	0.9909	0.4412	6.5827	1.8972E-03
7	0.9894	0.1393	23.5869	4.1163E-03
9	0.9856	0.1034	40.8333	1.1765E-02

Several conclusions can be drawn from this analysis:

- Mode 5 in Table 5.9 provides a good approximation to mode 3 in Table 5.8. Comparison of the mode shapes estimates in Table 5.10
- Also of interest, Koopman mode 6 appears to represent a second-order mode.

- Finally, following Property 2.3, a theoretical mode shape of the nonlinear mode related to the linear eigenmode of 0.2198 Hz is shown in Table 5.11 to be compared against the mode shape of the 0.4412 Hz of the approximation.

Table 5.10. Comparison among amplitudes and phases of the modes. The amplitudes are normalized

App. KM (0.2207 Hz)		Vector $\mathbf{u}_{7,8}$ (0.2198 Hz)	
Amplitude	Phase	Amplitude	Phase
0.8562	25.8286	0.8562	25.7167
0.8507	28.4999	0.8507	28.3128
1.0000	0.0000	1.0000	0.0000
0.9850	-2.5343	0.9850	-2.5102

Table 5.11. Comparison among mode shapes

App. KM (0.4412 Hz)		Theoretical mode shape (0.4396 Hz)	
Amplitude	Phase	Amplitude	Phase
0.3494	52.2018	0.7331	51.4333
0.3654	55.2006	0.7237	56.6256
1.0000	0.0000	1.0000	0.0000
0.9631	-5.0026	0.9703	-5.0203

As can be seen, the normalized amplitudes of the last two terms and all the phases of both mode shapes are almost the same. The discrepancy between the normalized amplitudes of the first and second generators is of almost the half. With a different amount of approximation of the optimized dynamical mode decomposition a similar result was achieved. By now there is not a clear explanation for that phenomenon.

The rest of the modes are approximations and mixtures of nonlinear modes which amplitude decay rapidly. Thus, they are not analyzed in depth in this work because the modes of lower frequency and damping rate are the most concerning.

5.3 The New-England 16-generator system

As a second test system, the 16-generator test system is adopted for further analysis with the classical system representation [1]. Here, emphasis is placed on improvements to the technique when observability information is incorporated to the estimation procedure.

5.3.1 Linear stability analysis

This system comprises 16 generators and 39 buses. Six modes of synchronizing power flow oscillations are of interest to this study (refer to Table 5.12).

Table 5.12. Eigenmodes of case of study C used for the observability study.

Mode j	Frequency Hz	Damping %
3	0.3799	14.8756
4	0.4892	12.2710
5	0.6267	9.1479
11	1.2227	3.2524
15	1.5051	2.6426
17	2.2854	1.7408

5.3.2 Observability analysis

Observability of the critical modes has an important effect on the ability of the Koopman decomposition to identify and characterize modal behavior. The reader is referred to Section 3.6.2 of this document for further information related to the computation of observability measures, and specifically in the evaluation of the matrix of observability of (3.44).

The observability measure of the modes is varied in this study by means of the vector of initial conditions $\mathbf{x}_0$. The modes that are taken for this study are the six modes of Table 5.12.

A summary of the results is shown in Table 5.13.

Table 5.13. Minimum values of the observability measure of the modes to be identified by DMD and optimized DMD algorithms.

	Mode of 2.2854 Hz	Mode of 1.5051 Hz	Mode of 1.2270 Hz	Mode of 0.6267 Hz	Mode of 0.4789 Hz	Mode of 0.3799 Hz
DMD	1×10^{-12}	1×10^{-12}	1×10^{-12}	1×10^{-12}	1×10^{-10}	1×10^{-10}
Optimized DMD	1×10^{-8}	1×10^{-6}	1×10^{-6}	1×10^{-7}	1×10^{-5}	1×10^{-6}

The minimum values of the observability measure shown in Table 5.13 were determined by the following procedure: the measure of observability was decreased until it was not identifiable.

The minimum observability measure value required to be identifiable by the dynamic mode decomposition was almost the same for all the modes. For the optimized dynamical mode decomposition, in change, the minimum required observability measure was alternating between 1×10^{-5} and 1×10^{-8}

The measure of observability of the other five modes practically did not have any influence in the results.

As can be seen in Table 5.13, the modes can be extracted from the observables even though they have a very low observability.

In Fig. 5.4 are shown the signals of the system when the observability measure of the mode of 0.6267 is fixed in 1×10^{-7} and the measures of the others at 1.0. The amplitude of the mode of Fig.5.4 (b) is of approximately 1.57×10^{-5} % of the original signal.

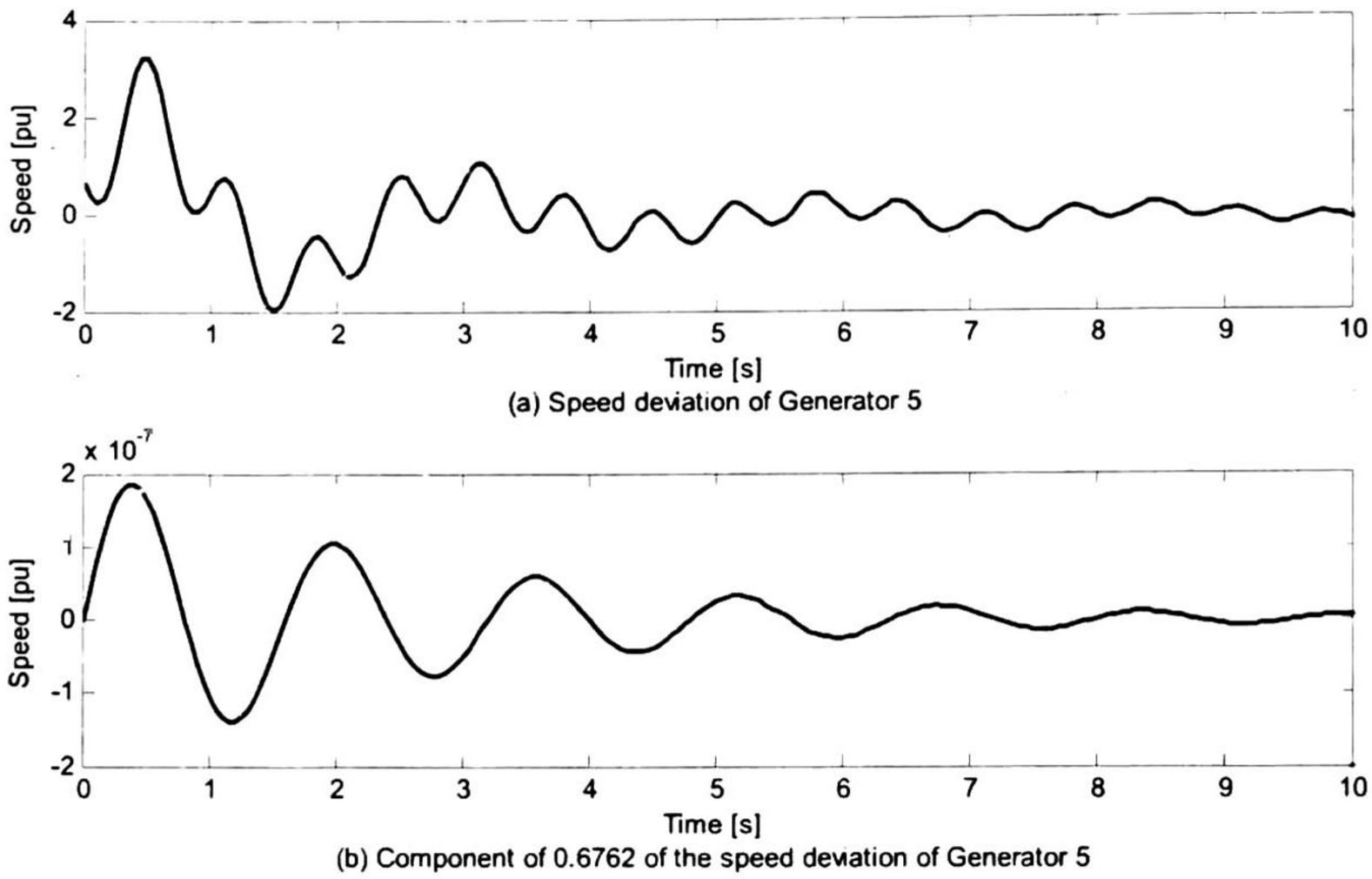

(a) Speed deviation of Generator 5

(b) Component of 0.6762 of the speed deviation of Generator 5

Fig. 5.4. Speed deviation of Generator 5, (a) original signal (b) the 0.6267 Hz component.

It must be noted that the damping ratio and the mode shape calculated for the mode of 0.6267 Hz are almost the same that those calculated by means of a linear stability analysis.

Based on the above analysis, a two-step strategy for an efficient computation of Koopman mode analysis for large sets of observables is proposed:

1. In the first stage, a few signals contain the modes of the system with a certain value of observability greater than a given threshold are selected

2. This subset of observables is used in an enhanced optimized dynamic mode decomposition to obtain the best approximations to the true Koopman modes

3. Finally, the best approximations are used to decompose the rest of the observables.

4. It is important to say that this last process can be made partially for smaller subspaces of observables in order to avoid numerical issues.

5.4 46-machine, 189-bus model of the Mexican power grid

The fourth case have been designed to be compared against results presented in [3] and [6], to show that Koopman mode analysis provides an extension of linear global analysis for nonlinear dynamics by extracting Koopman modes from simulation data of a large disturbance in a real, nonlinear system. It illustrates both, linear and nonlinear behavior, and was computed with a time step of 0.0128 s and a time window of 30 s.

A detailed 46-machine, 189-bus of the Mexican interconnected system (MIS) is used to assess the ability of the Koopman operator to characterize wide-area phenomena in complex power systems.

The disturbance of interest is the outage of the Merida (MDA) power station unit # 1 in the Peninsular system. This contingency is known from previous studies to excite the two slowest modes in the system [3], [6].

5.4.1 Modal characteristics

The 46-machine MIS model has 5 inter-area modes in the low frequency range that are of interest to this research. For reference and comparison, Table 5.14 lists the damping and frequency of the five slowest modes in the system [3].

Table 5.14. The five slowest mode of the system

Inter-area Mode j	Eigenvalue λ_j	Frequency (Hz)	Damping (%)
1	-0.011+ 2.010i	0.31	0.57
2	-0.032+3.251i	0.51	0.98
3	$-0.043 \pm 3.912i$	0.62	1.09
4	$-0.031 \pm 4.824i$	0.76	0.64
5	$-0.177 \pm 5.693i$	0.91	3.10

Discussion will be limited to the first four modes of Table 5.14 which dominate system response for most major contingencies of interest.

5.4.2 Koopman mode analysis

To identify the dynamics interacting in the observables is used the dynamic mode decomposition algorithm to obtain approximations to the true Koopman modes. Then, the ensemble of signals is decomposed with the optimized approach.

Figure 5.5 shows the time evolution of selected signals for analysis. Visual inspection suggests the presence of nonlinear trends and multicomponent behavior.

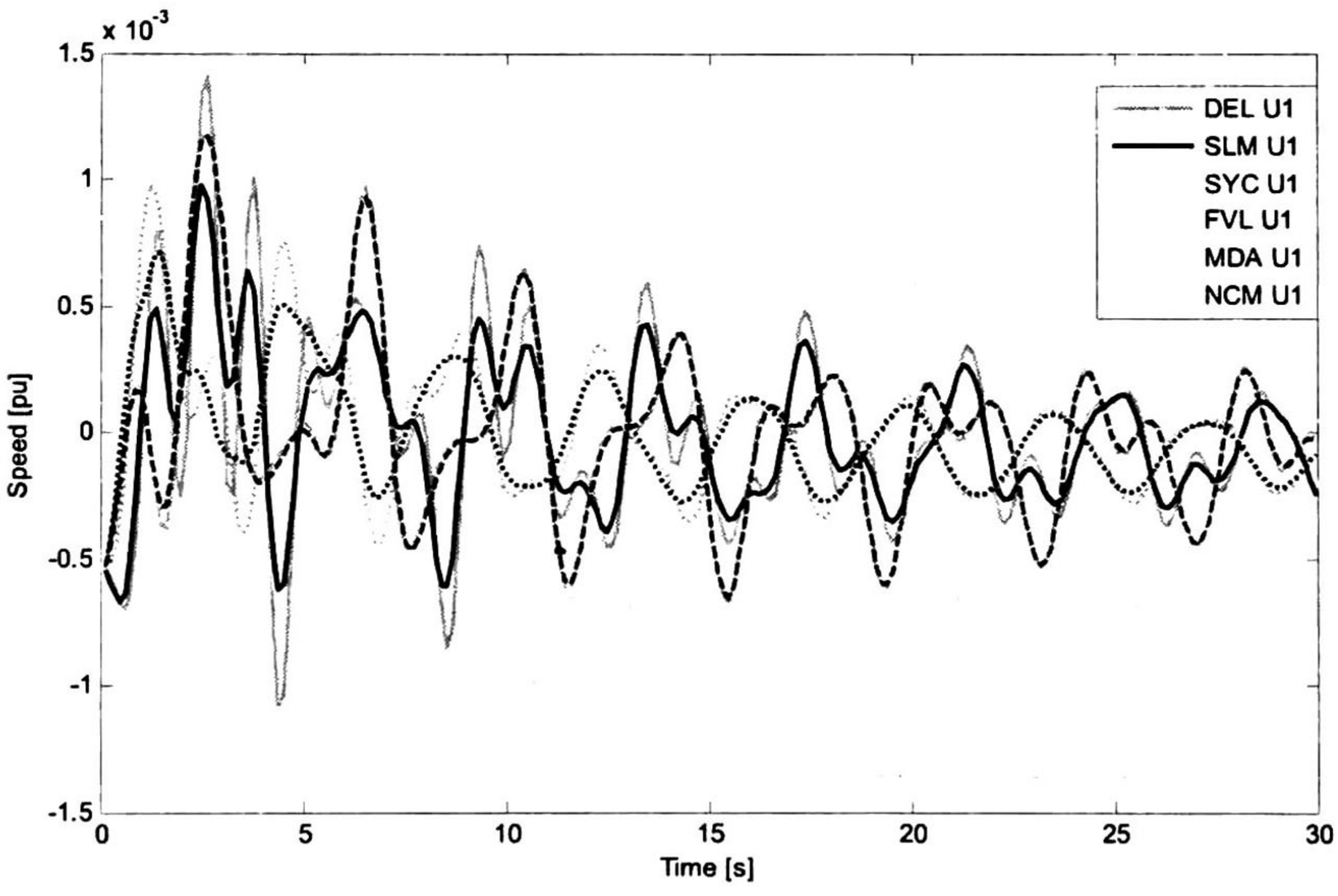

Fig. 5.5. Speed deviations of selected system generators.

The dynamic mode decomposition algorithm it has been used to analyze the set of observables of the Fig. 5.5.

With the entire collect of empirical Ritz vectors (237) gotten by the dynamic mode decomposition, the maximum error is of 6.63×10^{-13} %. The first 10 approximate Koopman modes are contained in Table 5.15.

Table 5.15. Approximate Koopman modes obtained by the DMD algorithm.

Mode j	$\lvert\tilde{\lambda}_j\rvert$	Frequency [Hz]	Damping [%]	Norm $\lVert\tilde{\mathbf{v}}_j\rVert$
1	1.0003	0.0000	-100.0000	0.2887
2	0.9969	0.5096	0.7781	0.3104
3	0.9961	0.2693	1.8128	1.0000
4	0.9953	1.1369	0.5206	0.0093
5	0.9953	2.3700	0.2499	0.0023
6	0.9949	2.4111	0.2688	0.0022
7	0.9938	1.0387	0.7554	0.0208
8	0.9937	1.6029	0.4991	0.0047
9	0.9936	1.2672	0.6432	0.0067
10	0.9934	1.8018	0.4632	0.0046

With these first 10 approximate Koopman modes, the error has a maximum value of 84.88%. Also, it is noted that the frequencies of second and third rows are similar to that of the inter-area modes provided in Table 5.14, and if just the first three empirical Ritz vectors are contemplated, the maximum error takes the value of 85.05%, what is not much different of the error of taking the first 10 modes.

Then the optimized dynamic mode decomposition is used. With 30 modes the maximum error value was of 0.69%. The first ten approximate Koopman modes found by the algorithm are shown in Table 5.16.

It can be observed that some modes with low frequencies as the first and the fifth provide an approximation to the trend of the signal.

Table 5.16. First 10 approximate KMs obtained by the optimized DMD algorithm for the data of Fig. 5.11.

Mode j	$\tilde{\lambda}_j$	Frequency [Hz]	Damping [%]	Norm $\tilde{\mathbf{v}}_j$
1	1.0960	0.0892	-79.2319	0.0000
2	1.0056	0.2602	-2.6878	0.0024
3	0.9978	0.5124	0.5543	0.0359
4	0.9947	0.2700	2.4748	0.1627
5	0.9938	0.0160	43.8355	0.0987
6	0.9904	0.7341	1.6522	0.0745
7	0.9882	0.2834	5.2640	0.0150
8	0.9844	0.5656	3.5085	0.0089
9	0.9824	1.6560	1.3554	0.0016
10	0.9804	0.6384	3.9097	0.0674

Additionally, the modes number 3, 4, 6, and 10 have frequencies similar to that shown in Table 5.14 so they can be interpreted as approximations to the inter-area modes of the system. Nevertheless, some other approximations seem to be residuals of these approximations to the inter-area modes. The second and seventh modes are similar to the third. Some other cases are present in the rest of the approximate Koopman modes.

Also, the fifth inter-area mode of Table 5.14 is contained in the list of the 30 approximate Koopman modes, but there are other several approximations with almost the same frequency that can be residuals or other local modes.

Figures 5.6 and 5.7 give the normalized mode shapes of the approximate Koopman modes of the inter-area modes 0.2700 Hz, 0.5656 Hz, and 0.7341 Hz. Results are in good agreement with previous small-signal stability results in [6].

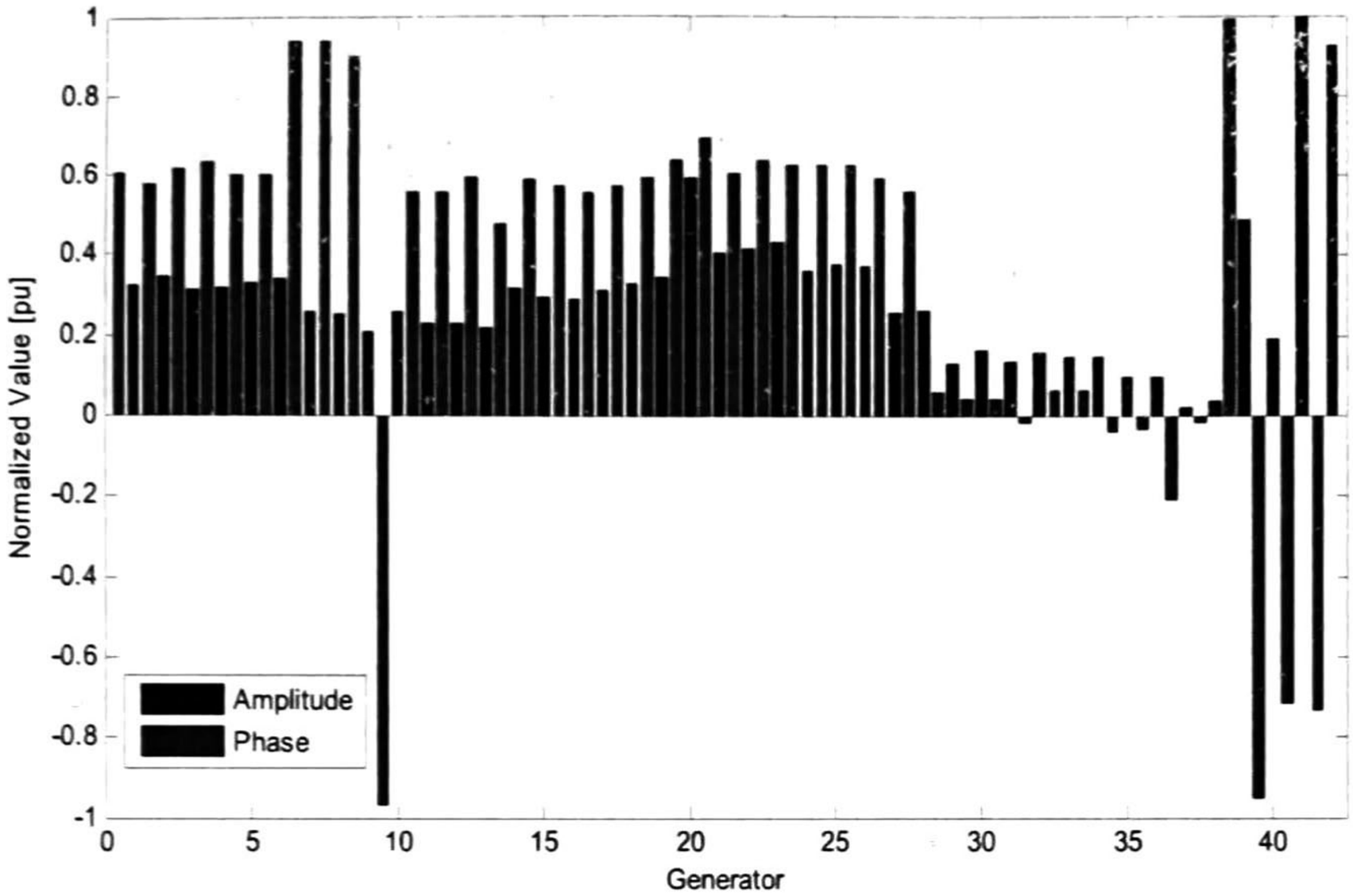

Fig. 5.6. Mode shapes of the approximate Koopman mode at 0.5656 Hz,

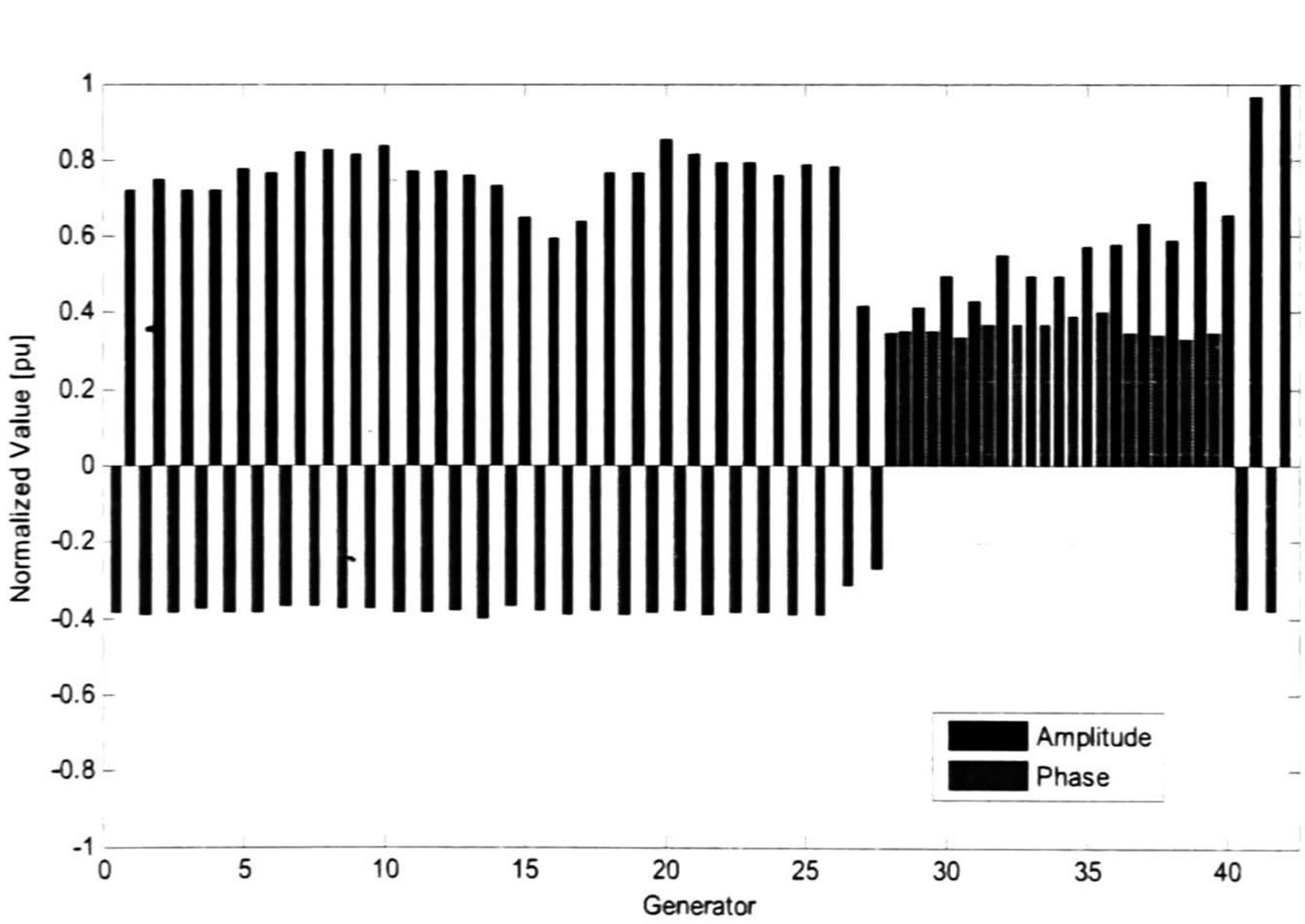

(a) 0.27 Hz mode

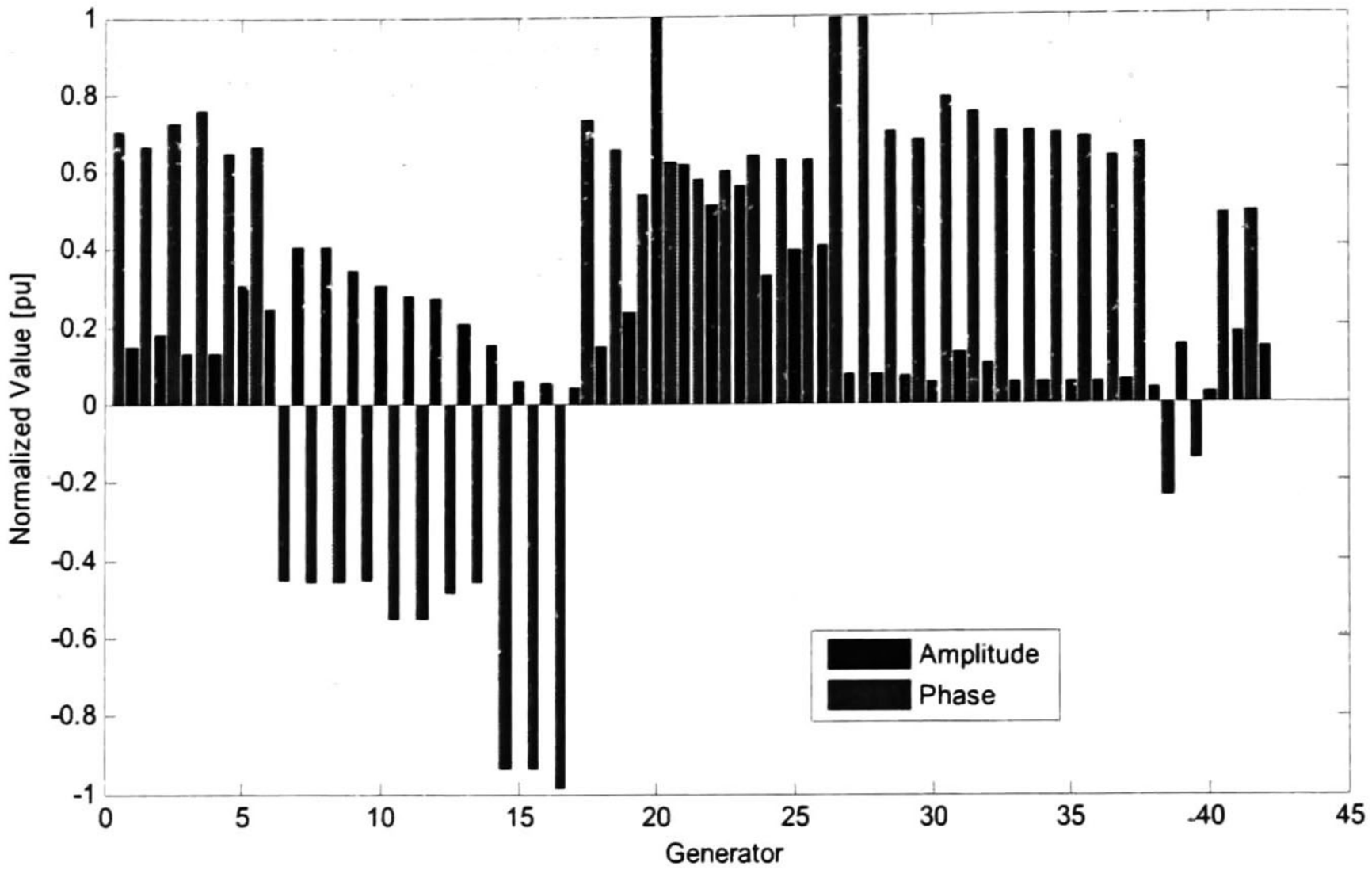

(b) 0.734 Hz mode

Fig. 5.7. Mode shapes of the approximate Koopman modes (a) 0.2700 Hz and (b) 0.7341 Hz

If the approximate Koopman modes that are similar to the trend and the four inter-area modes (6 in total) are taken to reconstruct the observables it rises a maximum error of 91.74%.

Figure 5.8 compares the original measured signal with the reconstructed signal using the dynamic mode decomposition and optimized DMD decomposition. Simulation results show that the two approaches provide a good approximation for the steady state system behavior. Clearly, the optimized DMD method outperforms the dynamic modes approximation.

In all cases, the dynamic mode decomposition technique fails to approximate system behavior following the inception of the fault, while the optimized DMD method provides an accurate modal approximation for the whole observation window.

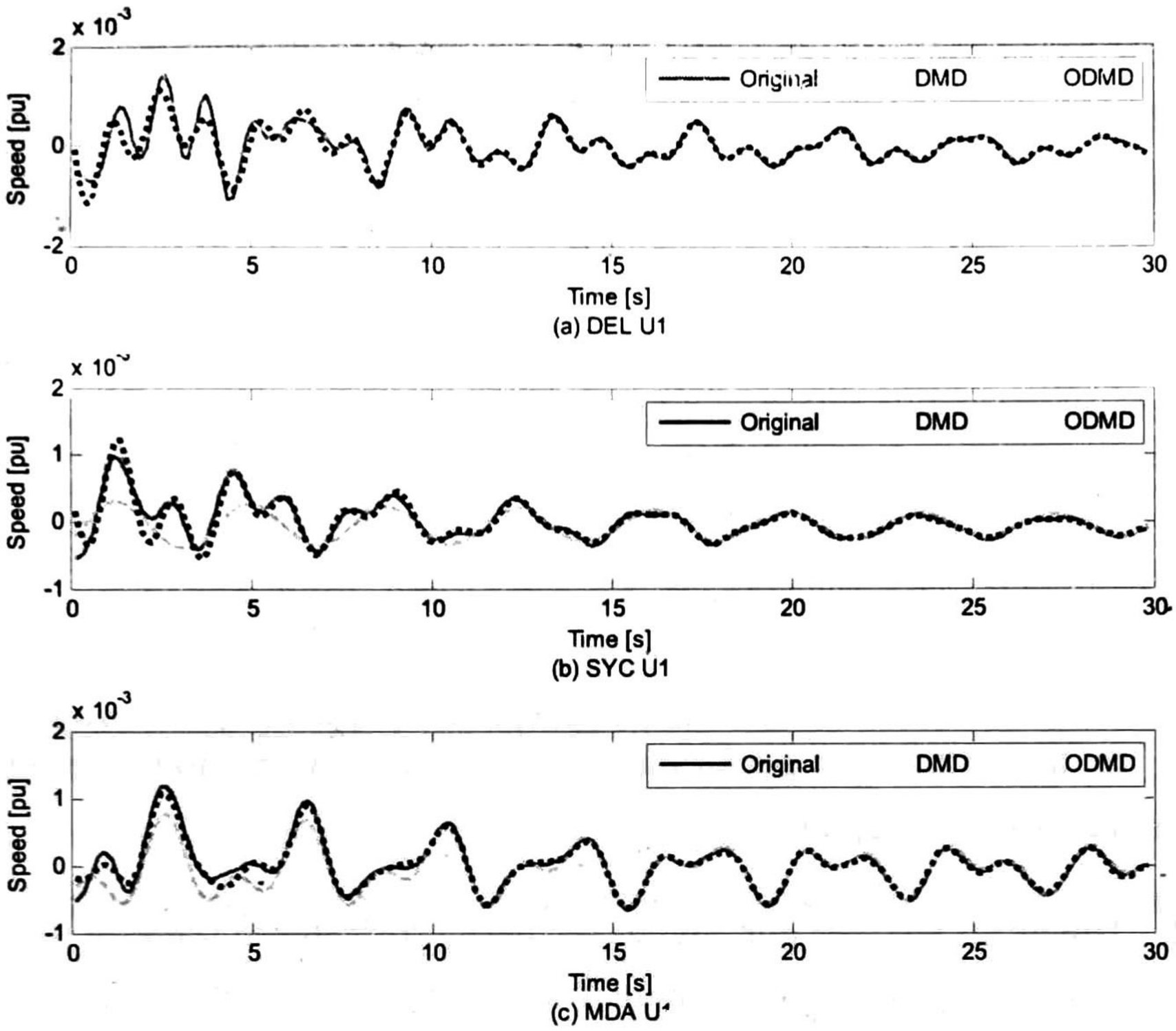

Fig. 5.8. Comparison of measured signals with the reconstructed mode shape estimates using the three dominant Koopman modes. Speed deviations of generators (a) DEL U1, (b) SYC U1, and (c) MDA U1.

5.5 Concluding remarks

Three types of test cases have been presented in this chapter: the linear case, the simulation of a real nonlinear power system and the simulation of a fault in a synthetic nonlinear system.

The linear case studied demonstrated that the Koopman modes converge to the linear eigenmodes. Then, for nonlinear observables it was shown that Koopman mode analysis is capable to decompose the set of signals into a few physically meaningful Koopman modes with an acceptably accuracy. Therefore, although the approximate Koopman modes can be a mixture of a few intrinsic modes of the observables, their properties are still preserved together in the

mode shape of the corresponding Koopman eigenvalue. Further results for observables with the adequate resolution are not presented in this research work due to the space and the aim of the investigation.

Then, it was found that though a component could have a very low measure of observability, Koopman mode analysis is still able to extract it.

Finally, in this chapter was performed an analysis of a nonlinear response and it was demonstrated that Koopman mode analysis provides analogous results to the method of Normal Forms. An important detail was that a theoretical approximation was used to calculate the second-order eigenmode of the main nonlinear mode identified. Nonetheless, more investigation is needed.

In the numerical performance of the Koopman mode decomposition, some details have been found:

1. The norm value is not always the best parameter to identify the empirical Ritz vectors that approximate in the best way the intrinsic dynamics.

2. The dynamic mode decomposition algorithm is faster than the optimized approach, but sometimes it cannot identify the most meaningful structures due to its dependence on the first and last vectors of the snapshots series.

3. The approach based on the singular value decomposition was not reported in this chapter because it got the worst approximation. Its results are useful mainly for some cases as initial set for an optimization process.

4. The optimized Koopman mode decomposition for large sets of approximate Koopman modes does not converge efficiently to the true Koopman modes.

5.6 References

[1] G. Rogers, *Power System Oscillations*, Massachsetts, USA; Kluwer Academic Publish rs, 2000.

[2] J. J. Sanchez-Gasca, V. Vittal, M. J. Gibbard, A. R. Messina, D. J. Vowles, S. Liu, and U. D. Annakkage, "Inclusion of higher order terms for small-signal (modal) analysis: committee report – task force on assessing the need to include higher order terms for small-signal (modal) analysis", IEEE Trans. Power Syst., vol. 20, no. 4, pp. 1886-1904, Nov. 2005.

[3] A. R. Messina and V. Vittal, "Nonlinear, non-stationary analysis of inter-area oscillations via Hilbert spectral analysis," *IEEE Trans. Power Syst.*, vol. 21, no. 3, pp. 1234–1241, Aug. 2006.

[4] K. K. Chen, J.H. Tu, C. W. Rowley, "Variants of Dynamic Mode Decomposition: Boundary Condition, Koopman, and Fourier Analyses", *J. of Nonlinear Science*, vol. 22, no. 6, pp. 887–915, Dec. 2012.

[5] S. Liu, A. R. Messina, V. Vittal, "Assessing placement of controllers and nonlinear behavior using normal form analysis", *IEEE Trans. Power Syst.*, vol. 20, no. 3, pp. 1486–1495, Aug. 2005.

[6] A. R. Messina and Vijay Vittal, "Extraction of dynamic patterns from wide-area measurements using empirical orthogonal functions", *IEEE Trans. Power Syst.*, vol. 22, no. 2, pp. 682–692, May 2007

Chapter6
Conclusions

6.1 General conclusions

In this thesis, a rigorous analytical framework for global nonlinear stability analysis of wide-area measurements is presented.

Drawing upon the theory of Koopman modes, variants of Koopman mode decomposition are introduced and tested on measured data. These include dynamic mode decomposition, SVD-based dynamic mode decomposition and optimized dynamic mode decomposition.

Extensive numerical simulations show that existing methods suffer from various limitations:

1) The SVD-based approach is severally affected by the number of observables and their correlation.

2) Dynamic mode decomposition is highly sensitive to the variation of the last snapshot.

3) The ranking criterion used for the approximate Koopman modes is deficient.

mode shape of the corresponding Koopman eigenvalue. Further results for observables with the adequate resolution are not presented in this research work due to the space and the aim of the investigation.

Then, it was found that though a component could have a very low measure of observability, Koopman mode analysis is still able to extract it.

Finally, in this chapter was performed an analysis of a nonlinear response and it was demonstrated that Koopman mode analysis provides analogous results to the method of Normal Forms. An important detail was that a theoretical approximation was used to calculate the second-order eigenmode of the main nonlinear mode identified. Nonetheless, more investigation is needed.

In the numerical performance of the Koopman mode decomposition, some details have been found:

1. The norm value is not always the best parameter to identify the empirical Ritz vectors that approximate in the best way the intrinsic dynamics.

2. The dynamic mode decomposition algorithm is faster than the optimized approach, but sometimes it cannot identify the most meaningful structures due to its dependence on the first and last vectors of the snapshots series.

3. The approach based on the singular value decomposition was not reported in this chapter because it got the worst approximation. Its results are useful mainly for some cases as initial set for an optimization process.

4. The optimized Koopman mode decomposition for large sets of approximate Koopman modes does not converge efficiently to the true Koopman modes.

5.6 References

[1] G. Rogers, *Power System Oscillations*, Massachsetts, USA; Kluwer Academic Publish rs, 2000.

[2] J. J. Sanchez-Gasca, V. Vittal, M. J. Gibbard, A. R. Messina, D. J. Vowles, S. Liu, and U. D. Annakkage, "Inclusion of higher order terms for small-signal (modal) analysis: committee report – task force on assessing the need to include higher order terms for small-signal (modal) analysis", IEEE Trans. Power Syst., vol. 20, no. 4, pp. 1886-1904, Nov. 2005.

[3] A. R. Messina and V. Vittal, "Nonlinear, non-stationary analysis of inter-area oscillations via Hilbert spectral analysis," *IEEE Trans. Power Syst.*, vol. 21, no. 3, pp. 1234–1241, Aug. 2006.

[4] K. K. Chen, J.H. Tu, C. W. Rowley, "Variants of Dynamic Mode Decomposition: Boundary Condition, Koopman, and Fourier Analyses", *J. of Nonlinear Science*, vol. 22, no. 6, pp. 887–915, Dec. 2012.

[5] S. Liu, A. R. Messina, V. Vittal, "Assessing placement of controllers and nonlinear behavior using normal form analysis", *IEEE Trans. Power Syst.*, vol. 20, no. 3, pp. 1486–1495, Aug. 2005.

[6] A. R. Messina and Vijay Vittal, "Extraction of dynamic patterns from wide-area measurements using empirical orthogonal functions", *IEEE Trans. Power Syst.*, vol. 22, no. 2, pp. 682–692, May 2007

CENTRO DE INVESTIGACIÓN Y DE ESTUDIOS AVANZADOS DEL I.P.N.
UNIDAD GUADALAJARA

El Jurado designado por la Unidad Guadalajara del Centro de Investigación y de Estudios Avanzados del Instituto Politécnico Nacional aprobó la tesis

"Avances en el monitoreo de la estabilidad de área amplia en sistemas de potencia mediante el análisis espectral de Koopman",
"Advances in wide-area power system stability monitoring using Koopman spectral analysis"

del (la) C.

Marcos Alfredo HERNÁNDEZ ORTEGA

el día 25 de Agosto de 2014.

Dr. Deni Librado Torres Román
Investigador CINVESTAV 3C
CINVESTAV Unidad Guadalajara

Dr. Juan Manuel Ramírez Arredondo
Investigador CINVESTAV 3C
CINVESTAV Unidad Guadalajara

Dr. Arturo Román Messina
Investigador CINVESTAV 3C
CINVESTAV Unidad Guadalajara

Dr. José Raúl Loo Yau
Investigador CINVESTAV 3B
CINVESTAV Unidad Guadalajara